BIOACTIVE PEPTIDE NANOFIBERS FOR TISSUE REGENERATION

A DISSERTATION SUBMITTED TO

THE GRADUATE SCHOOL OF ENGINEERING AND SCIENCE

OF BILKENT UNIVERSITY

IN PARTIAL FULFILLMENT OF THE REQUIREMENTS FOR

THE DEGREE OF

DOCTOR OF PHILOSOPHY

IN

MATERIALS SCIENCE AND NANOTECHNOLOGY

By

Gözde Uzunallı

January 2016

BIOACTIVE PEPTIDE NANOFIBERS FOR TISSUE REGENERATION

By Gözde Uzunallı
January 2016

We certify that we have read this thesis and that in our opinion it is fully adequate, in scope and in quality, as a thesis for the degree of Doctor of Philosophy.

Ayşe Begüm Tekinay (Advisor)

Mustafa Özgür Güler

Bahri Aydın

Çağlar Elbüken

Fatih Büyükserin

Approved for the Graduate School of Engineering and Science:

Levent Onural
Director of the Graduate School

ABSTRACT

BIOACTIVE PEPTIDE NANOFIBERS FOR TISSUE REGENERATION

Gözde Uzunallı
Ph.D. in Materials Science and Nanotechnology
Advisor: Ayşe Begüm Tekinay
January, 2016

Defects in the tissues or organs caused by trauma or diseases can have detrimental effects on all aspects of patients' life quality. During the last three decades, considerable developments have been made in tissue engineering and regenerative medicine in order to find alternative treatment methods to recover tissue function after injury. These methods are based on the development of materials that are uniquely suited to the specific requirements of the tissue type and the repair process itself. Consequently, the implanted biomaterial must be compatible with biological systems and capable of delivering the signals necessary to facilitate tissue repair. In the present thesis, peptide amphiphile molecules were used to meet these requirements and develop next-generation biomaterials that are able to enhance the repair process while minimally affecting the integrity of surrounding tissues. Peptide amphiphiles are molecules that naturally self-assemble into nanofibrous hydrogel structures that closely emulate the composition of the extracellular matrix. As peptide amphiphiles contain amino acid sequences, bioactive signals can also be integrated into their structure to create a biocompatible environment and enhance the survival and proliferation of the resident cell population. In the scope of the present thesis, peptide amphiphile systems

were utilized in three distinct applications. The first chapter covers the fundamentals of regenerative medicine and tissue engineering, the interactions between biomaterials and cells and extracellular materials, and the materials that are commonly used for these applications. The second chapter details the use of fibronectin- and laminin-derived peptide amphiphiles for the regeneration of corneal injuries. The third chapter investigates the ability of heparin-mimetic peptide hydrogels to facilitate the survival of pancreatic islets *in vitro* and demonstrates that islets transplanted in tandem with peptide gels trigger a local angiogenic response, decrease blood glucose levels and retain these functionalities even after 28 days of observation. The fourth chapter concerns the application of heparin-mimetic peptide amphiphile molecules for the recovery of acute wound injuries through the establishment of a well-ordered collagen matrix and the enhancement of the re-epithelialization process. Distinct peptide amphiphiles bearing bioactive signals conductive to tissue development were developed and utilized in all three studies, and the use of these materials has been demonstrated to serve as an adequate means of enhancing tissue repair.

Keywords: Extracellular matrix, peptide amphiphiles, self-assembly, cornea regeneration, islet transplantation, wound healing, angiogenesis

ÖZET

DOKU REJENERASYONUNDA BİYOAKTİF PEPTİT NANOFİBERLER

Gözde Uzunallı
Malzeme Bilimi ve Nanoteknoloji, Doktora
Tez Danışmanı: Ayşe Begüm Tekinay
Ocak, 2016

Doku ve organlardaki hastalık ya da travma kaynaklı hasarlar, hastaların yaşam kalitesi üzerinde ciddi etkilere yol açmaktadır. Son 30 yılda, doku mühendisliği ve rejeneratif tıp alanında hasar sonrası doku fonksiyonunun geri kazanılmasına alternatif tedavi yöntemleri bulmak adına önemli gelişmeler kaydedilmiştir. Bu yöntemler, özellikle doku tipine özgü gereksinimlere ve iyileşme sürecine elverişli malzemelerin geliştirilmesine dayanmaktadır. Bu nedenle implante edilecek biyomalzemelerin, biyolojik sistemlerle uyumlu ve doku tamirini gerçekleştirecek önemli sinyalleri iletmeye yetkin olması gerekmektedir. Bu tez çalışmasında, belirtilen gereksinimleri karşılamak için peptit amfifil molekülleri kullanılmış ve tamir sürecini hızlandırırken çevre dokuların bütünlüğünü minimal düzeyde etkileyen yeni nesil biyomalzemeler geliştirilmiştir. Peptit amfifil molekülleri, hücreler arası ortamın komposizyonunu taklit edebilen ve doğal olarak kendiliğinden bir araya gelebilen nanofiber hidrojel yapılardır. Peptit amfifiller aminoasit dizileri içerdikleri için yapılarına, biyouyumlu ortam yaratmak ve yerleşik hücre popülasyonunun sağkalımı ve çoğalmasını arttırmak için biyoaktif sinyaller entegre edilebilir. Bu tez çalışması kapsamında üç uygulama alanı için farklı biyoaktif peptit amfifil hidrojel sistemleri incelenmiştir. İlk bölümde rejeneratif

tıp ve doku mühendisliğinin temelleri, bunların hücreler arası ortam ile etkileşimleri ve temelde kullanılan malzemeler hakkında bilgiler verilmiştir. İkinci kısımda, fibronektin ve lamininde bulunan önemli biyoaktif dizileri içeren peptit amfifil moleküllerinin kornea stroma hasarı üzerindeki rejeneratif etkileri tartışılmıştır. Üçüncü kısımda, heparin benzeri peptit hidrojellerin *in vitro* ortamda pankreatik adacıkların sağkalımı üzerindeki etkileri incelenmiştir. Bununla beraber, peptit jelleri ile birlikte transplante edilen adacıkların bölgesel anjiyogenez yanıtını tetiklediği, kan glikoz seviyesini düşürdüğü ve bu fonksiyonelliği 28 boyunca koruduğu gösterilmiştir. Dördüncü bölüm ise anjiyogenik etkisi olduğu bilinen heparin benzeri peptit amfifil molekülleri uygulamasının, akut yara hasarında düzenli kollajen yapısı oluşturması ve epitelizasyonu hızlandırması üzerinedir. Doku gelişiminde etken biyoaktif sinyalleri taşıyan farklı peptit amfifiller bu iç çalışma içinde geliştirilmiş ve değerlendirilmiştir. Bu malzemelerin kullanımlarının elverişli bir şekilde doku tamiri hızlandırılmasına hizmet ettiği gösterilmiştir.

Anahtar kelimeler: Hücreler arası ortam, peptit amfifiller, kendiliğinden birleşme, kornea rejenerasyonu, adacık transplantasyonu, yara iyileşmesi, anjiyogenez

ACKNOWLEDGEMENT

Though only my name appears on the cover of this dissertation, a great many people who deserved more than I can say have made this dissertation possible and because of whom my graduate experience has been one that I will cherish during my way to this long journey.

First and foremost my sincerest gratitude is to my advisor Prof. Ayşe Begüm Tekinay for her knowledge and patience, whilst allowing me the room to work in my own way. She supported me not only by academically but also emotionally through the rough road to move on. Her support helped me overcome many crisis situations. My co-advisor, Prof. Mustafa Özgür Güler, has been always there to listen and give advice. I am deeply grateful to him for his knowledge, guidance and perspective.

I would like to thank Prof. Bahri Aydın and Prof. Fatma Yülek Turgut for their guidance and support during my PhD studies.

I would like to thank Rashad Mammadov, Turan Selman Erkal, Yasin Tümtaş, Melis Şardan, Çağla Eren and Öncay Yaşa for especially valuable discussions, mostly sleepless nights and their friendship. I also would like to acknowledge Büşra Mammadov, Burcu Gümüşçü, Melike Sever, Didem Mumcuoğlu, Melis Göktaş, Ruslan Garifullah, M. Aref Khalily, Göksu Çınar, Ceren Garip, Mustafa Beter, Gökhan Günay, Egemen Deniz Eren, Zeynep Orhan, Fatih Yergöz, Merve Şen, Seren Hamsici, Meryem Hatip, Aygül Zengin, Canelif Yılmaz, İbrahim Çelik, Idil Uyan, Şehmus Tohumeken, Ayşe Özdemir,

Nuray Gündüz, Gülcihan Gülseren, Nurcan Haştar, Özüm Günel, Oğuz Tuncay and Begüm Kocatürk for the their help and for all the fun we have had in these years. I am also so grateful to Alper Devrim Özkan for his help and suggestions for all my manuscripts. It has been my pleasure to know and work with all of you.

I would like to thank The Scientific and Technological Research Council of Turkey (TÜBİTAK BIDEB-2211C, 213M682, 110S010) for funding my PhD research.

Süleyman Gülsüner, Ali Hashemi, Deniz Özel… There has been no courage of me to start over without your support. Thank you for mentoring and trusting me.

Zeynep Aytaç, Aslı Çelebioğlu, David Slattery... Thank you for help me to stay sane through these years. Having such open hearted and incredible people like you is one of my greatest chances in my life. I am so grateful having you as a good friend and being my cheerfulness in this journey.

Gülnihal Coşkuntürk, Gülşah Kayserili, Gültaç Coşkuntürk, Nilay Göçet…When I look to my last 23 years, I see incredible memories which make me stronger even we are far away from each other. Physical presence does not matter, because I will always know that we are here for each other forever.

Betül Akpınar, Yıldız Gözde Sağlam, Sinem Gürbüz… Sometimes just a word explains the mystery of the whole world, so thank you for being my home.

Ahmet Kalır, Ozan Şişman, Alper Mortaş… My big or little brothers… Your keen interest was a great help throughout the course of this work. Growing with you is an invaluable experience in my life even though our crazy idiosyncrasies, immature personality and weird habits.

Ezgi Çalışkan, Cansu Özdemir and foremost Yamanitom… I feel myself as a luckiest person in the world since you spent all these years putting up with my everlasting ventures. Thank you for encouragements and bonding that will forever be my treasure.

Yılmaz Yıldız, Leman Akcan… We have felt at home since we cried, laughed and made fun of everything we went through. Thank you for being there for me in all forms. And Barış, it will be difficult to live in a world like this. I know that you will be upset, or filled with despair, or wish to rebel against it, but don't – Just remember, you are a part of a beautiful story with the greatest parents ever!

Rüya Turna, Pınar Erdem, Can Turan, Songül Kaynak Bayar, Özlem Telci Özkaya, Cem Erkan, Pervin İvegen, Çağrı Acar, Mübeccel Koyutürk, Seval İnceoğlu, Tuğba Okatan Aykar, Ümit Dedeoğlu. I owe a debt of gratitude to those incredibly amazing people who are my lighthouse for 'any step' of my life. I want to give my all appreciation for providing freedom to explore everything on my own with your full support and guidance to recover when my steps faltered.

Kazım Cihan Can, Nadir Çakır (Çona'm), Emiralp Emre… It is always difficult for one to bare their inner self to the world and live among others with

no fear or pain or regret. I deeply appreciate you doing this for me. Thank you for being my superheroes, mostly my İkinci “Yeni”, my tears and my laughter.

Lastly, Fırat Uzunallı, Ümit Demir, Levent Alkan, Emir Özçalışkan, Deniz Eyice (or Cep Rüya’m)… I would like to express my most sincere gratitude to my family. I am eternally grateful for supporting and allowing me to pursue my ambitions throughout my life. Thank you for letting me be the person I am today. I would like to let you to know that you all are my inspiration and motivation for entire my life. Without your endless support, enduring love, guidance and encouragement, I could not have made it this far. I love you all from the bottom of my hypothalamus or degraded megakaryocytes.

CONTENTS

ABSTRACT iii

ÖZET v

ACKNOWLEDGEMENT vii

CONTENTS xi

LIST OF FIGURES xvi

Abbreviations xxii

Chapter 1 1

INTRODUCTION 1

1.1 *The Fountain of Regeneration*: An approach in biology and engineering 2

1.2 Basic Principles of Tissue Engineering and Regenerative Medicine..... 7

1.2.1 Cell Types 9

1.2.2 Soluble macromolecules in ECM..... 12

1.2.3 Scaffolds..... 14

1.2.3.1 The extracellular matrix and the importance of its interactions with cells..... 14

1.2.3.2 Requirements of scaffolds 20

1.2.3.3 Biomaterials utilized for tissue engineering and regenerative medicine 22

1.2.3.3.1 Naturally derived biomaterials 22

1.2.3.3.2 Synthetic biomaterials 25

Chapter 2 30

BIOACTIVE SELF-ASSEMBLED PEPTIDE NANOFIBERS FOR CORNEAL STROMA REGENERATION..... 30

2.1 INTRODUCTION 31

2.2 MATERIALS & METHODS 35

2.2.1 Materials..... 35

2.2.2 Synthesis and Purification of PA Molecules 35

2.2.3 Physical and Chemical Characterizaiton of PA Molecules…….37

2.2.3.1. Atomic Force Microscopy 38

2.2.3.2 Transmission electron microscopy 38

2.2.3.3 Circular Dichroism 38

2.2.3.4 Scanning Electron Microscopy 39

2.2.4 Cell Culture & Maintenance..... 39

2.2.4.1 Analysis of *In Vitro* Effects of PA Molecules 40

2.2.4.2 Spreading 41

2.2.5 *In Vivo* Experiments..... 42

2.2.5.1 Surgical Procedure 43

2.2.5.2 Immunohistochemistry..... 44

2.2.6 Statistical analyses 45

2.3. RESULTS AND DISCUSSION..... 46

2.3.1 Synthesis of PA molecules 46

2.3.2 Characterization of Self-assembled PA Nanofibers..... 52

2.3.3. *In vitro* Characterization of Cellular Responses on PA Nanofibers 56

2.3.4 Histological Examination and Analysis of Rabbit Corneas 60

2.4 CONCLUSION 74

Chapter 3 75

IMPROVING PANCREATIC ISLET TRANSPLANTATION EFFICIENCY USING HEPARIN MIMETIC PEPTIDE AMPHIPHILE NANOFIBER GEL .. 75

3.1 INTRODUCTION 76

3.2 MATERIALS AND METHOD 79

3.2.1 Materials 79

3.2.2 Synthesis of Peptide Amphiphile Molecules 79

3.2.3 Purification of Peptide Amphiphile Molecules 80

3.2.4 Physical, Mechanical and Chemical Characterization of Self assembled Nanofiber Network 81

3.2.4.1 Transmission Electron Microscopy [30] 81

3.2.4.2 Atomic Force Microscopy (AFM) 81

3.2.4.3 Scanning Electron Microscopy (SEM) 82

3.2.4.4 Circular Dichroism (CD) 82

3.2.4.5 Oscillatory Rheology 83

3.2.5 Animals 83

3.2.6 Islet Isolation and Culture 83

3.2.6.1 Pancreatic Islet Viability 84

3.2.6.2 Glucose Stimulated Insulin Release 85

3.2.7 Transplantation 86

3.2.8 Scaffold Function Assessment 87

3.2.9 Histological Analysis 88

3.2.10 Statistical Analysis 89

3.3 RESULTS 89

3.3.1 Heparin Mimetic PA Molecules Self-assembles Into Nanofibers 89

3.3.2 HM-PA Improves Function of Islets *In Vitro* 95

3.3.3 Transplantation within Bioactive PA Scaffold Improves Glucose Responsiveness of the Transplanted Islets 100

3.3.4 PA Scaffold Supports Islet Integrity and Enhance Vascular Density of the Transplantation Site 103

3.4 DISCUSSION 110

3.5 CONCLUSIONS 114

Chapter 4 116

ANGIOGENIC HEPARIN-MIMETIC PEPTIDE NANOFIBER GEL IMPROVES THE REGENERATIVE HEALING OF ACUTE WOUNDS 116

4.1 INTRODUCTION 117

4.2 MATERIALS & METHOD 121

4.2.1 Materials 121

4.2.2 Synthesis and Purification of Peptide Amphiphile Molecules . 121

4.2.3 Physical and Mechanical Characterization of Self-assembled Nanofiber Networks 122

4.2.3.1 Scanning Electron Microscopy (SEM) 122

4.2.3.2 Oscillatory Rheology 122

4.2.4 Wound Healing Animal Model 123

4.2.5. Histological Analyses 124

4.2.6 Statistical Analysis 125

4.3 RESULTS 125

4.4 DISCUSSION..... 144

4.5 CONCLUSION 147

Chapter 5 149

CONCLUSION AND FUTURE PERSPECTIVES 149

Bibliography 155

APPENDIX..... 171

LIST OF FIGURES

Figure 1.1 Commercially available tissue engineering products. 5

Figure 1.2 Basics of tissue engineering. 8

Figure 1.3 Interactions between cells and their surrounding extracellular matrix organize the biological dynamic 16

Figure 1.4 Glycosaminoglycans and their structural units. 19

Figure 1.5 Schematic representations of peptide amphiphile molecules and nanofibers. (A) Chemical structure, (B) different regions of structure, (C) nanofibrous structure of peptide amphiphiles 28

Figure 2.1 Chemical structures of PA nanofibers. (A) YIGSR-PA, (B) KKRGD-PA, (C) K-PA, (D) E-PA 48

Figure 2.2 (A) HPLC chromatogram of purified YIGSR-PA molecule at 220 nm. (B) Mass spectrometry analysis of YIGSR-PA molecule..... 49

Figure 2.3 (A) HPLC chromatogram of purified KKRGD-PA molecule at 220 nm. (B) Mass spectrometry analysis of KKRGD-PA molecule. 50

Figure 2.4 (A) HPLC chromatogram of purified E-PA molecule at 220 nm. (B) Mass spectrometry analysis of E-PA molecule 51

Figure 2.5 (A) HPLC chromatogram of purified K-PA molecule at 220 nm. (B) Mass spectrometry analysis of K-PA molecule. 52

Figure 2.6 Circular dichroism spectra of the peptide nanostructures. 54

Figure 2.7 Transmission electron micrographs of (A) YIGSR-PA/E-PA, (B) KKRGD-PA/E-PA, (C) K-PA/E-PA, (D) YIGSR-PA/CS, and (E) KKRGD-PA/CS. 55

Figure 2.8 Atomic force microscopy of (A) YIGSR-PA/E-PA, (B) KKRGD-PA/E-PA, (C) K-PA/E-PA, (D) YIGSR-PA/CS and (E) KKRGD-PA/CS. 55
Figure 2.9 Scanning electron micrographs of (A) YIGSR-PA/E-PA, (B) KKRGD-PA/E-PA, (C) K-PA/E-PA, (D) YIGSR-PA/CS and (E) KKRGD-PA/CS. 56
Figure 2.10 Viability results of corneal fibroblast at 24 h. PA scaffolds do not exhibit any toxic effect on HTK cell line..... 58
Figure 2.11 Proliferation results of corneal fibroblasts at 72 h. The YIGSR-PA nanofibers exhibited a similar proliferation profile compared with collagen.. 58
Figure 2.12 SEM images of corneal fibroblasts cultured on (A) YIGSR-PA coated surface, (B) KKRGD-PA coated surface, (C) K-PA coated surface and, (D) collagen coated surface show the adhesion profiles of cells..... 59
Figure 2.13 Spreading and cellular morphology of corneal fibroblasts acquired by vimentin (blue), TRITC-conjugated phalloidin (red) and TO-PRO®-3 (green) iodide staining on (A) YIGSR-PA coated surface, (B) KKRGD-PA coated surface, (C) K-PA coated surface, (D) collagen coated surface..... 60
Figure 2.14 Representative images of injection process of KKRGD-PA..... 61
Figure 2.15 Thickness of the rabbit corneas at (A) week 3 and (B) week 7. 62
Figure 2.16 IHC analyses of YIGSR-PA injected samples at week 3..... 64
Figure 2.17 IHC analyses of KKRGD-PA injected samples at week 3..... 65
Figure 2.18 IHC analyses of damaged rabbit cornea samples at week 3. ... 66
Figure 2.19 IHC analyses of YIGSR-PA injected samples at week 7..... 68
Figure 2.20 IHC analyses of KKRGD-PA injected samples at week 7..... 69
Figure 2.21 IHC analyses of damaged rabbit cornea samples at week 7 70

Figure 2.22 Histological and immunohistochemical analyses of native rabbit corneas 70
Figure 3.1 Chemical structures of peptide amphiphiles used in this study... 90
Figure 3.2 (A) HPLC chromatogram of purified Heparin-mimetic PA molecule at 220 nm. (B) Mass spectrometry analysis of Heparin-mimetic PA molecule. 91
Figure 3.3 (A) HPLC chromatogram of purified K-PA molecule at 220 nm. (B) Mass spectrometry analysis of K-PA molecule 92
Figure 3.4 Circular dichroism spectra of the peptide amphiphile molecules. 93
Figure 3.5 Characterization of peptide amphiphile nanofiber and scaffolds at pH 7.4 94
Figure 3.6 Morphology of pancreatic islets cultured with HM-PA, HM-PA with growth factors (GF), HM-PA/K-PA, HM-PA/K-PA growth factors at day 7. .. 97
Figure 3.7 Viability analysis of the islets seeded on different PA hydrogels with or without growth factor (GF) by using the Alamar blue assay at (A) day 1, (B) day 3 and (C) day 7. 98
Figure 3.8 Results of glucose stimulation test at (A) day 1, (B) day 3, and (C) day 7 99
Figure 3.9 Technique used to implant peptide amphiphile gel into the omentum of rats.. 101
Figure 3.10 Blood glucose levels were measured 5 days before and throughout 28 days after transplantation. 102
Figure 3.11 Change of weight of animals during 28 days. 102

Figure 3.12 Intraperitoneal glucose tolerance test (IPGTT) at the end of 28 days. 103
Figure 3.13 H&E staining of (A) Sham, (B) PA hydrogel, (C) Islet, and (D) Islet + PA hydrogel groups. 105
Figure 3.14 Masson's trichrome staining of (A) Sham, (B) PA hydrogel, (C) Islet, and (D) Islet + PA hydrogel groups. 106
Figure 3.15 Immunohistological staining of (A) Sham, (B) PA hydrogel, (C) Islet, and (D) Islet + PA hydrogel groups using anti-insulin antibody. 107
Figure 3.16 Immunohistochemical staining of macrophages in omenta..... 108
Figure 3.17 Immunohistochemical staining of blood vessels by using anti-von Willebrand Factor in the omenta and quantification of blood vessels..... 109
Figure 4.1 Chemical structure of HM-PA molecule. 126
Figure 4.2 Chemical structure of K-PA molecule. 126
Figure 4.3 Chemical structure of E-PA molecule. 127
Figure 4.4 Purification and characterization of HM-PA. (A) HPLC chromatogram of purified heparin-mimetic PA molecule at 220 nm. (B) Mass spectrometry analysis of heparin-mimetic PA molecule..... 127
Figure 4.5 Purification and characterization of E-PA. (A) HPLC chromatogram of purified E-PA molecule at 220 nm. (B) Mass spectrometry analysis of E-PA molecule. 128
Figure 4.6 Purification and characterization of K-PA. (A) HPLC chromatogram of purified K-PA molecule at 220 nm. (B) Mass spectrometry analysis of K-PA molecule. 129

Figure 4.7 Scanning electron microscopy images of (A) HM-PA/K-PA and (B) E-PA/K-PA reveal the ECM-like morphology of the scaffolds. 130
Figure 4.8 Rheology results showed that HM-PA/K-PA and E-PA/K-PA combinations formed gels and that their mechanical properties were similar. 130
Figure 4.9 Representative images of wounds following hydrogel application 132
Figure 4.10 Wound areas of (A) sucrose, (B) E-PA/K-PA and (C) HM-PA/K-PA treated wounds at days 3, 7, 10 and 14. 132
Figure 4.11 Wound area (%) according to the location of wounds in control, E-PA/K-PA and HM-PA/K-PA treated groups on day 3. 133
Figure 4.12 Wound area (%) according to the location of wounds in control, E-PA/K-PA and HM-PA/K-PA treated groups on day 7. 133
Figure 4.13 Wound area (%) according to the location of wounds in control, E-PA/K-PA and HM-PA/K-PA treated groups on day 10. 134
Figure 4.14 Wound area (%) according to the location of wounds in control, E-PA/K-PA and HM-PA/K-PA treated groups on day 14.. 134
Figure 4.15 (A) H&E and (B) Masson's Trichrome staining (lower panel) of control group at day 7.. 136
Figure 4.16 (A) H&E and (B) Masson's Trichrome staining (lower panel) of E-PA/K-PA application at day 7.. 137
Figure 4.17 (A) H&E and (B) Masson's Trichrome staining (lower panel) of HM-PA/K-PA application at day 7. 138

Figure 4.18 (A) H&E and (B) Masson's Trichrome staining (lower panel) of control group at day 14. 139
Figure 4.19 (A) H&E and (B) Masson's Trichrome staining (lower panel) of E-PA/K-PA application at day 14. 140
Figure 4.20 (A) H&E and (B) Masson's Trichrome staining (lower panel) of HM-PA/K-PA application at day 14. 141
Figure 4.21 Quantitative analysis of granulation tissue of wound tissues at day 7 and 14. 142
Figure 4.22 Quantitative analysis of re-epithelialization of wound tissues at day 7 and 14. 143
Figure 4.23 Quantitative analysis of skin appendages of wound tissues at day 14. 143
Figure 4.24 Staining of blood vessels by anti-von Willebrand Factor (a-c) and quantification of blood vessels at day 7 and 14 (d-e). 144

Abbreviations

AFM	Atomic force microscopy
ANOVA	Analysis of variance
Boc	*Tert*-butoxycarbonyl
BSA	Bovine serum albumin
CD	Circular dichroism
CS	Chondroitin sulfate
DAB	3,3'-diaminobenzidine
DCM	Dichloromethane
DIEA	*N*,*N*-diisopropylethylamine
DMEM	Dulbecco's modified Eagle's medium
DMF	N,N-Dimethylformamide
DMSO	Dimethyl sulfoxide
ECM	Extracellular matrix
EDTA	Ethylenediaminetetraacetic acid
E-PA	Lauryl-VVAGE-OH
ESC	Embryonic stem cells
FBS	Fetal bovine serum
FDA	Food Drug Administration
FGF-2	Fibroblast growth factor-2
Fmoc	9-Fluorenylmethoxycarbonyl
GAG	Glycosaminoglycan
GF	Growth factor
H&E	Hematoxylin and eosin
HBTU	*N,N,N′,N′*-Tetramethyl-O-(1*H*-benzotriazole-1-yl) uronium hexafluorophosphate
HM-PA	Heparin mimetic peptide amphiphile
HPLC	High pressure liquid chromatography
HRP	Horseradish peroxidase
HTK	Human keratocyte
IHC	Immunohistochemistry
IPGTT	Intraperitoneal glucose tolerance test
iPSC	Induced pluripotent stem cell
K-PA	Lauryl-VVAGK- Am
KKRGD-PA	Lauryl-VVAGKKRGD- Am
LC-MS	Liquid chromatography-Mass spectroscopy
P/S	Penicillin/Streptomycin
PA	Peptide amphiphile
PBS	Phosphate buffered saline
PDGF	Platelet-derived growth factor

PEG	Poly ethylene glycol
PLA	Poly lactic acid
PGA	Poly glycolic acid
PLGA	Poly lactic-co-glycolic acid
RT	Room temperature
SEM	Standard error of mean
T1D	Type 1 Diabetes
TBS	Tris buffered saline
TEM	Transmission electron microscopy
TFA	Trifluoroacetic acid
YIGSR-PA	Lauryl-VVAGKYIGSR- Am

CHAPTER 1

INTRODUCTION

1.1 *The Fountain of Regeneration*: An approach in biology and engineering

From ancient times to the Age of Exploration –and perhaps even today– it has been a fundamental desire of Man to find a mystic source of water that cures all sickness and bestows eternal life. Although the Greek historian Heredotus and Alexander the Great were said to have believed in a *Fountain of Youth*, the myth is most closely associated with the 16th century Spanish explorer Juan Ponce de Léon. Urged by King Ferdinand to explore an island called Bimini, he discovered Florida and –according to the myth– the fountain. As legend has it, whoever bathes in the water or drinks from it is granted everlasting life and freedom from all sickness. Of course, no magical panacea is known to modern medicine, and no record confirms that Ponce indeed found the fountain of youth. But perhaps this is about to change.

It is not difficult to understand why people seek a cure for all sickness – including Shakespeare's "hideous winter", aging. Observations of the animal kingdom only raised further questions, as some organisms can apparently recover and re-grow after any injury, while Man may forever be crippled after superficial damage. In the regeneration process, injury is recognized and the original integrity of the damaged tissue is restored by complex mechanisms. However, the regenerative capacities of animals vary greatly between the nine major animal phyla, and may change considerably in even closely related species [1]. Réaumur and Trebmley's landmark experiments on starfish, crayfish and *Hydra* have greatly expanded the scope of research on regeneration, and comparative and descriptive characterization of the

regeneration process has become a topic of major scientific interest. Initial research into this process concerned whether there were differences in the regenerative capacity of various organs and tissues in various organisms, whether aging had any effect on the rate of regeneration, and whether regeneration would occur in a differentiative manner between different species and their tissues [2]. Following these investigations, more specialized questions began to arise: how did internal and external conditions affect this process?; how does the so-called “histogenesis” occur, when tissues are generated? These questions are not fully answered to date, and research into them forms the basis of current approaches in tissue engineering.

Regeneration is broadly seen in nature, but the extent of this process is variable between species and life stages [3]. Although limb regeneration in salamanders is one the best known examples of literature, other urodelan tissues may not exhibit the same capacity for regeneration, despite having an identical genetic composition [4]. We also know that identical injuries may result in complete regeneration or extensive scar formation in related species, between different organs and tissues, or in organisms at different life stages. Perhaps due to these observations, the molecular investigation of the repair process has been increasingly important in the past few decades, and modern biomaterials are commonly designed with molecular functions in mind.

The first signs of reconstruction, however, date back to 7000 BC [5]. Different materials were used in Incan Empire for cranioplasty and the usage of gold plates was reported by Fallopius in 16th century. In 1668, van Meekeren developed a xenograft model for the cranial defect of a man [6]. These

approaches started to spark interest into the use of bio-engineering as a solution for biological problems. Between 1660s and 1980s, many methods or approaches were developed for this purpose and, finally, *tissue engineering* emerged as a major research area in late 1980s. Following the founding of the Tissue Engineering and Regenerative Medicine International Society, the limitations of those methods came under scrutiny.

The primary goal of tissue engineering and regenerative medicine is to transplant biofactors such as cells, specific proteins or small molecules, signals, genes or their combinations within a scaffold. While biofactors initiate the repair process, the porous and degradable architecture of scaffolds (of which dimensions range from 10 to 10000 micrometers) imitates the volume and mechanical properties of lost tissue, and carries the biofactors in its structure [7-8]. It is, however, a major challenge to reform tissues from cells by triggering complex tissue repair processes in a reliable manner. Material costs, batch-to-batch variations, governmental regulations and social and religious views all contribute to the difficulty of designing an ideal scaffold. To date, several biomaterials were approved by the Food Drug Administration (FDA), European Union (EU) or the German government (Figure 1.1) [9]. Although there is considerable progress in biomaterial design, their commercial applications are nonetheless limited and next-generation materials are necessary for tissue engineering and regenerative medicine applications to be commonly utilized in clinical settings. As attempts to entirely replace the damaged organ can only serve as stopgap solutions and do not yield long-term results, it is important to define the problems associated with the repair of

damaged tissues and subsequently engineer biomaterials to enhance the natural repair process of the organism of interest.

Tissue	Product	Regulatory status	Description	Material						Cells		Use	Form
				Synthetic	Resorbable	Animal derived	Plant or bacteria derived	Human derived	Growth factor	Allogenic	Autologous		
Skin	TransCyte, Advanced Biohealing	1997	Nylon mesh coated with porcine collagen, containing non-viable human fibroblasts, with upper layer of silicon	✓	✓	✓				✓		Burns	Sheet
	Apligraf, Organogenesis	1998	Lower layer of human fibroblasts and bovine collagen, upper layer of keratinocytes		✓	✓				✓		Leg ulcers	Sheet
	Dermagraft, Advanced BioHealing	2001	Cryopreserved human fibroblasts on a polyglactin 910 (2-hydroxy-propanoic acid polymer with polymerized hydroxyacetic acid) mesh	✓	✓					✓		Diabetic foot ulcers	Sheet
	ICX-SKN, Intercytex	Phase II	Allogenic fibroblasts and human collagen with additional layer of keratinocytes		✓			✓		✓		Burns and acute wounds	Sheet
	Integra Dermal Regeneration Template, Integra Lifesciences	1996	Porous bovine collagen crosslinked with chondroitin-6-sulphate with upper layer of silicon	✓	✓	✓						Burns	Sheet
	Integra Flowable Wound Matrix, Integra Lifesciences	2007	Granulated bovine collagen crosslinked with chondroitin-6-sulphate		✓	✓						Ulcers	Gel
	Oasis Wound Matrix, Healthpoint	2006[a]	Decellularized porcine small intestinal submucosa		✓	✓						Burns, ulcers, other wounds	Sheet
	PriMatrix, TEI Biosciences	2008	Decellularized fetal bovine skin		✓	✓						Wounds	Sheet
	Xelma, Molnlycke	2005 EU	ECM protein (amelogenins) in propylene glycol alginate carrier		✓	✓	✓					Leg ulcers	Gel
Bone	INFUSE Bone Graft, Medtronic	2002	Bovine type I collagen sponges soaked in rhBMP-2 in LT-CAGE Lumbar Tapered Fusion Device	✓	✓	✓			✓			Spinal fusion	Solid
	OP-1, Stryker	2001	Bovine type I collagen with rhBMP-7		✓	✓			✓			Bone injury	Paste
	PuraMatrix, 3DM	Preclinic	Synthetic 16-amino-acid peptide, forming nanofibres	✓	✓							Dental bone defects	Gel
	Vitoss Scaffold FOAM, Orthovita	2004	Porous foam comprising β-TCP and bovine type I collagen	✓	✓	✓						Bone injury	Foam
	Bioset IC, Pioneer surgical	2008	Human demineralized bone matrix with bovine bone chips in type I collagen carrier		✓	✓		✓				Bone injury	Paste
	FortrOss, Pioneer Surgical	2008	Nanocrystalline hydroxyapatite and E-matrix (porcine collagen co-polymerized with dextran)	✓	✓	✓	✓					Bone injury	Paste
	Regenafil, Regeneration Technologies/Exatech	2005	Human mineralized bone matrix in porcine gelatin carrier		✓	✓		✓				Bone injury	Paste
	GEM 21S, BioMimetic Therapeutics	2005	β-TCP particles and recombinant human platelet-derived growth factor-BB (PDGF-BB)	✓	✓				✓			Dental bone/ gum defects	Paste
	BCT001, Bioceramic Therapeutics	Preclinic	Strontium releasing bioactive glasses	✓	✓							Bone defects	Granules, paste

Figure 1.1 Commercially available tissue engineering products. (Reproduced from Ref. [9] with permission from Nature Publishing Group.).

Cartilage	Synvisc, Genzyme	1997	Hyaluronic acid (Hylan GF-20 and Hylan B) from chicken combs		✓	✓					Synovial fluid replacement	Gel
	CaReS, Arthro Kinetics	2007 Germany	Rat-tail type I collagen matrix seeded with chondrocytes		✓	✓				✓	Articular cartilage injury	3D disc
	Bioseed-C, Biotissue Technologies	Clinic 2001[b]	Polyglycolic/polylactic acid and polydioxane scaffold containing chondrocytes	✓	✓					✓	Articular cartilage injury	3D disc
	Menaflex, Regenbiologics	2008	Bovine type I collagen with hyaluronic acid and glycosaminglycans, hydrated		✓	✓					Meniscus cartilage injury	Mesh
	Hyalograft C autograft, Fidia advanced biopolymers	2008 EU[c]	HYAFF (esterified derivative of hyaluronic acid) scaffold with autologous chondrocytes		✓		✓			✓	Articular cartilage injury	3D disc
	MACI, Genzyme	Unreg EU[d]	Type I collagen membrane seeded with chondrocytes		✓	✓				✓	Articular cartilage injury	Sheet
T/L	GraftJacket, Wright Medical Technology	Unreg[e]	Decellularized human skin		✓			✓			Tendon and ligament repair	Sheet
	X-Repair, Synthasome	FDA review[f]	Poly-L-lactic acid woven mesh	✓	✓						Tendon and ligament repair	Sheet
BV	VascuGel, Pervasis	Phase II	Gelfoam porcine gelatin foam sponges seeded with endothelial cells		✓	✓				✓	Vessel reconstruction	Tubular
	Vascu-guard, Synovis	1994	Decellularized bovine pericardium		✓	✓					Vessel reconstruction	Sheet
HV	Cryovalve SG pulmonary human heart valve, Cryolife	2008	Decellularized human heart valves		✓			✓			Heart valve replacement	Valve
Retina	NT-501, Neurotech	Phase II/III	Genetically modified cells secreting ciliary neurotrophic factor in hollow permeable polyethersulphone fibres	✓						✓	Retinitis Pigmentosa	Tubular
Nerve	NeuraGen, Integra	2001	Semipermeable bovine type I collagen nerve conduits		✓	✓					Nerve injury	Tubular
Pancreas	Islet Sheet, Cerco Medical	Preclinic	250-μm-thick alginate sheet with encapsulated pancreatic islets (pig or human)				✓			✓	Diabetes mellitus	Sheet
	Amcyte/ReNeuron	Phase II	Alginate/poly-L-lysine encapsulated human pancreatic islets	✓			✓			✓	Diabetes mellitus	Bead
	Novocell	Phase I/II	Alginate/polyethylene glycol encapsulated human pancreatic islets	✓			✓			✓	Diabetes mellitus	Bead
Bladder	Neo-bladder, Tengion	Phase II	Poly(lactic-co-glycolic acid) seeded with urothelial and smooth muscle cells	✓	✓					✓	Spina bifida, bladder dysfunction	Sheet
Dura	DurADAPT, Pegasus Biologicals	2005	Decellularized, crosslinked equine pericardium		✓	✓					Reconstruction of dura mater	Sheet
Various	Extracel, Glycosan Biosystems	Preclinic	Crosslinkable bacterial hyaluronic acid, bovine and porcine gelatin, porcine heparin and PEG derivatives	✓	✓	✓	✓		*g*	*g* *g*	Examples: cartilage, bone, vocal fold TE	Gel, sheet, tubular

Figure 1.1 (continued) Commercially available tissue engineering products. Tissue abbreviation: T/L, tendon and ligament; BV, blood vessel; HV, heart valve. Regulatory status: dates indicate year approved by regulatory body (FDA unless stated as EU or Germany). Preclinic indicates preclinic development, phase I and II indicate clinical trial stage. Date of regulatory approval does not necessarily coincide with market release. [a]Reclassified in 2006 from an earlier product. [b]First clinical trials in 200. [c]Commercial sale

began in 2000. [d]Unregulated in EU, not available in the United States. [e]Unregulated product. [f]Decision expected 2009. §Addition of growth factors and cells is dependent of application. (Reproduced from Ref. [9] with permission from Nature Publishing Group.).

1.2 Basic Principles of Tissue Engineering and Regenerative Medicine

Organ transplantation is the ideal means of replacing organs or tissues lost due to trauma or other causes. However, a substantial number of people die annually without being included in waiting lists. Organ transplantations are limited by high costs, the lack of available donors and immune rejection of the organ [10]. Beyond these problems, even successful organ transplants face a series of problems. The field of regenerative medicine and tissue engineering has emerged largely with the intent to eliminate the problems associated with organ transplants, and utilizes the tenets of biology, engineering and materials sciences to maintain and renew damaged tissues and organs [11]. The three-dimensional (3D) composition of tissue microenvironments can be imitated by seeding patient- or donor-derived cells into the porous scaffold. The scaffold can be enriched with growth factors and small molecules according to the specific needs of the tissue of interest and subsequently transplanted into the patient (Figure 1.2) [10].

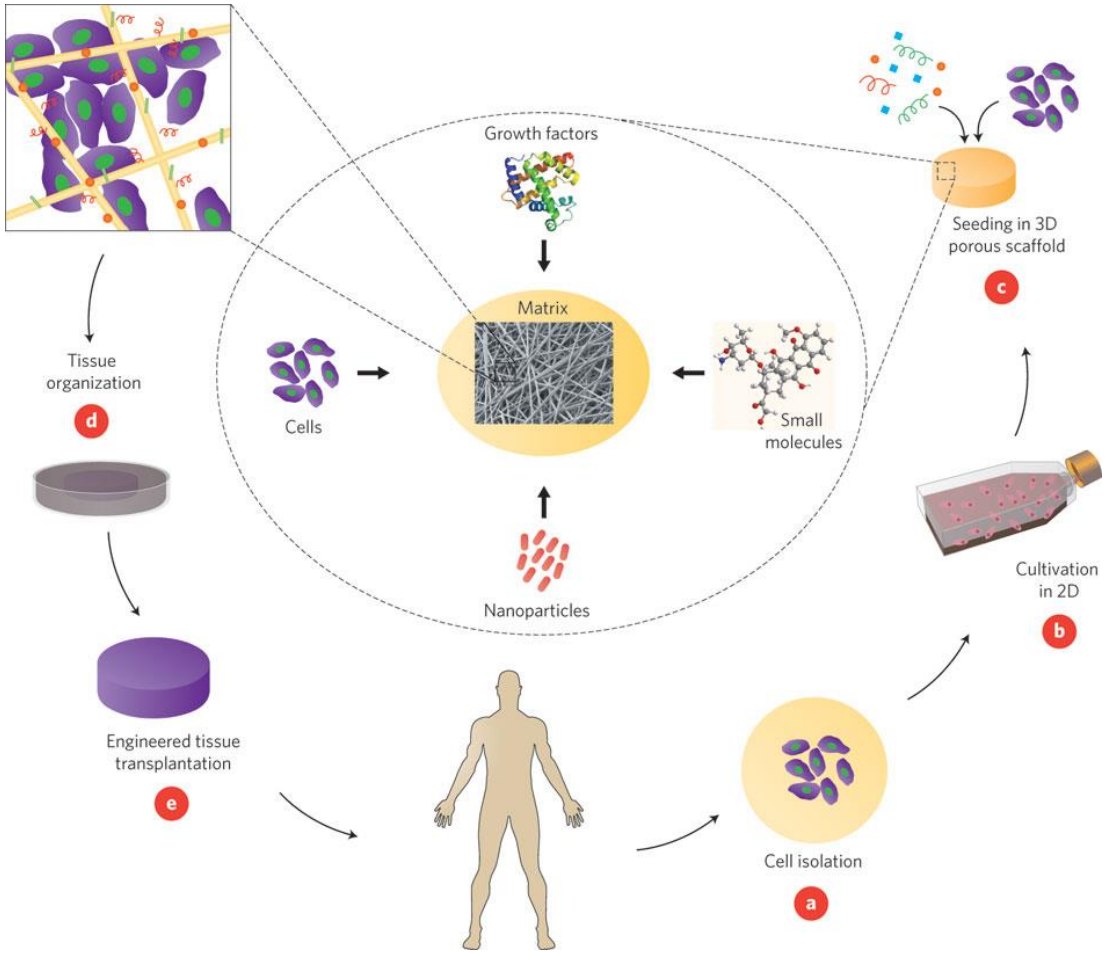

Figure 1.2 Basics of tissue engineering. Cells are initally isolated from the patient or a donor **(A)** and expanded in cell culture **(B)**. Expanded cells are seeded into a porous scaffold, which is decorated with the necessary signals for tissue repair **(C)** and incubated in a bioreactor to provide the optimal growth conditions **(D)**. The constructed tissue is later transplanted to the damaged site **(E)** (Reproduced from Ref. [10] with permission from Nature Publishing Group.).

Tissue engineering and regenerative medicine approaches have been developed to provide cells with a facsimile of their natural microenviroment, which supports them and allows the formation of replacement tissues by

triggering the differentiation process. The main elements of this approach are cells, scaffold and signal molecules; and different combinations of these elements can be altered depending on the needs of the injured or diseased tissue [12].

1.2.1 Cell Types

The choice of cell type is vital to ensure that a sufficient number of cells can be generated to meet the needs of the damaged tissue. Three types of cell sources can be utilized for tissue engineering: Autologous, allogeneic and xenogeneic. Autologous cells are the patient's own cells, which are isolated and subsequently expanded in cell culture for regenerative applications. The use of these cells is typical for tissue engineering, because there is no risk of immunogenity and no need for immunosuppressive treatment. In addition, they can be utilized for the repair many organs, such as the liver, blood vessels, bone, cartilage and skin. However, autologous cells have their own set of limitations. First of all, the tissue of interest should be reachable by biopsy, as the cells must be a derived from the patient [13]. Harvesting cells can also be a problem; *e.g.* if there is myocardial infarction in the patient's medical history, it is not possible to obtain cardiac cells in sufficient numbers. The age of the patient also affects the amount of harvested cells, and even if the harvesting process is successful, contamination in culture environment is another potential risk. In addition to issues with the culture equipment, it is known that sera used for cell culture may lead to viral contamination. Allogeneic (from different individuals of the same species) or xenogeneic (cells from different species) sources are also utilized for tissue repair. However, immunogenicity

is the most common problem in both approaches. In addition, zoonoses can also pose a problem, as Patience *et al.* reported that porcine endogenous retrovirus can transfer from donor to acceptor [14]. Despite these limitations, allogeneic cells have been used as effective wound covers [15] and in the treatment of diabetes [16] and liver disease [17] (Figure 1.1), while feeder cells from xenogeneic sources have been evaluated for the formation of epidermal tissue[18].

Stem cells are another major source for regeneration of tissues. Stem cells have the exclusive capacity to proliferate in an undifferentiated state and differentiate under special conditions (which may be delivered through cell culture media) into various cell types [19]. These cells can be derived from both embryonic and adult tissues. Embryonic stem cells (ESC) have the potential to differentiate into all three germ lines: ectoderm [20], mesoderm [21] and endoderm [22]. However, controlling the fate of these cells is not easy and teratomas can form under *in vivo* conditions [23]. In addition to this, there are some ethical issues about the usage of ESCs, which is still forbidden in many countries – although the United States lifted the ban in 2009. Nevertheless, limitations associated with ESCs can be overcome with the use of induced pluripotent cells (iPSC), which closely resemble their embryonic counterparts but are derived from somatic cells that are transformed through Yamanaka factors [24-27].

Because of the tumorigenic potentials of ESCs and iPSCs, adult stem cells such as hematopoietic (HSC), mesenchymal (MSC) or adipose derived stem cells (ADSC) are generally preferred for regenerative medicine. These

cells are easily accessible, can be obtained in large amounts and pose fewer safety issues compared to ESCs and iPSCs. Somatic cells generally reach their fully differentiated forms soon after birth [28]. However, HSCs have the potential to facilitate tissue regeneration throughout the entire life span. HSCs have a high tendency to maintain myogenesis and cardiomyogenesis [29-31], and can also trigger the formation of liver cells [31]. Unlike HSCs, MSCs are found not only in bone marrow but also in bone [32], skeletal muscle [33], skin [34], pericytes [35], peripheral blood [36] and teeth [37]. They have attracted great attention for tissue engineering approaches because of their capability to differentiate into muscle, blood vessels, bone, tendon, cartilage, skin, nerve and adipocytes [18, 38]. In addition to HSCs and MSCs, ADSCs are popular for tissue engineering. Since adipose tissue is pervasive and easily accessible, they can be obtained in large amounts with less morbidity. The differentiation capacity of ADSCs is high and encompasses chondrogenic [39], myogenic [40], adipogenic [41], osteogenic [42], angiogenic [43] and neuronal lineages [44].

Stem cells are highly promising for the clinical applications of tissue regeneration. However, they still suffer from certain limitations; in particular, their quantity is typically insufficient to facilitate tissue repair. Although stem cells can be expanded in two dimensional cell culture environments, dedifferentiation eventually takes place before the desired number of cells is reached. In addition, the proliferation capacity of stem cells is quite low in 3D cultures. Another problem is the necessity of xenogeneic serum, which provides growth supplements to the cells but can also lead to contamination

[45]. While synthetic sera can be used instead of fetal calf serum, the proliferative capacity of cells decreases under these conditions.

1.2.2 Soluble macromolecules in ECM

Tissue engineering is a complex process that requires acts through several signal cascade events and ultimately culminates in the initiation of the repair process at the tissue of interest. Under natural conditions, repair-associated signals are activated through proteins called growth factors (GFs). GFs may be secreted endogenously to stimulate the cell itself (autocrine signaling) or to communicate with other cells (paracrine signaling). Although the effects of many growth factors are not fully described, stem cell research in particular led to a greater understanding of the remarkable capacity of growth factors to initiate and regulate processes such as development, differentiation and regeneration.

The delivery of growth factors into tissues of interest is a difficult prospect. While soluble GFs may be injected, their systemic dispersion prevents them from reaching the concentrations necessary for initiating local tissue repair. As such, three methods have been developed to selectively deliver GFs to a specific organ or tissue. The first is to use a DNA plasmid that codes for a given GF, allowing its continued in-site production. The second is to transfect the GF-coding gene to a certain cell type, and subsequently inject these cells to localize to the tissue of interest [18]. Lastly, GFs can be delivered without genetic engineering through the assistance of a carrier matrix called a scaffold. This is the most popular method for GF delivery, as it can readily overcome

the short half-lives associated with the injection of soluble GFs. However, the degradation kinetics of the scaffold should also be determined to ensure optimal release of GFs in tissue environments.

Bone morphogenic proteins (BMPs), fibroblast growth factor-2 (FGF-2), transforming growth factor-β (TGF- β) and vascular endothelial growth factor (VEGF) are the most commonly used GFs in tissue engineering. Some of these GFs are already available in commercial tissue engineered products (Figure 1). Recombinant BMP-2, for example, has been embedded into a collagen sponge and used for spinal fusion, tibial shaft fractures and oral-maxillofacial procedures [46]. In addition to ensuring direct delivery, the controlled release of GFs may also enhance their activity: for instance, the extracellular matrix production of vascular smooth muscle cells was found to increase in the presence of TGF-β1 immobilized in polyethylene glycol (PEG) hydrogel compared to the soluble TGF- β1[47].

Carrier systems can be decorated with specific structures to enhance their ability to bind to growth factors. It is known that glycosaminoglycan molecules can bind to and protect growth factors from degradation [48-49]. In addition, some growth factors such as FGF-2 have heparin-binding domains which establish an electrostatic interaction between the GF and the molecule through sulfate and carboxylic acid groups [50-51]. It has been shown that this binding interaction increases GF stability compared to the unbound form [52]. As such, the heparin molecule has been studied extensively for slow release applications.

1.2.3 Scaffolds

As a definition, a scaffold is a temporary platform used for the cultivation of cells and tissues [53]. The efficiency of tissue engineering approaches depends heavily on the ability of the scaffolds to provide cells with conditions closely resembling their native environment. Chemical and physical cues inherent to *in vivo* tissue environments are often mimicked for this purpose, and scaffolds are typically designed to facilitate the recruitment, attachment and proliferation of cells, imitate the mechanical properties of the tissue of interest and allow the exchange of oxygen, nutrients and waste products across the scaffold matrix. In addition, biochemical signals should be presented or retained in the scaffold structure to ensure the optimal growth and differentiation of the resident cell population [54].

As many of these requirements are met by the extracellular matrix (ECM) in the native tissue microenvironment, the investigation of ECM structure and function is a major aspect of tissue engineering.

1.2.3.1 The extracellular matrix and the importance of its interactions with cells

The ECM is the non-cellular part of tissues and contains proteins, proteoglycans, water and minerals. The formation, function, homeostasis and regeneration of tissues are orchestrated by the spatial and temporary organizations of signals arising from the ECM (Figure 1.3). The ECM provides not only a mechanical support to cells but also takes part in determining cellular fates, facilitating the replication, migration, differentiation, apoptosis or

proliferation of cells through molecules such as growth factors and pH adjustments [55-56]. The ECM is a dynamic 3D microenvironment and consists of different combinations of at least 100 types of molecules, which depend on the organ or tissue, age and physiological condition. Fibrillar proteins (collagens and non-collagenous glycoproteins), proteoglycans and glycosaminoglycans are the main components of the ECM, and serve as a reserve for soluble macromolecules such as growth factors, cytokines and chemokines [57].

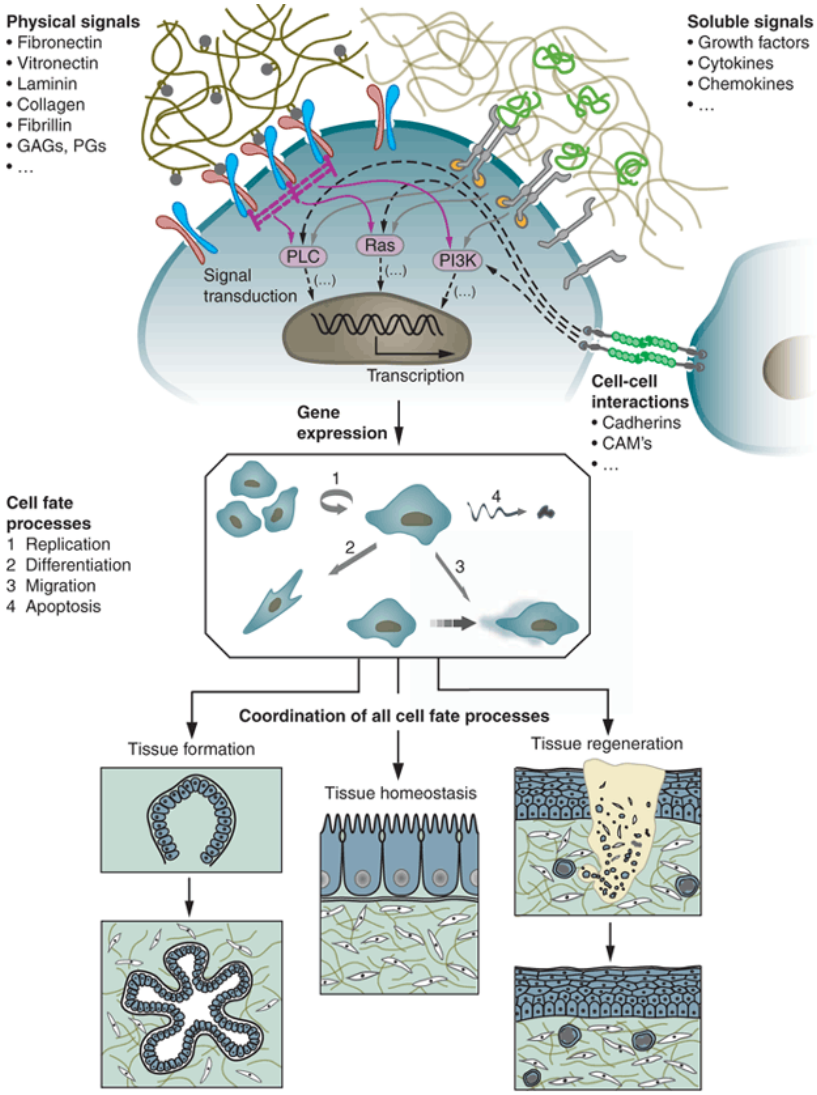

Figure 1.3 Interactions between cells and their surrounding extracellular matrix organize the biological dynamic. Specific binding of physical and soluble signals to cell surface receptors or cell-cell interactions initiate the signaling cascade inside the cells and fate of cells is determined by genetic regulation. PLC, phospholipase C; GAGs, glycosaminoglycans; PGs, proteoglycans; CAMs, cell adhesion molecules (Reproduced from Ref. [57] with permission from Nature Publishing Group.).

Collagen is the most common protein type in the ECM, and exhibits a triple helix (homo or heterotrimer) organization due to its α-chain structure [58]. There are 28 known members of the collagen family, which are derived from different combinations of 48 α-chains [59]. Other proteins may also bear collagen-like domains that allow them to exhibit similar properties [60]. Collagen fibers can form large-scale bundles, which play a major role in providing tensile strength to tissues and exhibit a variety of structures depending on the collagen types involved in network formation. In addition to its mechanical properties, collagen is also responsible for regulating cellular behaviors such as differentiation, adhesion and migration; thereby controlling the tissue development process [61-62]. In addition to collagen, elastin and fibrilin are the other fibrillar proteins in ECM, and largely exhibit similar properties [55].

Fibronectin is another key molecular player in the ECM. It can bind to GAGs, cell surface receptors such as integrins and other ECM proteins, and may also self-assemble by binding to other fibronectin molecules [63]. One of the most important roles of fibronectin is cell adhesion. The 'RGD' sequence found in fibronectin shows a strong affinity for integrins, including α5β1, αvβ3 and αIIbβ3 [64-65]. Recent research also suggests that this sequence is responsible not only for cell attachment, but also for cellular migration during the development and self-renewal of stem cells [66-68].

Laminin is another major protein of the ECM, and consists of epidermal growth factor-like repeats and globular and coiled domains [56]. This molecule commonly occurs in the basal lamina of tissues [69]. The modular domains in

the laminin molecule can interact with cell surface receptors, such as integrins, and other components of ECM, such as entactins, perlecan and collagens [70]. Like fibronectin, a variety of peptide epitopes have been derived from the laminin sequence; including “YIGSR” and “IKVAV”. The YIGSR peptide is associated with cell attachment and migration, metastasis and the inhibition of angiogenesis [71-72]; while IKVAV plays a role in neurite outgrowth, angiogenesis and tumor and cell growth [73-75].

Bornstein identified another class of ECM proteins, which are called matricellular proteins and include the tenascin family, thrombospondins, osteopontin and SPARC/osteonectin. These proteins also interact with cell surface receptors, other proteins and molecules such as cytokines, but are not involved in structural tasks [55, 76].

Proteoglycans are another important class of ECM proteins and typically consist of glycosaminoglycan (GAG) chains that are bound to a core protein [77-78]. Because of their structures, proteoglycans can bind to growth factors and cytokines [79]. They are categorized according to their GAG chains, core proteins and location, as cell-surface proteoglycans, modular proteoglycans and small leucine-rich proteoglycans (SLRPs) [78]. GAGs are long and charged molecules that consist of repeating disaccharide units [D-glucuronic or L-iduronic acid, sulfated N-aceltylglucosamine or N-acetylgalactosamine, and galactose (4 N-acetylglucosamine-β1,3-galactose-β1)]. These molecules can be further classified as sulfated and non-sulfated GAGs. Sulfated GAGs include chondroitin and dermatan sulfate (which are composed of galactosamine and either glucuronic acid or iduronic acid) heparin and

heparan sulfate (which are composed of glucosamine and either glucuronic acid or iduronic acid), and keratin sulfate (which is composed of glucosamine and galactose). Hyaluronan is the only non-sulfated GAG and does not bind to any core protein (Figure 1.4) Because of their hydrophilic structures, GAGs can interact with water molecules and form highly hydrated structures, thereby providing compressive strength to the tissues in which they are abundant [57].

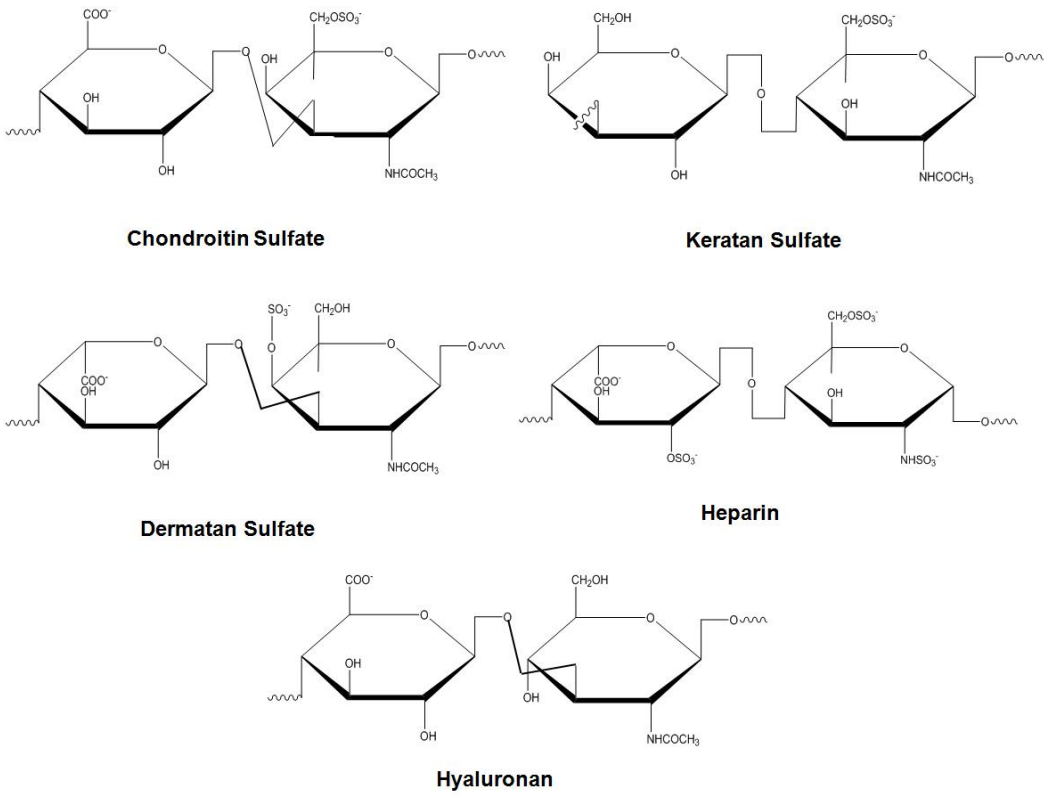

Figure 1.4 Glycosaminoglycans and their structural units.

GAGs are one of the most studied polysaccharides and have substantial roles in various biological processes, including angiogenesis [80], cancer pathogenesis [81], neural development [82], embryogenesis [83] and anticoagulation [84]. These molecules modulate cells and their microenvironments through their interactions with ECM proteins, growth

factors, enzymes and cytokines. In addition, they can direct signaling by allowing the formation of enzyme-substrate and growth factor-receptor complexes.

1.2.3.2 Requirements of scaffolds

Numerous scaffolds have been developed to regenerate different tissues and organs in the literature, using a great variety of materials and fabrication techniques. Even though we do not have clear-cut rules of thumb to define an ideal scaffold, these materials must nevertheless meet certain general criteria to facilitate the regeneration of the tissue or cell of interest.

The decisive criterion for any scaffold for any tissue is biocompatibility. Neither the scaffold itself nor its degradation byproducts should raise any immune or inflammatory response in the body. Immune responses can delay the healing process or affect the acceptance of the scaffold [85]. Moreover, cells should function normally within the scaffold, which should be free of external contaminants and exhibit no toxic or mutagenic activity towards any organ or tissue.

The main aim of tissue engineering and regenerative medicine is to provide support to injured tissue until the recovery is completed. Therefore, the scaffold should be designed such that the regenerating tissue can gradually replace it. Tissue repair and scaffold degradation should be synchronous to ensure that this process occurs smoothly.

The optimization of mechanical properties is another other key element in tissue engineering. During the implantation or application process, the

structure should not be damaged as a result of surgical handling. Scaffolds intended to replace hard and ductile tissues, such as bone, cartilage and cardiovascular muscle, should be particularly resistant to mechanical stress and support the tissue during the healing process. Since the repair of injuries is slower in older patients, the degradation-resorption kinetics of scaffold should also be considered on a patient-dependent basis [86]. Nonetheless, the production of materials with ideal mechanical properties may also indirectly affect other aspects of tissue regeneration, possibly resulting in insufficient vascularization and cell infiltration [87].

The porous architecture of scaffolds is another crucial point. Scaffolds are typically intended to facilitate tissue regeneration at the site of implantation, and the infiltration of the scaffold by surrounding cells is essential for this process. Porous materials allow the exchange of nutrients and gases, which is necessary for the continuity of biological activities. Furthermore, the byproducts of the scaffold (and, if any, its resident cells) should be eliminated without damaging the newly formed tissue [88]. As cells communicate with the ECM through specific chemical groups and are heavily reliant on their microenvironment to establish these connections, pore size is also important for scaffold design. While pores should be large enough to allow cell movements, they should also be small enough for efficient cell binding [89].

Finally, it is important to mention the processes involved in scaffold production. Efforts in regenerative medicine generally aim for the clinical use of the scaffold. As such, the scaffold should be reproducible, cost effective and commercially available. Scaffolds that do not require any extra steps prior to

implantation (such as *in vitro* culture for cell growth) are preferred for this purpose [89].

1.2.3.3 Biomaterials utilized for tissue engineering and regenerative medicine

Providing an optimized milieu to regenerating tissue by using biomaterials is the primary aim of tissue engineering and regenerative medicine applications. The materials that have been chosen for this purpose can be divided into two categories called natural and synthetic. Decellularized biological materials will be discussed in naturally derived biomaterials part. Figure 1 has detailed examples of all materials.

1.2.3.3.1 Naturally derived biomaterials

The first materials used in clinical applications are naturally derived materials [89]. They carry the biological cues and other physical features to provide a better environment for cells to attach, proliferate, migrate and differentiate. Since they are extracted from natural sources such as skeleton and blood plasma, they do not have any toxicity [12]. The degradation is achieved by natural enzymatic system in the host. However, there are several disadvantages of these materials. Their degradation kinetics can be rapid and some chemical modifications such as cross-linking, which can cause toxicity, can be needed [90]. The other problem can be, albeit small, the inflammatory response.

Collagen is the most studied natural molecule for tissue engineering applications. It can be obtained from both animal and human sources.

According to used density, the degradation kinetics and the pore size can be controlled [91]. In addition, its combination with other synthetic materials increases the mechanical properties of collagen [92]. Development of organisms is based on cell-ECM interactions which are the communications between cell surface receptors and specific epitopes on molecules. These interactions can be direct like integrin family and discoidin domain 1 and 2 which bind GFO (Gly-Phe-Hyp) motif [93-94] and indirect like RGD (Arg-Gly-Asp) sequence in fibronectin [95]. In the indirect cell-collagen interaction, proteins containing RGD motif bind to both integrin and collagen. These binding profiles can lead the cellular behaviors like adhesion and proliferation and increase the importance of collagen scaffolds [96]. Collagen scaffolds have been widely investigated in neural system disorders [97], bone [98] and cartilage [99] disorders, cardiovascular system disorders [100], blood vessels [101], skin [102-104], cornea [105-107] and urogenital system regeneration [108].

Hyaluronan (hyaluronic acid or hyaluronate) is a GAG which iscomposed of β-(1,4) or β-(1,3) linked D-glucuronic acid and D-N-acetylglucosamine (Figure 1.4). Due to its water holding capacity, it has great viscoelastic properties. Hyaluronan can be obtained via bacterial production. It is found in wound sites, vitreous chamber of eye and synovial fluid in joints [109]. It has been also reported that hyaluronan has important roles in cell migration, inflammation, fertilization, mitosis and angiogenesis [110]. There are several applications of hyaluronan based scaffolds. It is extensively studied for cartilage repair due to its effect on chondrocyte proliferation and production of

GAGs and type II collagen [111-112]. In addition, it was shown that hyaluronan improves cartilage histogenesis and promote cellular condensation in chondrogenesis [113]. Hyaluronan-polyethylene glycol complex has been investigated for controlled release of BMP-2 and this complex contributed to the bone regeneration [114]. Apart from these applications, it was used for nerve and brain repair [115]; wound healing [116]; and as space filling material in otolaryngology [117] and reconstructive surgery [118].

As a polysaccharide, alginate is the main component of seaweeds, and is composed of β-(1,4) D-mannuronic acid and α-(1,4) Lguluronic acid [119]. This polysaccharide forms ionotropic and elastic gel with divalent cations including calcium and magnesium [120]. $CaCO_3$ and $CaSO_4$ salts affect the mechanical properties of alginate gels [121]. Alginate gels are biocompatible and injectable systems that form at physiological pH and temperature [122]. One of the limitations of the system is its slow degradation kinetics [123]. Alginate gels were used in pancreatic islet delivery [124], cell mobilization [125], wound dressing [126] and cartilage tissue engineering [120].

Chitosan is another biomolecule that has been widely investigated for biomedical applications. It is a soluble derivative of chitin, and has great properties for tissue engineering applications including biocompatibility, biodegradability, non-toxicity, hemostatic potential [127], antimicrobial activity and easy process ability. It can be processed as different forms such as sponges, hydrogels, membranes and fibers [128]. Due to its remarkable features, it has been investigated for bone and cartilage [129] regeneration, wound dressing [130] and nerve conduits [131].

Decellularized materials are prepared by removing all cell and remaining proteins and other biological elements. The source of material can be allogenic or xenogenic. They are also biodegradable and biocompatible materials, however, the cross-linking methods for improving the mechanical properties can evoke immune response [79]. The most common applications of decellularized matrices are in wound healing area [132]. Although studies on decellularized matrices increase the potential use of xenogenic sources in tissue engineering applications, there are still some issues that should be overcome including size differences between human and animal organs and difficulties in complex systems like heart and liver [13].

Except above mentioned materials, fibrinogen [133], fibrin [134], silk[135], agarose [136], dextran [137] *etc* have also been reported for tissue engineering and regenerative medicine applications.

1.2.3.3.2 Synthetic biomaterials

Naturally derived scaffolds have many advantages for supporting cells and creating the natural environment. However, concerns about immunological response due to xenogenic viral infections of natural materials have prompted researchers to develop synthetic materials with no immunogenicity responses, controllable properties and processing flexibility [138]. These materials can be fabricated according to the tissue needs. Their degradation can be controlled by material itself or its composites [139]. As biodegradable polyesters, poly (lactic acid) (PLA), poly (glycolic acid) (PGA), and poly (lactic-co-glycolic acid) (PLGA) have FDA approval in clinical

applications. In addition, their degradation byproducts are not toxic to body [140]. The degradation kinetics can be controlled from weeks to years. These polymers are biocompatible except from PGA. However, CO_2 is the degradation products of PLA and PGA, which decrease the pH of environment and cause necrosis [88]. They are suitable for mass production with long shelf lives and are cheaper than biological polymers [53]. Other polymers which are used in tissue engineering applications include polyurethanes (for vascular valves and grafts, prostheses and catheters [141]); polyanhydrides (for drug-delivery applications [142]); and polyphosphazenes (for soft tissue regeneration [143]).

Despite their mechanical, physical and porous structures, one of the common drawbacks of these materials is lacking of bioactive signals for cell attachment, migration, differentiation and so on. However, they can be conjugated with essential peptide sequences to help cell-integrin recognition [144]. Hydrogel scaffolds made by these materials are biodegradable and have many similarities with ECM. Their applications are less invasive and site specific due to the injectable properties [145].

Hydrogels are hygroscopic materials that can harbor large amounts of water, up to thousands times than their own dry weight. Biocompatibility of hydrogels increases because of their high water content [146]. One of the first examples of polymeric hydrogels is PEG which is a well known polymer as food additive. Forming hydrogel from PEG is done by cross-linking that determine the mechanical properties and degradation kinetic of gel [142]. Photocross-linking approach for making PEG hydrogels has been used for

regenerative approaches including encapsulation of pancreatic islets [147], chondrocytes [148], osteoblasts [149], and mesenchymal stem cells and for delivery of nitric oxide to eliminate thrombosis and restenosis [150].

Unlike cross-linking, self-assembly mechanisms do not use any covalent interactions [151]. Self-assembly is used in biological system for macromolecular assembly without any external forces such as adjusting lipid content of cell membrane or correct folding of proteins [152]. During self-assembly, building blocks come together through non-covalent interactions such as electrostatic interactions, hydrogen bonding, π–π stacking, van der Waals interactions, and hydrophobic-hydrophilic forces [153]. Niece *et al*. described a new method by combining two oppositely charged peptide amphiphile (PA) molecules to form a hydrogel at aqueous and physiological environment [154]. Nanofibrous structure of the mixture is provided by hydrophobic collapse of molecules and intermolecular noncovalent interactions in aqueous solution (Figure 1.5). PA molecules are composed of amino acid sequences which can be degraded by natural enzymatic system in organisms [155]. They can also be designed to bear biological signals to create a system which is suitable for *in vivo* conditions. They have ability to be decorated with biological signals as well as present ligands or carry small molecules or GFs. Self-assembling peptide amphiphiles have been investigated in preclinical applications including cartilage regeneration [156], nerve regeneration [157], cardiac repair [158], bone regeneration [159], drug delivery systems [160] and stem cell differentiation [161] etc.

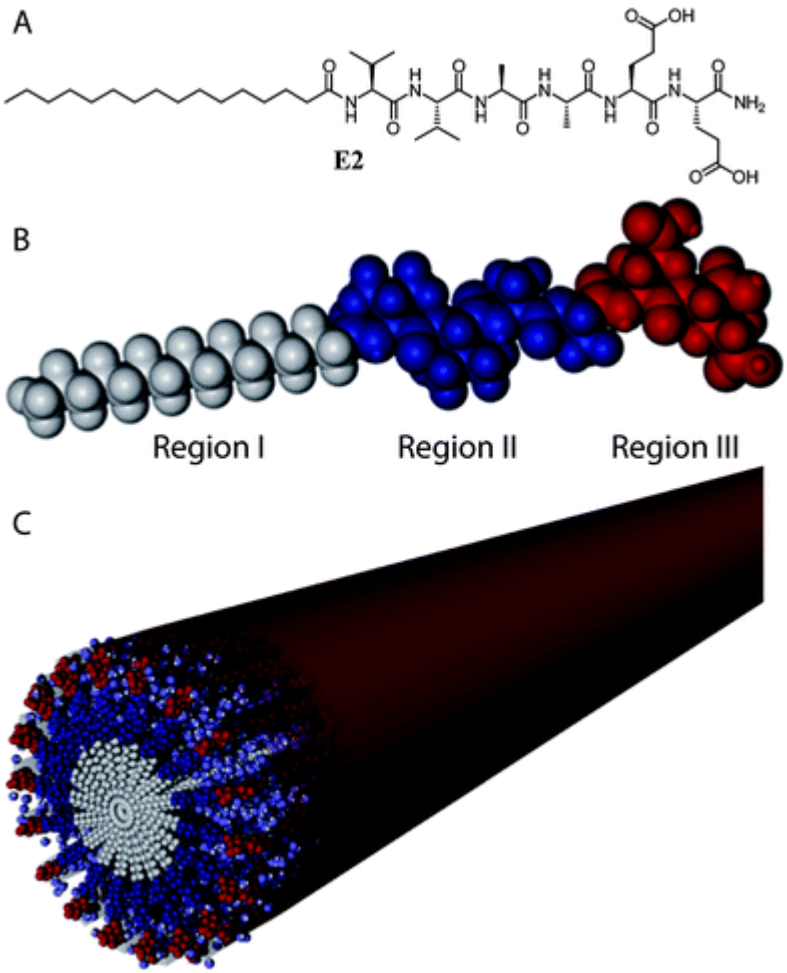

Figure 1.5 Schematic representations of peptide amphiphile molecules and nanofibers. **(A)** Chemical structure, **(B)** different regions of structure, **(C)** nanofibrous structure of peptide amphiphiles (Reproduced from Ref. [162] with permission from Royal Society of Chemistry).

Self-assembled peptide gels are extensively studied in tissue engineering and regenerative medicine applications. Their porous and nanofibrous structures mimic the natural environment of ECM. In addition, decoration of these molecules with important biological signals can lead the regenerating tissues.

In this thesis, three different studies about applications of bioactive peptide amphiphile hydrogels on corneal stroma regeneration (Chapter 2), pancreatic islet culture and transplantation (Chapter 3) and wound healing (Chapter 4).

CHAPTER 2

BIOACTIVE SELF-ASSEMBLED PEPTIDE NANOFIBERS FOR CORNEAL STROMA REGENERATION

Part of this chapter of thesis is published in the following article [163] ;

Reprinted from Bioactive self-assembled peptide nanofibers for corneal stroma regeneration; Uzunalli, G., Soran, Z., Erkal, T.S., Dinc, E., Hondur, A. M., Guler, M.O., and Tekinay, Acta Biomaterialia, 10 (2014),1156–1166, with permission from Elsevier

2.1 INTRODUCTION

The cornea acts as a barrier to protect the eye from external effects and has a major role in the refractive nature of the eye [164]. It is a dome-shaped, transparent, avascular and immune privileged tissue. Packed and well-ordered collagen fibrils provide its transparency. In addition, the fibril density and diameter are arranged by the interactions between keratan sulfate proteoglycans and collagen [165]. Cornea contains five major layers: the epithelium layer; Bowman's layer; the stroma; Descment's membrane and endothelium layer [166]. Epithelial layer of the cornea protects the inner layers from the external effects and provides gas exchange and nutrient supply to the cornea. Bowman's layer, which is an acellular zone, places beneath the epithelium. Bowman's layer and stroma are responsible for tensile strength of cornea due to their collagen content [167]. Descemet's membrane has a potential to extend, and because of its low stiffness, it protects endothelial layer from physical pressure [168]. Innermost layer of cornea is endothelium which regulates fluid balance inside the cornea, preserving the transparency of the tissue. The destruction of this layer causes corneal edema and blindness.

The structure and thickness of these layers are crucial for the cornea's transparency. Corneal opacification due to inflammation, trauma or corneal dystrophies such as keratoconus or keratoglobus results in vision loss affecting ten million people worldwide annually, who are generally treated by cornea transplantation [169-170]. Even though the need for cornea donation increases each year, the number of suitable donors decreases owing to

widespread use of laser vision corrective surgery, which makes the cornea unusable for transplantation.

The stroma is the thickest and transparent part of the cornea. It plays an important role as a refractive layer and transmits the light to the retina. It is formed by quiescent corneal fibroblasts, keratocytes, which are sandwiched between collagen lamellae [171]. Uniform spacing between collagen fibers and their parallel organization are thought to have roles in corneal transparency. There are 200-250 lammellas of collagen bundles which primarily consist of collagen type I and lesser amount of collagen type V and VI in the stroma [172-173]. Apart from collagenous fibers, stroma hosts some extrafibrillar materials called proteoglycans including chondroitin sulfate/dermatan sulfate and keratin sulfate. Decorin is one of the chondroitin sulfate/dermatan sulfate proteoglycans which binds to type VI collagen [174]. Lumican, keratocan and mimecan are the other water-retentive proteoglycans in stroma which create a sulfated environment for hydration.

Damage to the ultrastructural organization of the corneal stroma can lead to irreversible loss of transparency. Stroma thinning, which is observed in keratoconus, also prevents the cornea from proper functioning. To address problems associated with corneal stroma, many different corneal substitutes, such as keratoprosthesis [175] or tissue engineered corneal equivalents [176], have been constructed. Keratoprosthesis has been employed for more than a century, but even the most promising commercial keratoprostheses [175, 177] were reported to cause progressive stroma melting and epithelial defects [178]. Stromal healing consists of collagen and proteoglycan synthesis and

gradually regaining of tensile strength. Immediately after injury, quiescent keratocytes lose their interconnections to activate and proliferate [179]. Although these activated cells participate in the healing process and secrete some fetal antigens to reduce the scar formation, healing tissue mostly consists of type III collagen, poorly sulfated keratan sulfate and laminin, which are associated with scar tissue [180]. In addition, the tensile strength cannot be regained even after 4 years [181].

Various biomaterials have been suggested for use in tissue engineered corneal equivalents, including collagen [182-183], fibrin-agarose [184] and decellularized cornea [185]. Because of its high optical clarity, it is important to design a scaffold that preserves the transparency of the cornea. Moreover, this scaffold should possess high biocompatibility ad non-immunogenicity [186].

Peptide amphiphile (PA) molecules self-assemble into nanofibers through intermolecular forces [187]. The self-assembly mechanism is based on hydrophobic interactions of alkyl tails, intermolecular hydrogen bonding and electrostatic interactions between the charged groups. At physiological pH, electrostatic interactions between oppositely charged molecules promote self-assembly without any external trigger [154]. Therefore, oppositely charged peptide molecules are mixed to form nanofibers at the physiological pH. The interactions between these nanofibers make up a three-dimensional (3-D) network, which encapsulates water and results in a hydrogel structure. Since the peptide segment of the PA molecules can be designed to provide biological signals, PA nanofiber networks are promising biomaterials for achieving controlled cell–material interactions. Because of their versatile physical,

chemical and biological features, they have been used as synthetic extracellular matrix (ECM) mimicking agents for cartilage [188], bone [189] and neural regeneration [190] and angiogenesis [191]. Various sets of peptide epitopes, which are found in ECM proteins such as laminin, collagen and fibronectin, are known to play crucial roles in the maintenance of cell survival and function. For example, the YIGSR sequence derived from laminin β-chain regulates cell adhesion through binding to laminin binding protein [192-194]. As an alternative to YIGSR, the RGD sequence derived from fibronectin can also be used for attachment of the cells to the ECM. Previously, RGD-containing peptides were observed to act as cell adhesive agents when they were immobilized on the surface [195]. These characteristic sequences regulate biological activities through activating and/or inhibiting protein targets with high specificity [196]. Owing to the short lengths of these peptide sequences, they are more stable and easier to manipulate, and show fewer conformational changes compared to whole proteins [197]. Therefore, it is convenient to use such sequences in pharmaceutical and clinical applications.

Versatile functional groups, the easy implementation capability and the self-assembly property of PA networks make them promising biomaterials for corneal tissue engineering. In this study, PA molecules carrying bioactive peptide sequences, YIGSR and RGD derived from laminin and fibronectin, were used to induce corneal regeneration. Healing of corneal wounds depends on the balance between cellular proliferation, differentiation, apoptosis and motility in the damaged area. Materials that can regulate these behaviors

simultaneously can mimic the native environment of cells and play vital roles in the maintenance of normal corneal function [198].

2.1 MATERIALS & METHODS

2.1.1 Materials

9-fluorenylmethoxycarbonyl (Fmoc) and other protected amino acids, lauric acid, [4-[a-(20,40-dimethoxyphenyl) Fmoc-amino methyl] phenoxy] acetomidonorleucyl-MBHA resin (Rink amide MBHA resin), 2-(1H-Benzotriazol-1-yl)-1,1,3,3-tetramethyluronium hexafluorophosphate (HBTU) and diisopropylethylamine were purchased from Merck and ABCR. The 100–200 mesh Wang resin was purchased from NovaBiochem, and valine was loaded on it for producing Fmoc-Val-Wang resin. All other chemicals and materials used in this study were analytical grade and obtained from Invitrogen, Fisher, Merck, Alfa Aesar and Sigma–Aldrich.

2.2.2 Synthesis and Purification of PA Molecules

All four PA molecules were synthesized using solid phase peptide synthesis method. The sequences of molecules are as follows: YIGSR-PA (Lauryl-VVAGKYIGSR-Am), KKRGD-PA (Lauryl-VVAGKKRGD-Am), K-PA (Lauryl-VVAGK-Am), E-PA (Lauryl-VVAGE-OH). YIGSR-PA, KKRGD-PA and K-PA were synthesized on Rink amide resin, while E-PA was synthesized on Fmoc-Glu-Wang resins. Peptide synthesis was achieved using 50 mL vessel on a wrist action shaker on a 1 mmole scale. To complete amino acid coupling, Fmoc group removal was done in the mixture of 20% piperidine and N,N-dimethylformamide (DMF) for 20 min. Resin was washed with DMF,

dichloromethane (DCM) and DMF three times after each reaction. Amino acid activation was performed with 2 molar equivalents of amino acid to 1.95 equivalents of O-Benzotriazole-N,N,N',N'-tetramethyl-uronium-hexafluoro-phosphate (HBTU) dissolved in DMF. Then, molar equivalents of N-ethyl-diisopropylamine were added to the amino acid solution and mixed thoroughly. The solution was added to the resin and shaken 2h for performing the coupling reaction. To monitor each coupling reaction, Kaiser Test was applied. This detects primary and secondary amines of molecule. If the yield is colorless, it shows that the amino acids attached to the chain and there is no deprotected nitrogen. Otherwise, blue color is observed and coupling is repeated. After test yielded negative result, 10% acetic anhydride in DMF solution was added and shaken for 30 min to block the remaining free amine groups. Alkylation of peptides was performed by coupling lauric acid to the chain. Cleavage of peptide molecules from the resin was achieved within trifluoroacetic acid (TFA):triisopropylsilane:water (95:2.5:2.5) for 2 hs at RT. Following the collection of PA molecules in round bottom flask, solution was rotary evaporated. Then, remaining peptide solution was incubated with ice-cold diethyl ether at -20 °C overnight. The following day, mixture was collected in tubes and centrifuged at 6000 rpm for 20 min. Supernatant was discarded and remaining diethyl ether was evaporated in a fume hood. Dissolving of pellet was peformed in deionized water at a resistance of 18.2 Ω and was lyophilized.

Characterization of synthesized PA was done using Agilent 6530 quadrupole time-of-flight mass spectrometry with an electrospray ionization source equipped with reverse-phase analytical high-performance liquid

chromatography (HPLC) with an Agilent Zorbax Extend-C18 2.1 X 50 mm column for basic conditions or a Zorbax SB-C8 4.6 X 100 mm column for acidic conditions. A gradient of 0.1% formic acid/water for acidic conditions or 0.1% ammonium hydroxide/acetonitrile for basic conditions were used as mobile phase for analytical HPLC. An Agilent preparative reverse-phase HPLC system equipped with a Zorbax Extend-C18 21.2 X 150 mm column for basic conditions and a Zorbax SB-C8 21.2 X 150 mm column for acidic conditions were used for the purification of PA molecules. The residual TFA in PA samples was removed by HCl treatment by dissolving in 0.01 M HCl solution and freeze drying. An Agilent preparative reverse-phase HPLC system equipped with Zorbax Extend-C18 21.2 X 150 mm column was used for purifying E-PA molecule.

2.2.3 Physical and Chemical Characterization of PA Molecules

YIGSR-PA, KKRGD-PA and K-PA were positively charged molecules while E-PA was negatively charged. Because the PA nanofiber systems form gel when mixed with oppositely charged molecules, E-PA was used as a gelator for physical and chemical characterizations *in vitro*. Electrostatic interactions of PA molecules formed a nanofibrous system. Because the natural environment of cornea tissue is highly negative due to the presence of negatively charged molecules such as chondroitin sulfate (CS) and keratin sulfate, PA solutions were injected into the corneal pocket. For characterizing the peptide nanofiber systems used for *in vivo* studies, CS was used as an inducer. In *in vivo* experiments, PA molecules were dissolved in 0.25 M sucrose solution instead of water.

2.2.3.1. Atomic Force Microscopy

Nanofibers were formed by mixing 0.05 wt % positvely-charged PA molecules and negatively-charged E-PA at pH 7.4 at 2:1 volume ratio for *in vitro* characterization, while 0.05 wt % YIGSR-PA and KKRGD-PA were mixed with 0.1% CS at a 7:1 volume ratio for *in vivo* on silicon wafers. Samples were air dried for 30 min at RT. All PA molecules were dissolved in ddH_2O because the cantilever mobility was affected by sucrose solution. Images were taken by using MFP-30 Asylum Research atomic force microscopy (AFM) in tapping mode, using a cantilever with stiffness of k = 40 N m^{-1} and resonance frequency of f = 250–350 kHz.

2.2.3.2 Transmission Electron Microscopy

Transmission electron microscopy (TEM) samples were prepared on a Lacey carbon-coated 300-mesh copper grid, and 10 µL of the solutions were dropped on a grid and incubated for 3 min before staining. The excess amount was removed by tissue paper, and 2 wt % uranyl acetate solution was used for staining the organic nanostructures. The samples were imaged by FEI Tecnai G2 F30.

2.2.3.3 Circular Dichroism

Circular dichroism (CD) spectra of the PA solutions were obtained on a J-815 Jasco CD spectrophotometer in the far UV region using quartz cuvettes with a 1 mm path length. The CD spectra of YIGSR-PA/E-PA, KKRGD-PA/E-PA, K-PA/E-PA, YIGSR-PA/CS and KKRGD-PA/CS were acquired. For preparation of YIGSR-PA/E-PA, KKRGD-PA/E-PA and K-PA/E-PA samples,

PA molecules were dissolved in deionized water at a concentration of 0.01 wt % and mixed at a 2:1 ratio. For preparation of YIGSR-PA/CS and KKRGDPA/CS samples, PA molecules were dissolved in 0.25 M sucrose solution at a concentration of 0.01 wt %, CS was dissolved in deionized water at a concentration of 0.02 wt %, and they were mixed at a ratio of 7:1. The pH value of each solution was adjusted to 7.4 with 1 M NaOH before characterization. An average of three scans of each sample was used. CD spectra were obtained from 190 nm to 300 nm, using a digital integration time of 1 s, a band width of 1 nm and a data pitch of 0.1 nm.

2.2.3.4 Scanning Electron Microscopy

The nanofiber network formation of PA molecules was investigated by scanning electron microscopy imaging performed with a FEI Quanta 200 FEG under high vacuum. For preparation of YIGSR-PA/E-PA, KKRGD-PA/E-PA and K-PA/E-PA samples, 1 wt % PA solutions were mixed at a ratio of 2:1. For YIGSR-PA/CS and KKRGD-PA/CS samples, PA solutions and CS solution were mixed at a volume ratio of 9:1. Gels were incubated for 20 min for maturation, and dehydrated gradually with increasing concentrations of ethanol. Samples were dried in a critical-point dryer (Tousimis, Autosamdri-815B) and coated with 6 nm of Au/Pd.

2.2.4 Cell Culture & Maintenance

Human corneal keratocyte (HTK) cell line was used for the *in vitro* experiments, were previously developed by Jester et al. [199]. The cell culture conditions were determined as 10% fetal bovine serum (FBS) and 1%

penicillin/streptomycin (p/s)-supplemented Dulbecco's Modified Eagle Medium (DMEM) and cells were cultured in 75 cm^2 polystyrene flasks [208]. Cells were used when they reached ~80% confluency for both experiments and passaging.

2.2.4.1 Analysis of *In Vitro* Effects of PA Molecules

Bioactivity and biocompatibility of PA molecules were assessed in three experimental groups: K-PA/E-PA combination as a control group, YIGSR-PA/E-PA and KKRGD-PA/E-PA as a bioactive nanofiber network. Since collagen is the native extracellular component of cornea, collagen coated surface was used as a positive control. For all *in vitro* experiments, surface-coating was performed by mixing positively charged (YIGSR-PA or KKRGD-PA or K-PA) and negatively charged E-PA molecules. According to their molecular weight, 0.2 wt % YIGSR-PA/E-PA, KKRGD-PA/E-PA and K-PA/E-PA were mixed at 1.85:1, 1.7:1 and 2:1 volume ratios, respectively. For collagen coating, 0.01 wt % collagen solution was used. For proper coating procedure, 100 µL of total PA solution was added in 96-well plates while 40 µL of collagen solution was added. Following the coating, plates were incubated at 37 °C for 30 min and air-dried in a sterile laminar flow hood overnight. Before cell seeding, plates were sterilized with ultraviolet light for 30 min. For 96-well plates, 3 x 10^3 HTK were seeded into each well.

Alamar blue assay was performed for evaluation of viability and proliferation. 3 x 10^3 cells were seeded in 96-well plates and cultured for viability and proliferation for 24 h and 72 h, respectively. After 24 or 72 h,

alamar blue was added into wells and incubated for 4 h. Fluorescence excitation of 540–570 nm and emission of 580–610 nm were measured.

2.2.4.2 Spreading

HTK cell spreading profiles were investigated by nuclei and actin filament staining with TRITC-conjugated phalloidin and TO-PRO®-3 iodide, respectively. In addition, a specific keratocyte marker, vimentin, staining was performed with anti-vimentin antibody. For this purspose, YIGSR-PA/E-PA, KKRGD-PA/E-PA, K-PA/E-PA or collagen coated on 15-mm glass cover slips were placed in 24 well plates. 2 x 10^4 HTK were seeded in each well, and were incubated for at 37 °C with 5% CO_2. At the end of the 24 h, 4% paraformaldehyde was applied for 15 min as a cell fixative and washed three times with phosphate buffered saline (PBS). Permeabilization of cells was performed via 0.1% Triton X-100 treatment in PBS with 1% bovine serum albumin (BSA). Then, cells were incubated for 2 h in blocking solution. Anti-vimentin antibody staining was performed (1:200) overnight at 4 °C following the blocking step. Alexafluor-488 conjugated secondary antibody was diluted in PBS (1:500) and applied to samples for 1h at RT. Samples were washed with 300 µL PBS three times. Phalloidin binds to F-actin in cells. Here, we used Tetramethylrhodamine (TRITC) conjugated phalloidin (1:500) and a monomeric cyanine TO-PRO®-3 iodide (1:1000) to stain F-actins and nuclei, respectively. They were incubated with cells for 20 min each at RT. At the end of the each incubation, cells were washed with PBS three times. Then, 15 mm cover glasses were taken out from the wells and were mounted on glass slides via ProLong anti-fade mounting media. Samples were left to dry overnight in

dark. The imaging of samples was performed with Zeiss LSM 510 confocal microscope. Since excitation/emission ranges of Alexa flour 488 (495/519), TRITC (557 nm/576 nm) and TO-PRO®-3 iodide (642/661) were different from each other; we were able to image the three dyes by changing the filter system in confocal microscope.

In order to understand the cell behaviors on nanofiber system in more detail; electron microscopy images were taken to evaluate the cell-nanofiber interactions. For this purpose, the coating procedure was followed as mentioned above. 2.5% gluteraldehyde and, 1 wt % OsO_4 were used as fixatives. Water content of samples was removed by increasing concentrations of ethyl alcohol (20%, 40%, 60%, 80% and 100% respectively). Samples placed in 100% ethanol were dried via a Tourismis Autosamdri®-815B critical-point dryer. Before imaging under high vacuum mode with SEM with a FEI Quanta 200 FEG instrument equipped with an ETD detector, samples were coated with 4 nm Au/Pd.

2.2.5 *In Vivo* Experiments

5 adult New Zealand white rabbits were used for corneal damage model. The weights of animals were between 2.5 and 3.0 kg. Rabbits were given ad libitum access to food or water in a 12 h–12 h light–dark cycle. All animal studies were approved by Mersin University Animal Studies Ethical Committee, and all experiments were conducted in accordance with the Animal Care and Use Committee and the ARVO statement for the Use of Animals in Ophthalmic and Vision Research.

2.2.5.1 Surgical Procedure

Before corneal damage model, PA molecules that were going to be injected were prepared at 1 wt % final concentration. For *in vivo* studies, only YIGSR-PA and KKRGD-PA molecules were used. Because cornea is a highly negatively charged tissue due to the keratin sulfates and dermatan sulfates, negatively charged PA molecules were not used. To not affect the osmotic balance of the tissue, 0.25 M sucrose solution was used to dissolve PA molecules. PA solutions were sterilized under UV for 2 h before use. 50 mg kg^{-1} ketamine hydrochloride and 5 mg kg^{-1} xylazine were used as anesthetic agents. After intramuscular injection of these agents, muscle tone and response to pinching fingers were monitored. Then, 7-8 mm diameter corneal stromal pockets were created using a fine corneal spatula by lamellar dissection. After PA solutions were injected, the entrance of the corneal stromal pocket was sutured. The group that is referred as ‘‘corneal pocket without injection’’ is the negative control where the corneal pocket was made and 0.25 M sucrose solution was injected. 0.1 mL dexamethasone/netilmicin was injected to subconjunctiva at the end of the surgery. To prevent the any infection in the first week of surgery, dexamethasone/netilmicin (0.1%/0.3%) eye drops were applied 4 times a day. During the experiment, eyes of rabbits were examined clinically for corneal clarity and for any sign of inflammation or infection. Corneas were surgically removed at weeks 3 and 7. YIGSR-PA was injected to 4 rabbits for each time point; KKRGD-PA was injected to 3 rabbits for week 3 group and 4 rabbits for week 7 group. In addition, for negative control 3 and 2 rabbits were used for week 3 and 7 groups, respectively. As a

positive control, native corneas were used. All rabbits were sacrificed with an intravenous injection of 100 mg kg^{-1} sodium pentobarbital. Cornea thickness was measured before and after injection, and before the cornea excision process via a pachymeter.

2.2.5.2 Immunohistochemistry

After removal of corneas, they were fixed in 4% paraformaldehyde for 36h. Tissues, dehydrated with 70%, 80%, 95% and 100% ethanol series for each 1h. Samples were incubated in last 100% ethanol overnight, and the next day they were treated with xylene for 3h. Tissues were placed in melted paraffin for 3h for paraffin infiltration, and then embedded in paraffin. Sectioning was performed with a Leica microtome and 5 µm thickness was determined as proper for further staining procedures. Samples were collected onto positively charged slides.

Hematoxylin and eosin (H&E), which is a commonly used histological method, was performed to understand the tissue morphology. Before staining, slides were incubated at 58 °C for an hour for melting paraffin. Remaining paraffin was removed in xylene and samples were rehydrated in 100%, 95% and 70% ethanol and water, respectively. Following hematoxylin staining, eosin staining was performed. Remaining water was removed in 95% and 100% ethanol, and samples were placed in xylene again before mounting. A xylene based mounting medium was used to cover the stained tissues.

Immunohistochemistry staining was carried out with anti-collagen I and anti-vimentin antibodies. Slides were incubated at 58 °C for an hour for melting

paraffin. Deparaffinization and rehydrated steps were similar with H&E staining with different incubation times. Following these steps, to increase the antibody binding, enzymatic antigen retrieval was performed using pepsin. Samples were incubated at 37 °C for 10 min. In order to provide enough permeabilization, 0.025% Triton X-100 in Tris-base saline (TBS) was applied to the samples twice 5 min each. Blocking step was performed to prevent any other specific binding except from antibodies. Therefore, samples were incubated with 10% normal serum with 1% BSA in TBS for 2h at RT in a humidified chamber. For antibody dilution, 1% BSA in TBS was used and dilutions were determined for collagen I at a ratio of 1:600; for vimentin at a ratio of1:200. Following the overnight incubation at 4 °C, samples were washed with 0.025% Triton X-100 in TBS for 5 min twice. Alexafluor-488 conjugated or Cy2-conjugated secondary antibodies were diluted at ratios 1:600 and 1:300. Secondary antibody incubation was carried out for an hour at RT and samples were mounted onto glass slides using Prolong anti-fade mounting media.

2.2.6 Statistical analyses

Statistical analyses were performed using GraphPad Prism 5. To determine the statistical difference for both viability and proliferation assays, one-way ANOVA and Bonferroni's multiple comparison post-tests were employed. Error bars indicate standard error of mean (SEM).

2.3. RESULTS AND DISCUSSION

2.3.1 Synthesis of PA molecules

Two different bioactive PA molecules were designed and synthesized and used in *in vitro* and *in vivo* experiments (Figure 2.1 A-B). YIGSR-PA molecule, which is inspired from laminin, was designed to enhance cell adhesion and proliferation. Boateng et al. [192] previously demonstrated that YIGSR affects cell adhesion on neonatal myocytes and provides resistance to mechanical strain in cultured cells. In another study, YIGSR epitope was observed to promote adhesion and proliferation of human skin fibroblasts [198]. Fibronectin, which is an ECM glycoprotein, is involved in cell attachment like laminin. Since RGD, which is found in the fibronectin sequence, was reported to be important for recognition by integrins [199]. KKRGD-PA was used to mimic the cell adhesive function of fibronectin. K-PA (Figure 2.1 C) was used as a control nanofiber matrix without YIGSR or RGD epitopes, to test the bioactivity of the PA, and collagen was used as a positive control.

Three-dimensional networks composed of peptide nanofibers were obtained through inducing self-assembly via mixing two oppositely charged PA molecules. The PA molecules self-assemble via electrostatic interactions and hydrophobic collapse at physiological pH, and encapsulation of water in 3-D networks of nanofibers results in gelation [154]. E-PA is a non-bioactive and negatively charged molecule (Figure 2.1 D), which was used for neutralization of positively charged YIGSR-PA, KKRGD-PA and K-PA molecules. All peptide molecules were characterized by liquid chromatography–mass spectrometry (LC–MS) and purified by preparative HPLC (Figure 2.2, 2.3, 2.4, 2.5)

In vitro studies were carried out with positively charged PA molecules gelled with negatively charged E-PA addition. For analysis of the nanofibers that were formed in *in vivo* studies, nanofibers were formed by mixing CS with YIGSR-PA and KKRGD-PA, since the adult human corneal stroma, similar to rabbit, contains 65 wt % keratan sulfate and 30 wt % chondroitin/dermatan sulfate (CS/DS) [200]. Because these glycosaminoglycans (GAG) are highly negatively charged molecules, positively charged PA molecules formed gels upon injection into cornea.

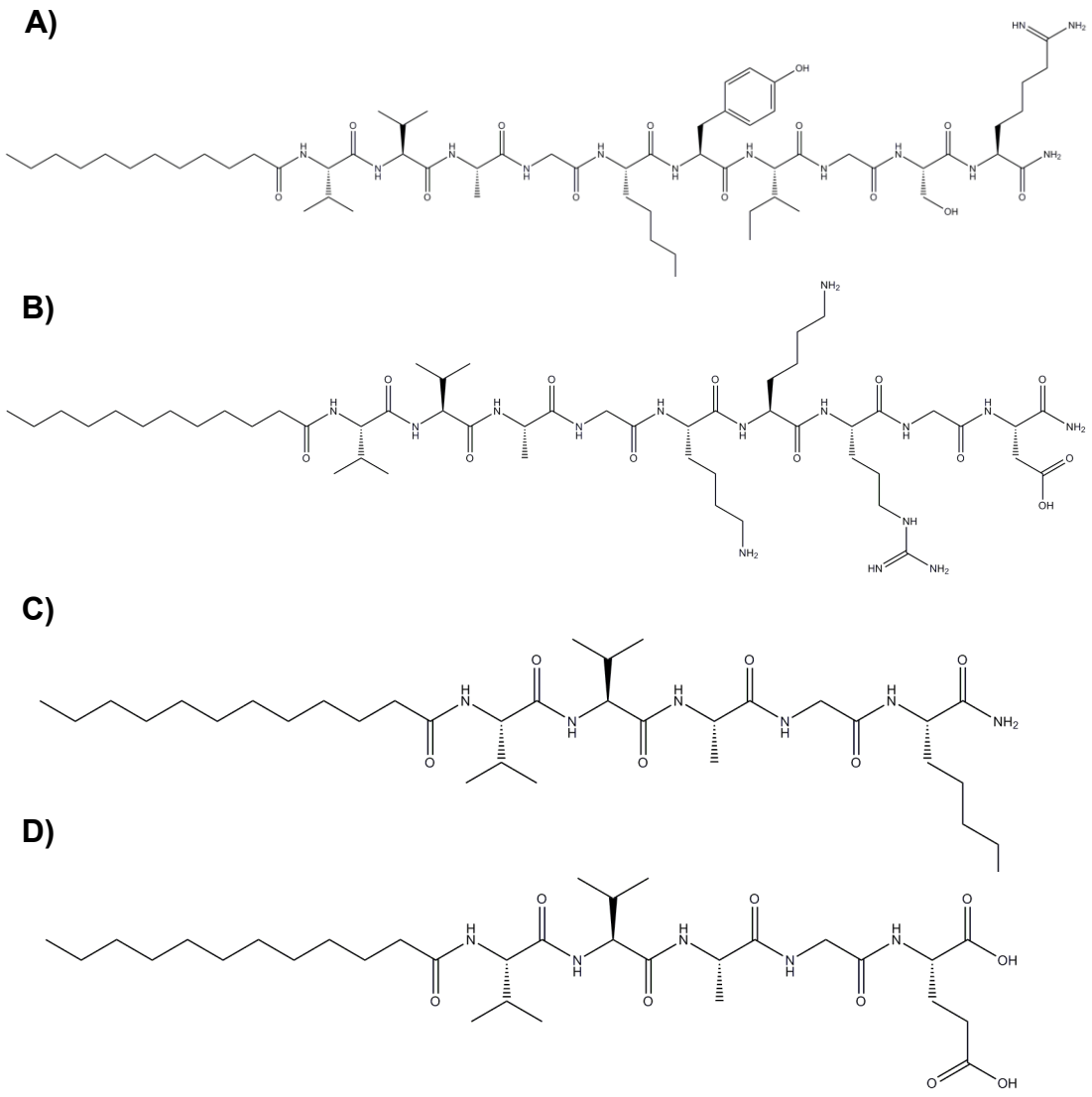

Figure 2.1 Chemical structures of PA nanofibers. **(A)** YIGSR-PA, **(B)** KKRGD-PA, **(C)** K-PA, **(D)** E-PA

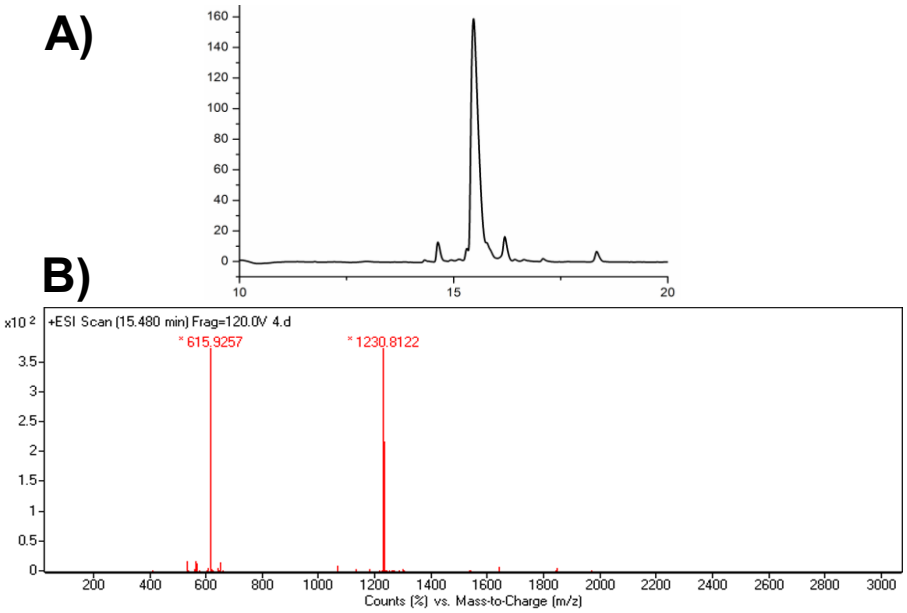

Figure 2.2 (A) HPLC chromatogram of purified YIGSR-PA molecule at 220 nm. **(B)** Mass spectrometry analysis of YIGSR-PA molecule. $[M+H]^+$ (observed)= 1230.81, $[M+H]^+$ (calculated)= 1230.79, $[M+2H]^{2+}$ /2 (observed)= 615.92, $[M+2H]^{2+}$/2 (calculated)= 615.89.

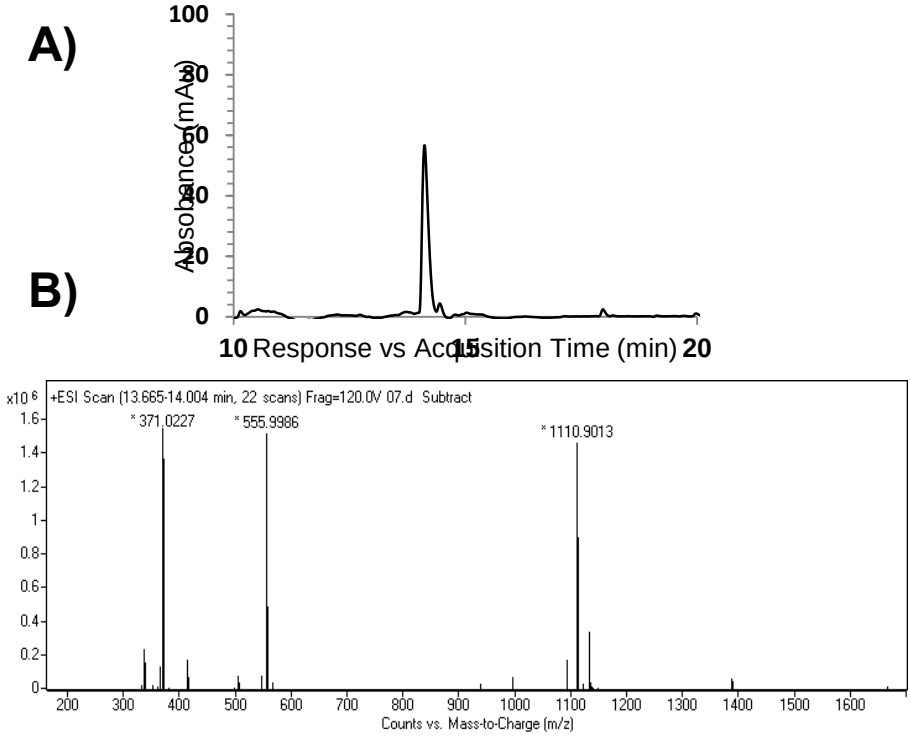

Figure 2.3 (A) HPLC chromatogram of purified KKRGD-PA molecule at 220 nm. **(B)** Mass spectrometry analysis of KKRGD-PA molecule. $[M+H]^+$ (observed)= 1110.90, $[M+H]^+$ (calculated)= 1110.73, $[M+2H]^{2+}$ /2 (observed)= 555.99, $[M+2H]^{2+}$/2 (calculated)= 555.86.

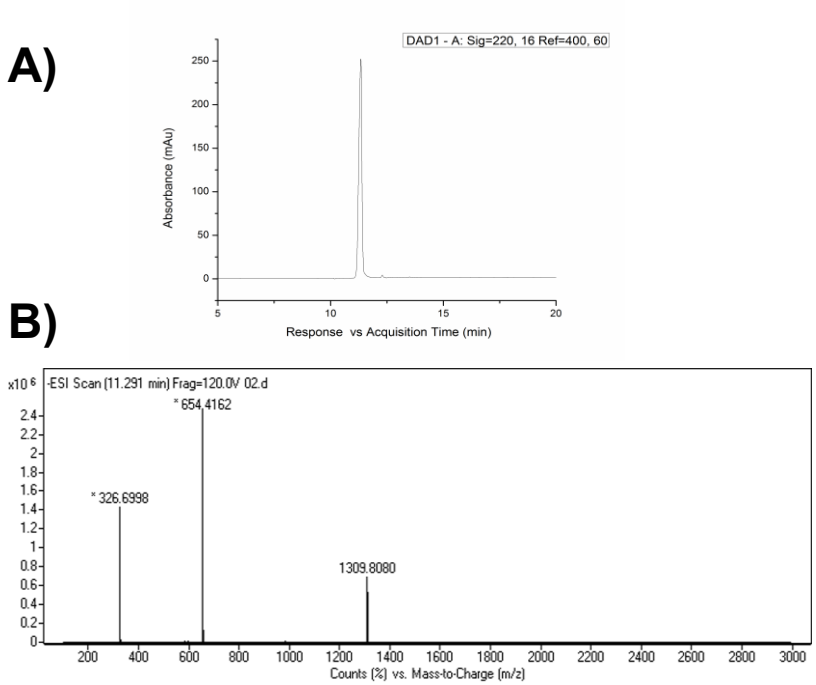

Figure 2.4 (A) HPLC chromatogram of purified E-PA molecule at 220 nm. **(B)** Mass spectrometry analysis of E-PA molecule. $[M-H]^-$ (observed)= 654.42, $[M-H]^-$ (calculated): 654.42, $[M-2H]^{2-}/2$ (observed)= 326.69, $[M-2H]^{2-}/2$ (calculated)= 326.71, $[2M-H]^-$ (observed)= 1309.80, $[2M-H]^-$ (calculated)= 1309.84.

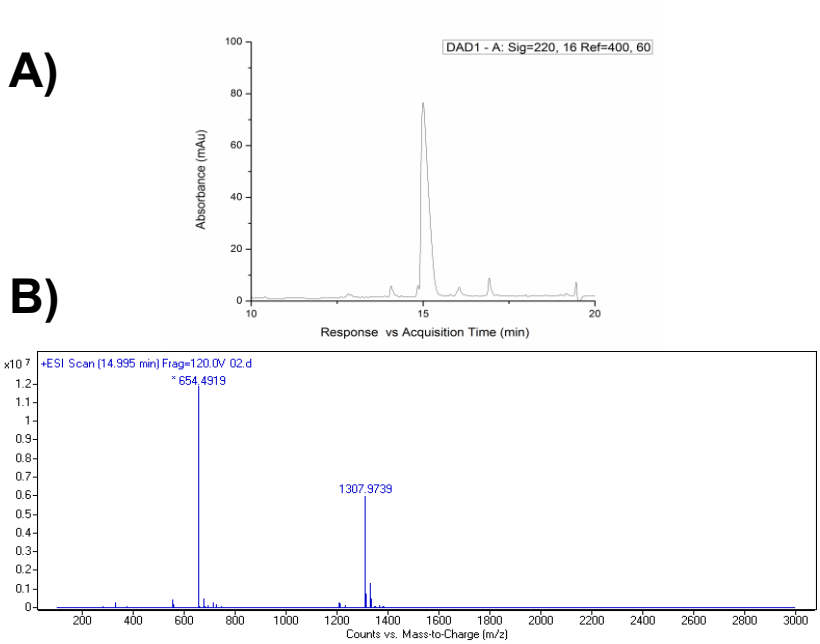

Figure 2.5 (A) HPLC chromatogram of purified K-PA molecule at 220 nm. **(B)** Mass spectrometry analysis of K-PA molecule. $[M+H]^+$ (observed) = 654.49, $[M+H]^+$ (calculated)= 654.49, $[2M+H]^+$ (observed)= 1307.97, $[2M+H]^+$ (calculated)= 1307.96.

2.3.2 Characterization of Self-assembled PA Nanofibers

Circular dichroism spectroscopy was used to characterize the formation of peptide nanostructures. β-sheet secondary structure was found to be prevalent for all samples, which also indicates nanofiber formation was driven by β-sheet formation (Figure 2.5 A) [201]. CD spectra of PA-CS nanofibers are shown in Figure 2.5 B. Nanofibers were visualized by TEM and AFM imaging. TEM images of nanofibers formed with E-PA or CS are shown in Figure 2.6. These images reveal that all the PA combinations that were used for *in vitro* and *in vivo* experiments formed uniform nanofibers with diameters of ~20–30 nm. The fiber diameters were similar for all PA combinations. The bundles

formed by PA nanofibers were analyzed by AFM (Figure 2.7). AFM images revealed that the nanofibers formed by all PA combinations used showed similar heights and morphologies.

The natural ECM is composed of a fibrous network and other structural and functional components that interact with cells. The organization of fibrils and lamellae affects the tensile strength of cornea and its transparency significantly [202]. Thus, when developing synthetic extracellular matrices, mimicking this fibrous network structure is an important task. PA molecules were previously shown to form nanofibrous networks similar to natural ECM. SEM imaging was used to investigate the general morphology of the hydrogels formed by the PA nanofibers. Critical-point drying was used to preserve the structure of the gels. The SEM images of YIGSR-PA/E-PA, KKRGD-PA/E-PA, K-PA/E-PA and of YIGSR-PA/CS and KKRGD-PA/CS nanofiber networks are shown in Figure 2.8.

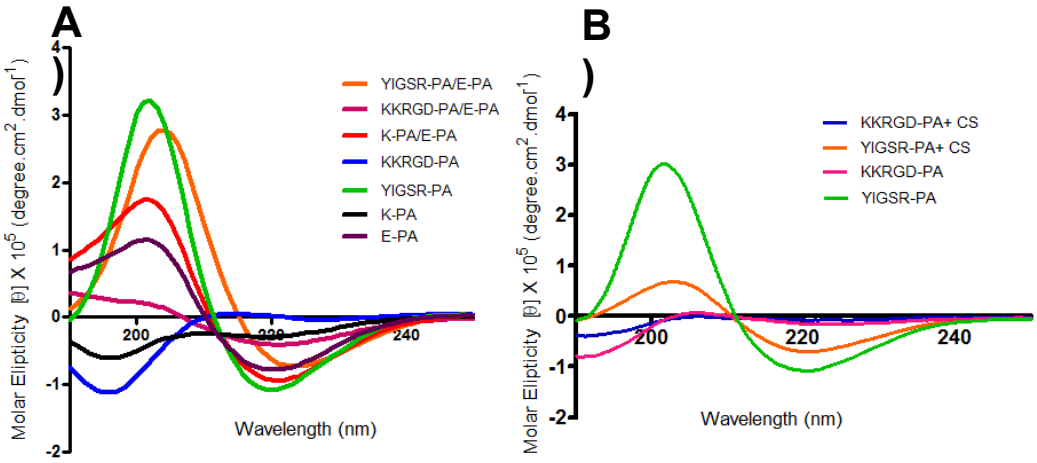

Figure 2.6 Circular dichroism spectra of the peptide nanostructures. The PA molecules showed characteristic β -sheet structure at physiological pH. **(A)** PA combinations were prepared using distilled water at physiological pH for *in vitro* study characterization, and **(B)** PA combinations were prepared using chondroitin sulfate at physiological pH for *in vivo* study characterization.

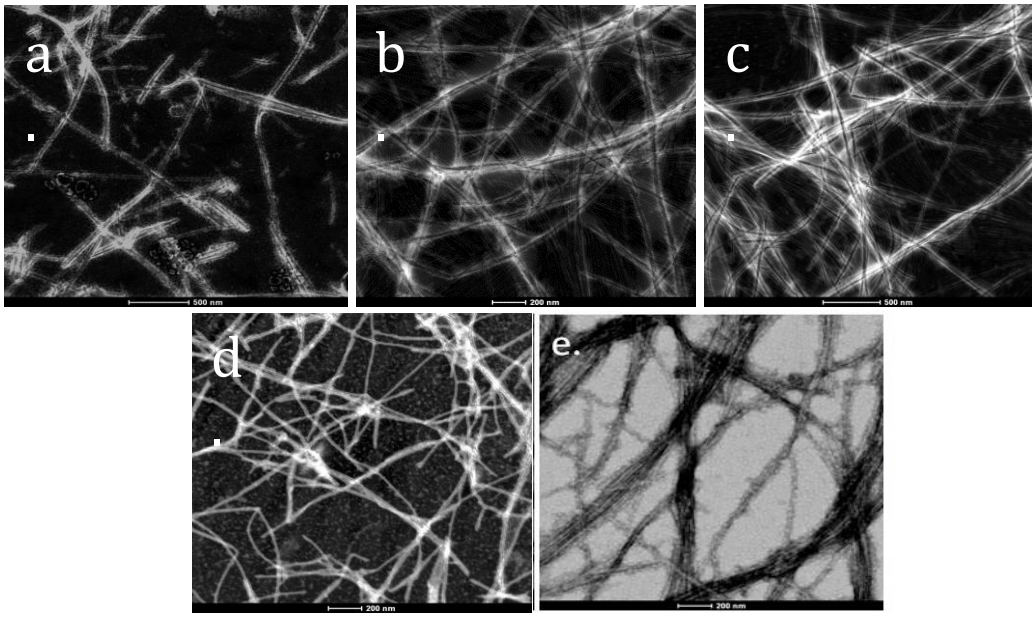

Figure 2.7 Transmission electron micrographs of **(A)** YIGSR-PA/E-PA, **(B)** KKRGD-PA/E-PA, **(C)** K-PA/E-PA, **(D)** YIGSR-PA/CS, and **(E)** KKRGD-PA/CS. Scale bars are 200 µm.

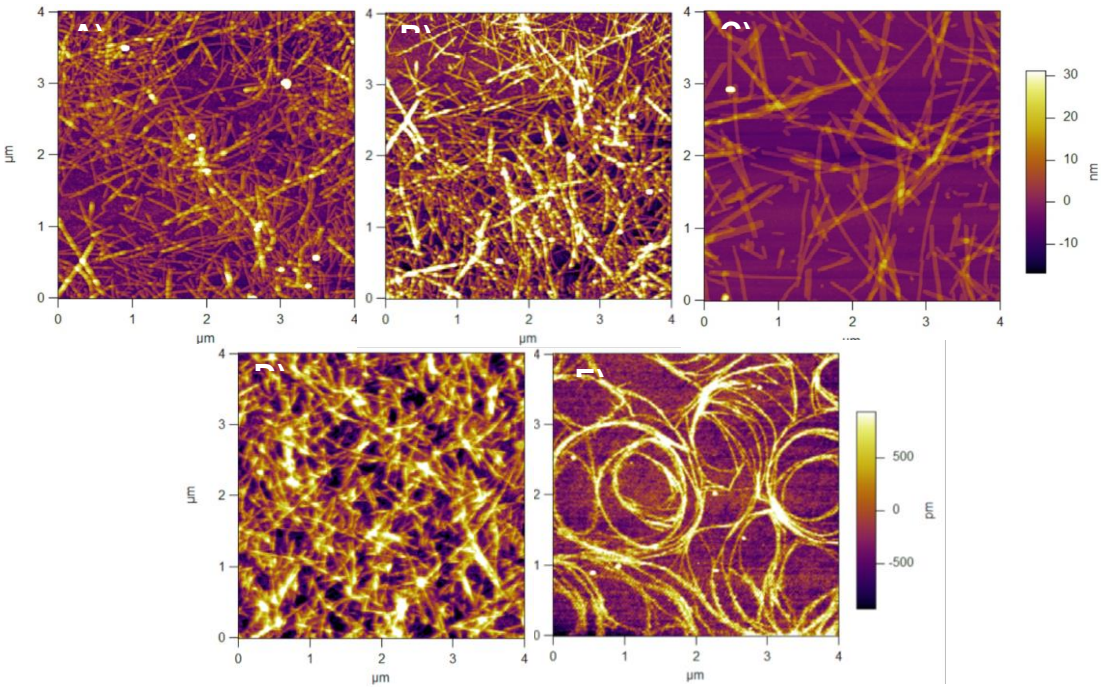

Figure 2.8 Atomic force microscopy of **(A)** YIGSR-PA/E-PA, **(B)** KKRGD-PA/E-PA, **(C)** K-PA/E-PA, **(D)** YIGSR-PA/CS and **(E)** KKRGD-PA/CS.

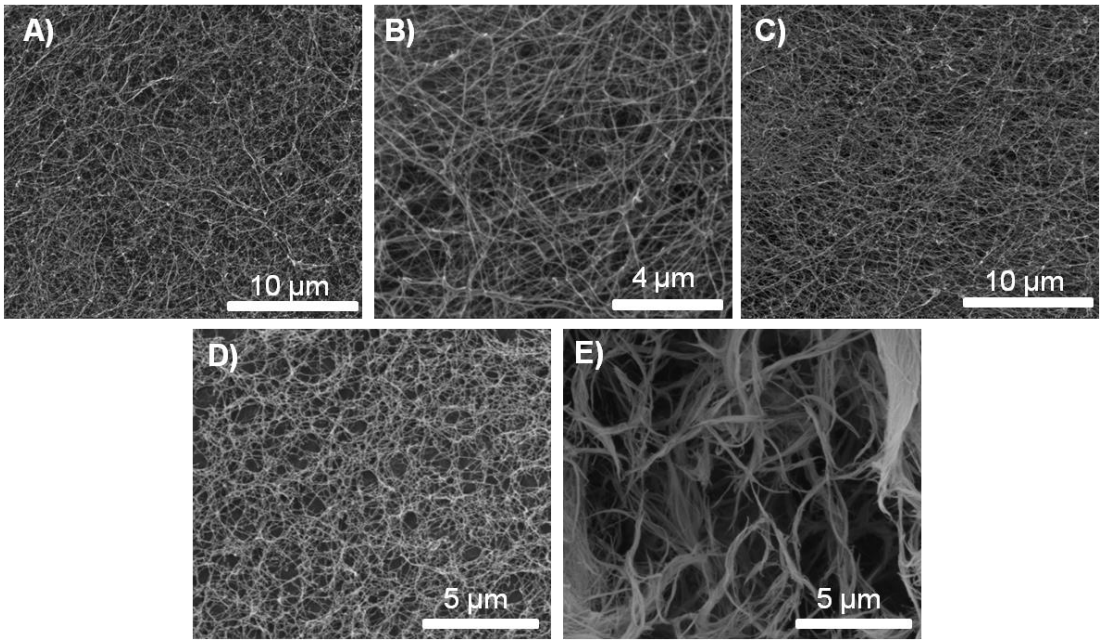

Figure 2.9 Scanning electron micrographs of **(A)** YIGSR-PA/E-PA, **(B)** KKRGD-PA/E-PA, **(C)** K-PA/E-PA, **(D)** YIGSR-PA/CS and **(E)** KKRGD-PA/CS.

2.3.3. *In vitro* Characterization of Cellular Responses on PA Nanofibers

The HTK cell line was developed and investigated by Jester et al. [199]. Karyotype, morphological and physiological analyses showed that these immortalized cells have similar properties to primary corneal keratocytes [198]. HTK cells were used in order to investigate the effects of bioactive peptide nanofibers on keratocyte viability and proliferation *in vitro*. Cell viability was determined by Alamar blue assay after culturing cells on the nanofibers for 24 h. Viability results indicated no significant difference among laminin-mimetic YIGSR-PA/E-PA, fibronectin mimetic KKRGD-PA/E-PA and non-bioactive K-PA/E-PA nanofiber scaffolds (Figure 2.9), suggesting that the bioactive sequences did not cause enhanced viability of corneal fibroblasts. HTK cells cultured on collagen showed higher viability than all PA groups. This might

have been caused by the fact that collagen, as a natural component of ECM combines a comprehensive array of biological and mechanical signals supporting the viability of these cells. In order to analyze the effects of the bioactive PA on proliferation of HTK cells, the cells were analyzed by Alamar blue assay after 72 h of incubation. While HTK cells cultured on laminin mimetic YIGSR-PA/E-PA nanofibers showed enhanced proliferation compared to cells cultured on K-PA/E-PA nanofibers, it was similar to that of cells on collagen coated wells (Figure 2.10). However, HTK cells cultured on fibronectin mimetic KKRGD-PA/E-PA nanofibers exhibited a slower proliferation rate than cells cultured on control nanofibers.

In their natural milieu, keratocytes need to adhere to the ECM in order to direct their cellular processes such as survival, migration or proliferation. When adhesion of cells on laminin mimetic YIGSR-PA/E-PA or fibronectin mimetic KKRGD-PA/E-PA nanofibers was investigated through SEM imaging, HTK cells grown on laminin mimetic nanofibers exhibited adhesion and spreading profile similar to cells cultured on collagen (Figure 2.11). However, the adhesion and spreading profiles of cells cultured on fibronectin mimetic nanofibers were similar to cells cultured on non-bioactive K-PA/E-PA nanofibers (Figure 2.12). Immunohistochemical staining for vimentin, which is a major structural protein of keratocytes, also revealed a morphological profile of cells grown on different scaffolds similar to those observed in the SEM analysis (Figure 2.12).

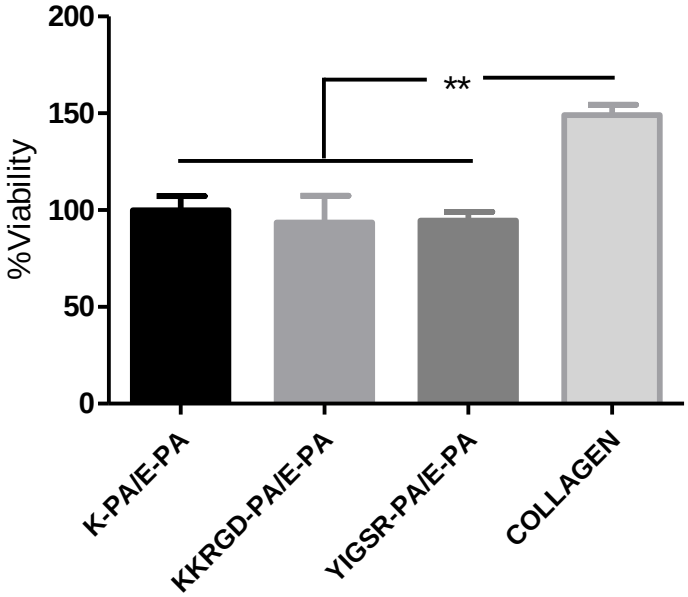

Figure 2.10 Viability results of corneal fibroblast at 24 h. PA scaffolds do not exhibit any toxic effect on HTK cell line.

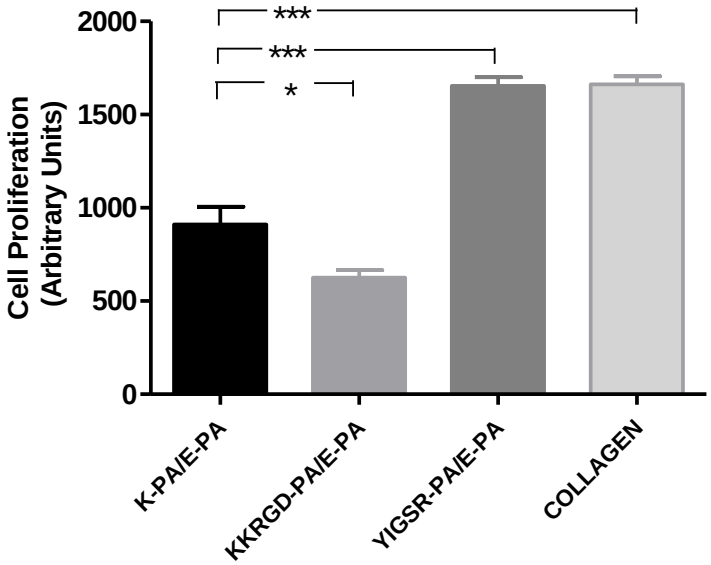

Figure 2.11 Proliferation results of corneal fibroblasts at 72 h. The YIGSR-PA nanofibers exhibited a similar proliferation profile compared with collagen.

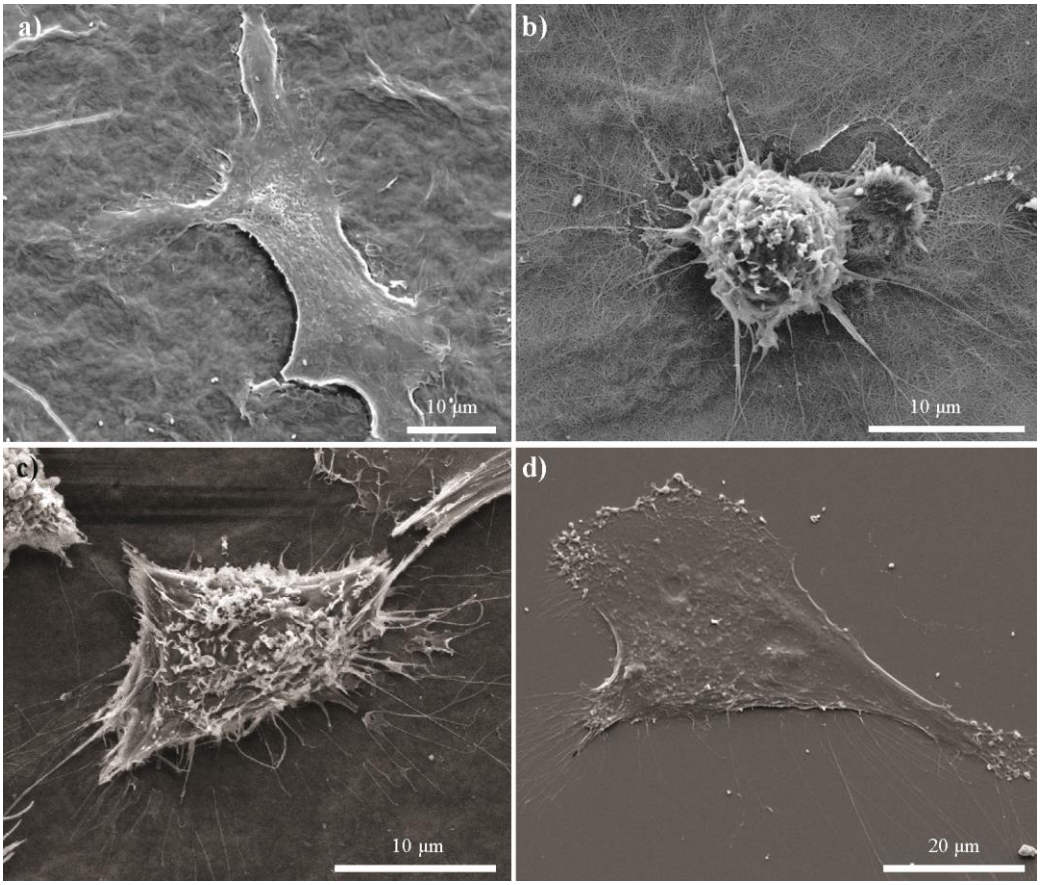

Figure 2.12 SEM images of corneal fibroblasts cultured on **(A)** YIGSR-PA coated surface, **(B)** KKRGD-PA coated surface, **(C)** K-PA coated surface and, **(D)** collagen coated surface show the adhesion profiles of cells.

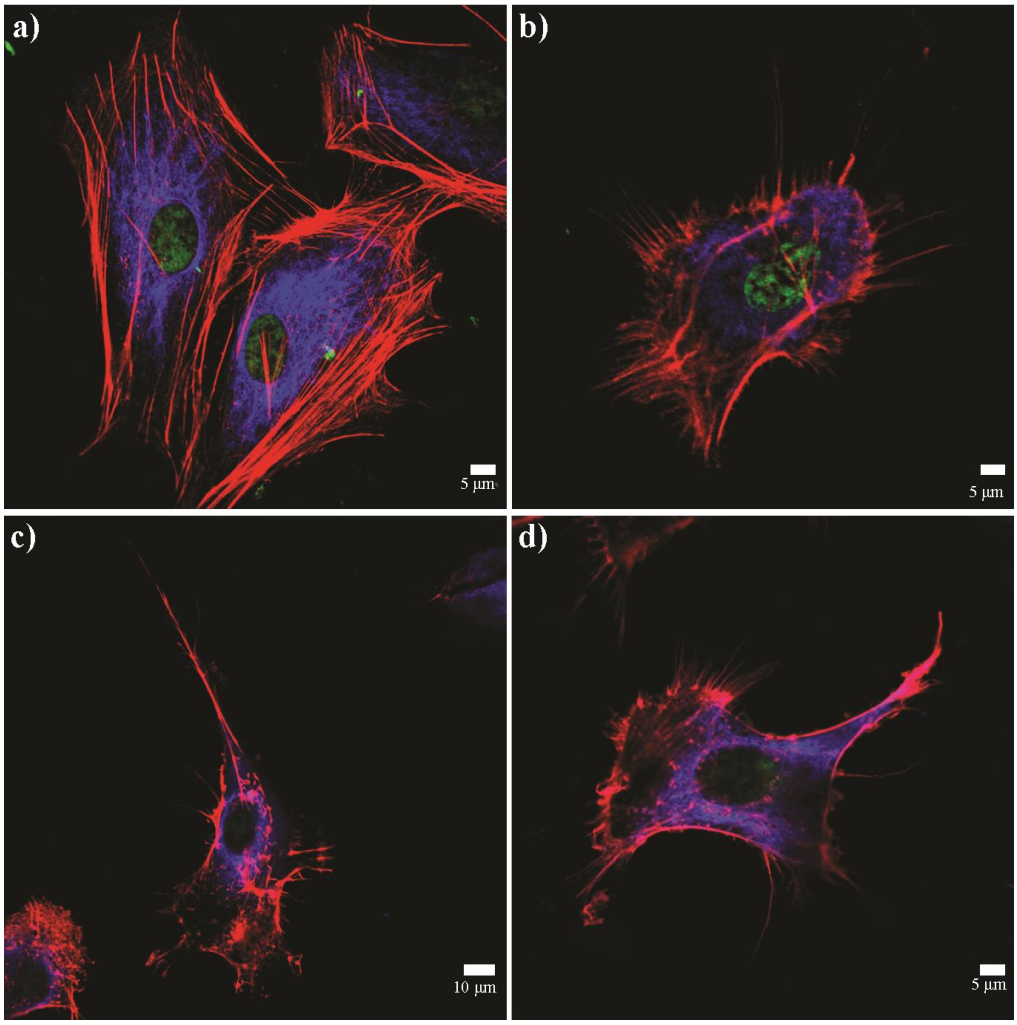

Figure 2.13 Spreading and cellular morphology of corneal fibroblasts acquired by vimentin (blue), TRITC-conjugated phalloidin (red) and TO-PRO®-3 (green) iodide staining on **(A)** YIGSR-PA coated surface, **(B)** KKRGD-PA coated surface, **(C)** K-PA coated surface, **(D)** collagen coated surface.

2.3.4 Histological Examination and Analysis of Rabbit Corneas

The effects of laminin mimetic and fibronectin mimetic PA gels on *in vivo* regeneration of corneal stroma were investigated using a rabbit corneal stromal pocket model. Corneal stromal pockets were surgically created as described in the methods section and filled with either YIGSR-PA or KKRGD-

PA (Figure 2.13), or left empty as negative controls. A pachymeter was employed to measure the central corneal thickness of the rabbit corneas (n = 5), and changes in the cornea thickness were investigated before and after injection. Since the stromal thickness profile provides information about changes in corneal regeneration [203], measurements were performed at 3 or 7 (Figure 2.14 A-B) weeks after surgery before sacrificing the animals. After injection, there was an average increase of 100 µm and 200 µm in corneal thickness, for YIGSR-PA and KKRGD-PA treated animals, respectively. However, after 3 weeks, the increase in corneal thickness of PA injected samples disappeared, and no significant difference was observed among PA injected groups, the native group and the corneal pocket without injection group. Measurements at 7 weeks also revealed a similar profile.

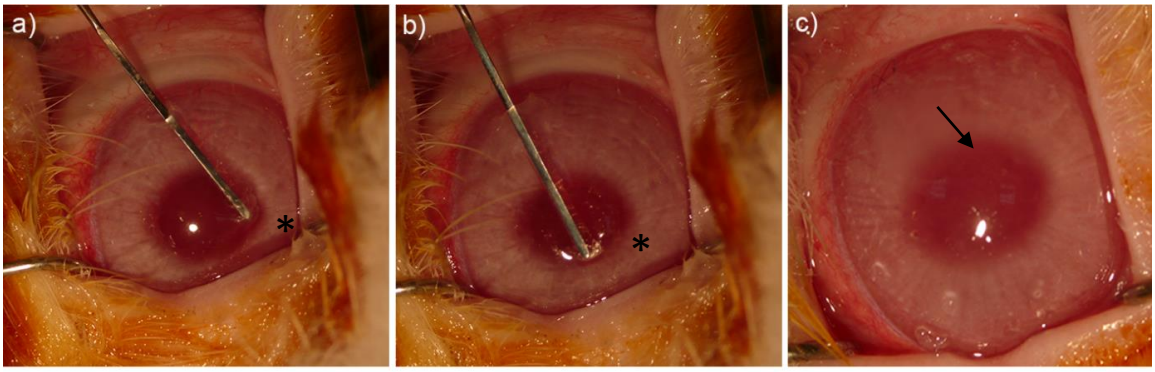

Figure 2.14 Representative images of injection process of KKRGD-PA. **(A,B)** Damaging of stromas by corneal dissector; **(C)** image of cornea after KKRGD-PA molecule injection (Asterisks indicate damaged area of corneal stroma and white arrows indicate the PA gels).

In order to investigate the regeneration process in PA gel injected and control cornea samples, histological and; immunohistochemical analyses were carried out. H&E staining was performed to observe the morphology of damaged and newly formed ECM and cell migration after surgery (Figure 2.15). H&E staining revealed that laminin mimetic YIGSR-PA (Figure 2.15 C-D) induced keratocyte migration and stromal regeneration in the stromal dissection site without any changes in the corneal morphology compared with native cornea (Figure 2.18). The corneal morphology was not preserved in the case of fibronectin-mimetic KKRGD-PA injection when inspected 3 weeks after surgery (Figure 2.16 A). In addition, there was no cell migration to the stromal dissection site in KKRGD-PA injected samples, which was similar to corneal pocket without injection samples, where no PA was injected (Figure 2.17 A). These results show that laminin-mimetic YIGSR-PA was the driving factor for inducing cellular migration to the stromal dissection site after surgery.

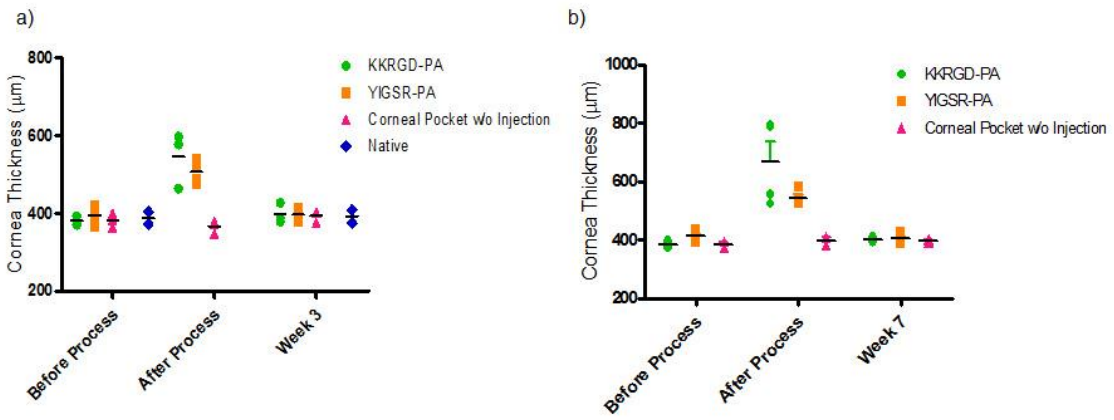

Figure 2.15 Thickness of the rabbit corneas at **(A)** week 3 and **(B)** week 7.

The morphology and protein content of the stromal ECM were further investigated by anti-collagen I and anti-vimentin immunostaining. Collagen forms ~80% of the organic content of the corneal stroma, and type I collagen is the most abundant collagenous component contributing to corneal transparency through the well-organized collagen I fibrils [204]. In order to regenerate damaged stroma, collagen I synthesis and lamellar organization of the fibrils is necessary. Thus, anti-collagen I staining was performed to observe its synthesis and organization. Three weeks after surgery, collagen I expression was observed in all groups. However, although lamellar organization of collagen I in the corneal dissection area was similar in YIGSR-PA, non-dissected control group and corneal pocket without injection group, the KKRGD-PA injected samples exhibited a wavy organizational pattern, which shows that the type of bioactive epitope is an important determinant of the regeneration inducing capability of hydrogels formed by PA molecules.

Anti-vimentin staining was performed to visualize the cells that migrated to the corneal dissection site. Vimentin is an intermediate filament protein and a well-known keratocyte marker. An increased amount of cells migrated to the corneal dissection site in the presence of YIGSR-PA injection in all four animals tested, and these cells were positive for anti-vimentin staining. However, no cell migration to the damaged area was observed in KKRGD-PA injected animals (n = 3) and the corneal pocket without injection group (n = 3) (Figure 2.16 C and 2.17 D).

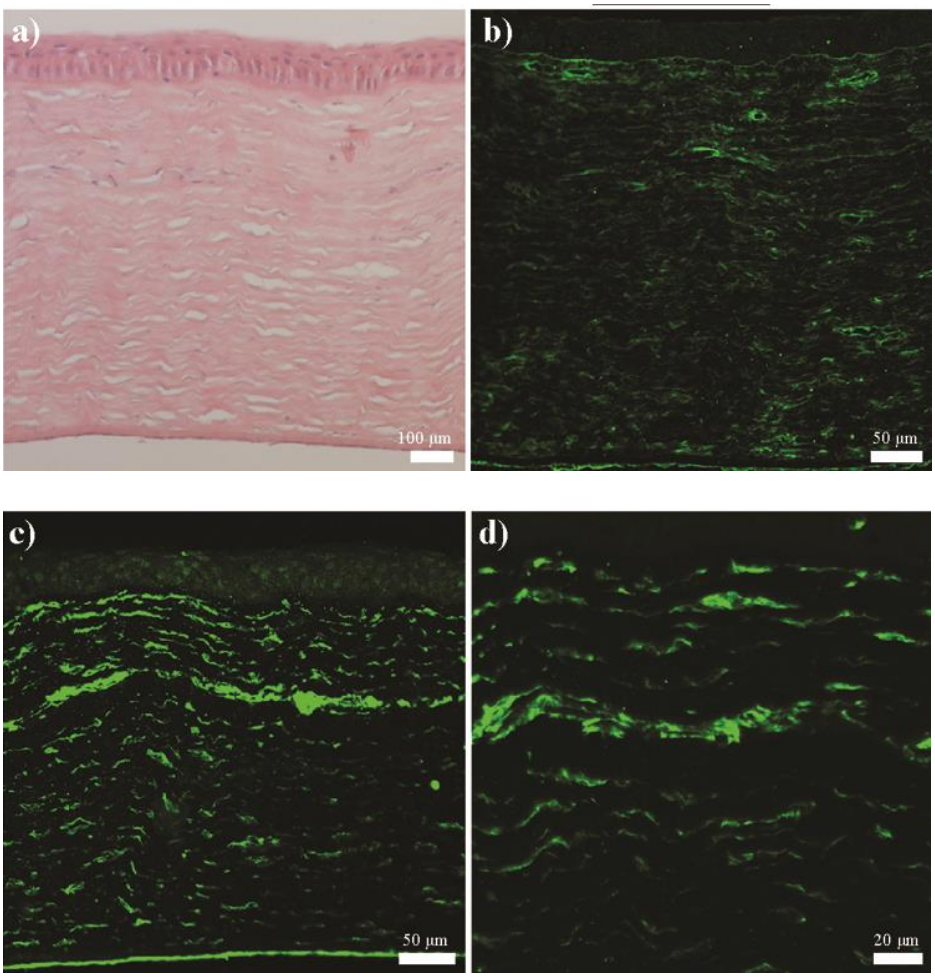

Figure 2.16 IHC analyses of YIGSR-PA injected samples at week 3. **(A)** H&E staining, **(B)** collagen staining and **(C-D)** vimentin staining. Scale bars: a) 100 µm, b-d) 50 µm.

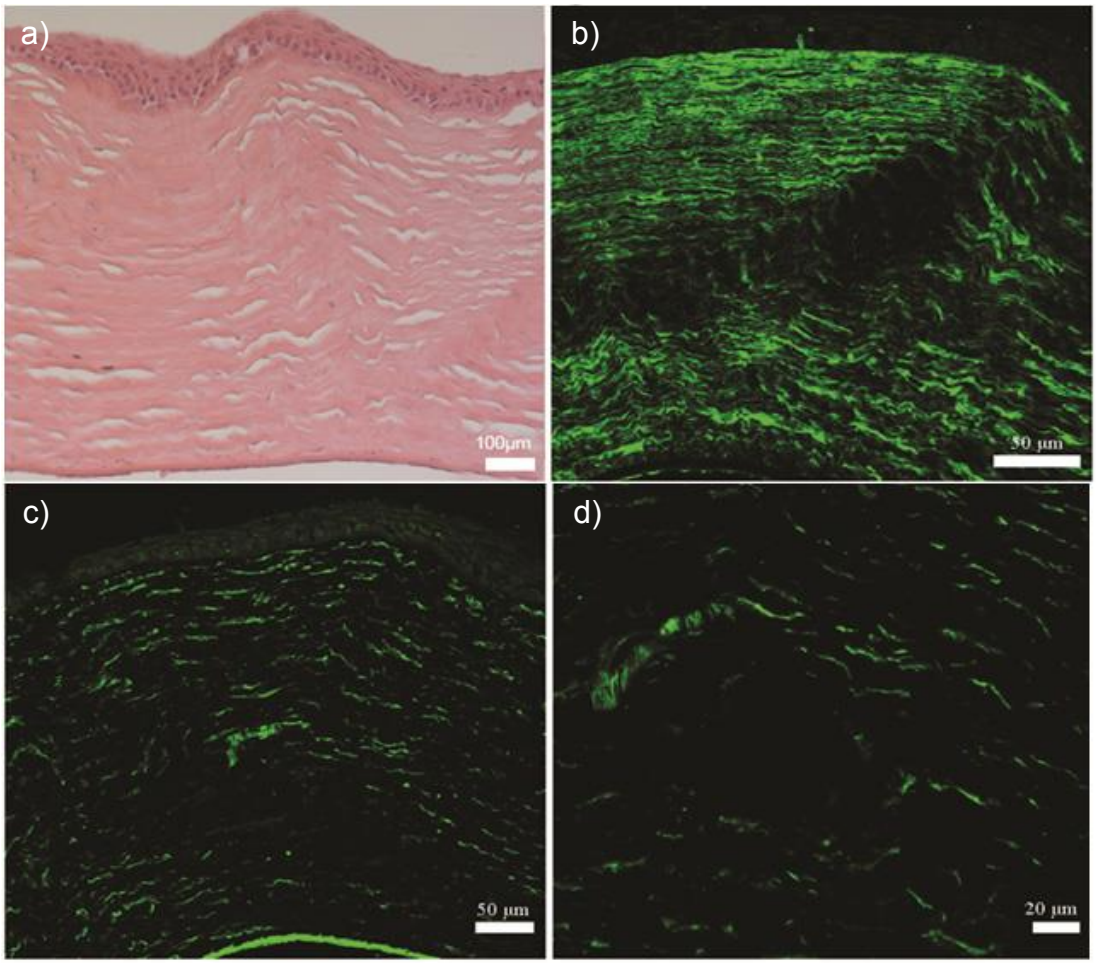

Figure 2.17 IHC analyses of KKRGD-PA injected samples at week 3. **(A)** H&E staining, **(B)** collagen staining and **(C-D)** vimentin staining. Scale bars: a) 100 µm, b-d) 50 µm.

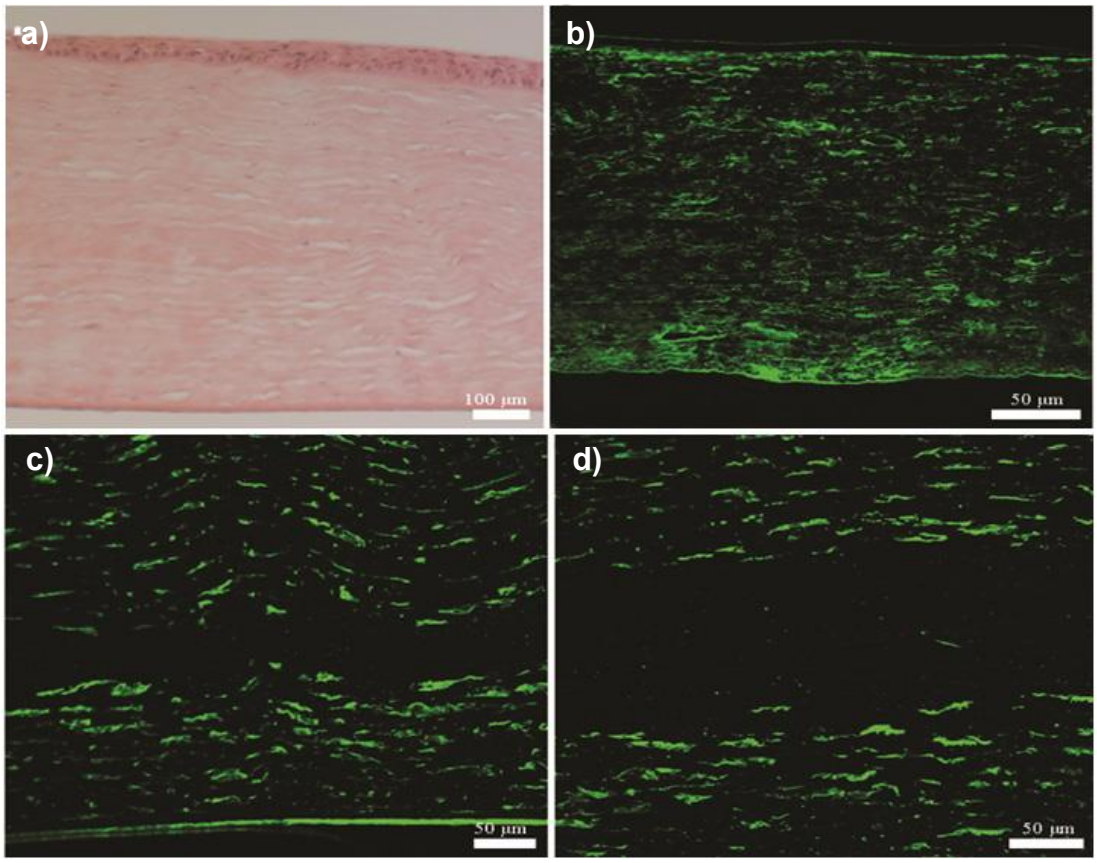

Figure 2.18 IHC analyses of damaged rabbit cornea samples at week 3. **(A)** H&E staining, **(B)** collagen staining and **(C-D)** vimentin staining. Scale bars: **(A)** 100 µm, **(B-D)** 50 µm.

After corneal dissection, while some keratocytes undergo apoptosis, others secrete ECM, which fills the gap in the damaged area [201]. Injection of YIGSR-PA gel to the corneal stromal pocket induced keratocyte migration and collagen I expression, enhancing stroma regeneration 3 weeks after surgery. In the corneal pocket without injection group, even though there was collagen I synthesis, keratocytes were not observed inside the newly formed tissue. A similar pattern was also observed for KKRGD-PA injected corneas. Lack of cell migration into the peptide nanofiber gels in KKRGD-PA group suggests

that the type of bioactive epitope that is presented on the PA nanofibers is important for achieving keratocyte migration.

Late stromal regeneration was investigated by histological and IHC staining at 7 weeks after surgery. In YIGSR-PA injected samples, H&E staining as well as anti-collagen I and anti-vimentin staining exhibited a similar profile to that observed at week 3, where keratocyte migration and collagen I synthesis was induced (Figure 2.18 a, b). The cell migration profile and collagen I organization of the corneal pocket without injection group were also similar to those observed at 3 weeks (Figure 2.19 A, B). However, KKRGD-PA injected samples showed a different profile at week 7 compared to week 3, where collagenous lamellae were more organized and similar to healthy cornea, although there was still no keratocyte migration (Figure 2.20 A, B).

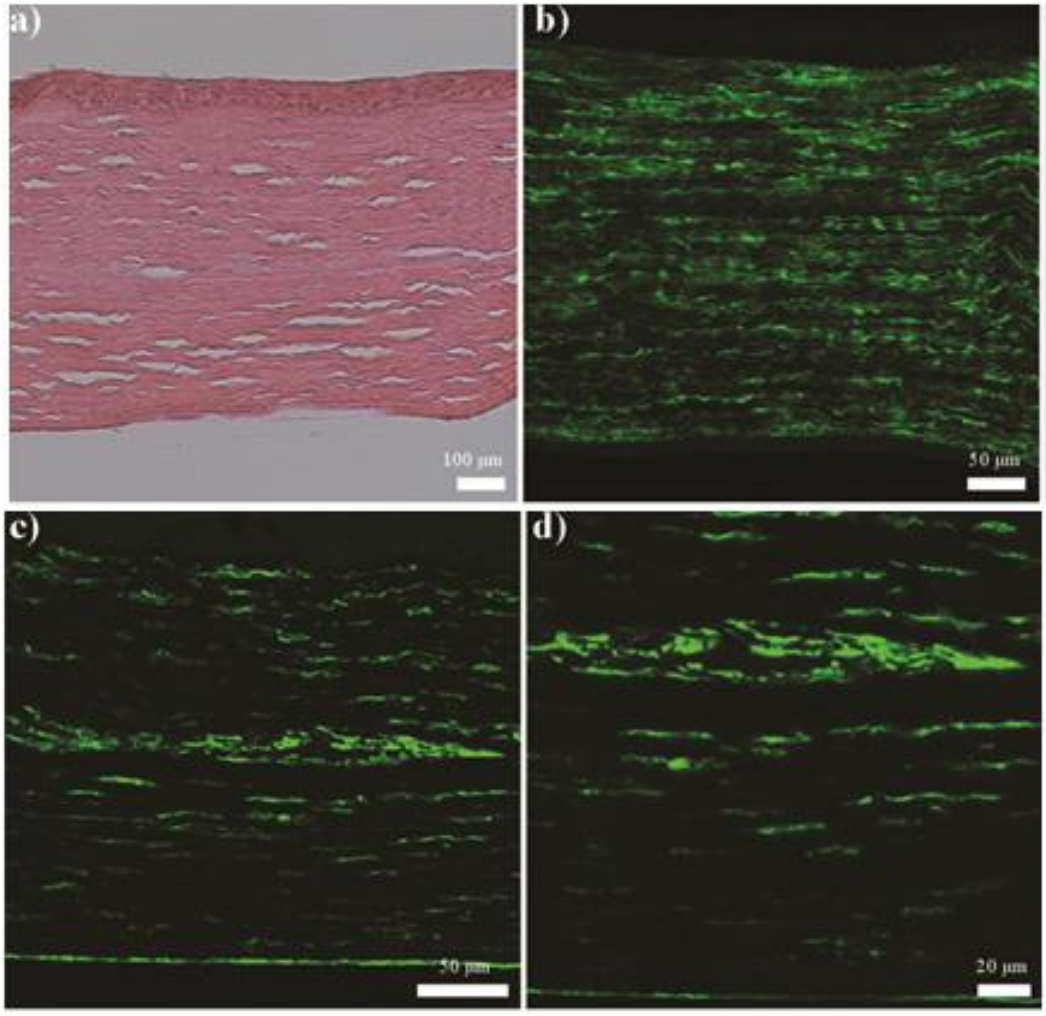

Figure 2.19 IHC analyses of YIGSR-PA injected samples at week 7. **(A)** H&E staining, **(B)** collagen staining and **(C-D)** vimentin staining. Scale bars: **(A)** 100 µm, b-d) 50 µm.

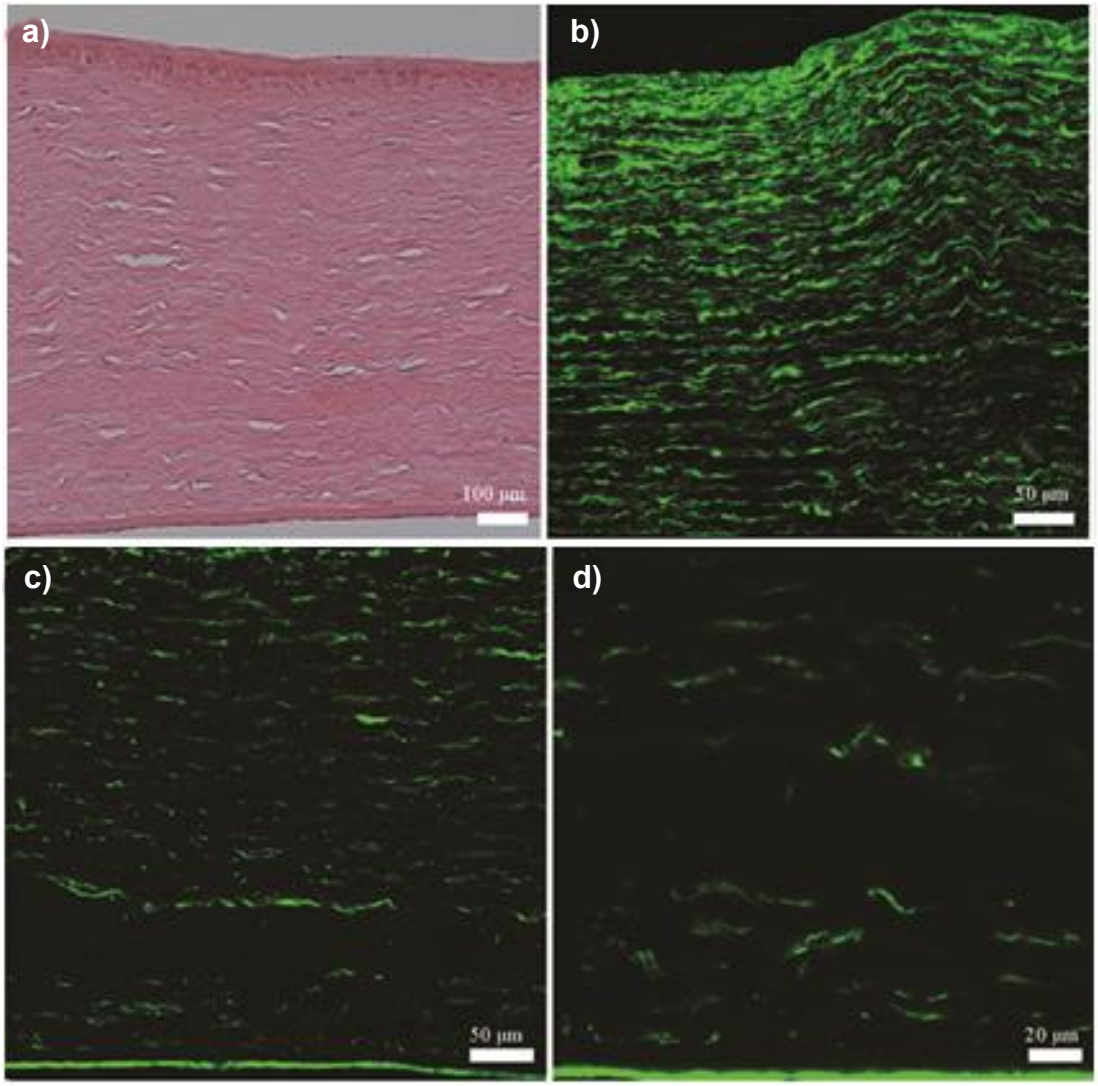

Figure 2.20 IHC analyses of KKRGD-PA injected samples at week 7. **(A)** H&E staining, **(B)** collagen staining and **(C-D)** vimentin staining. Scale bars: **(A)** 100 µm, **(B-D)** 50 µm.

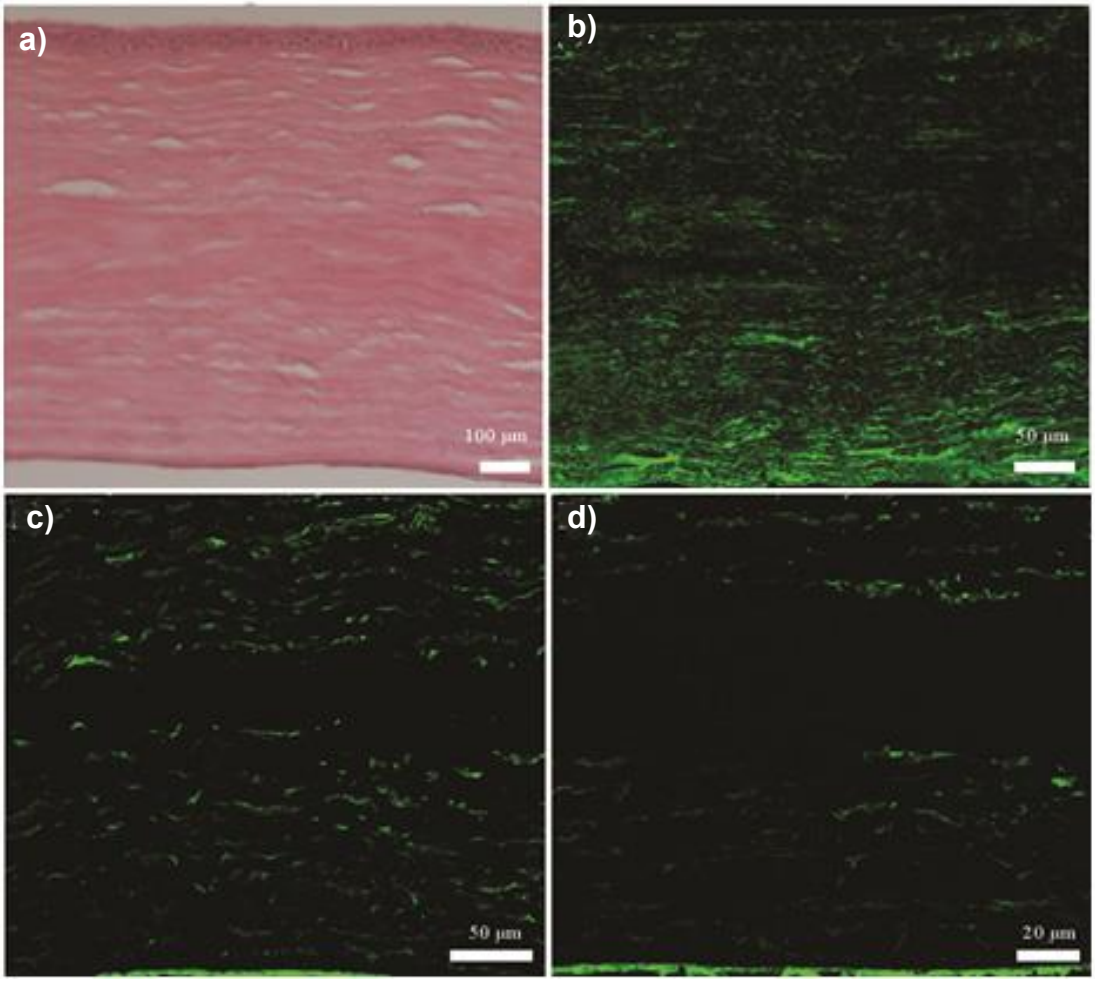

Figure 2.21 IHC analyses of damaged rabbit cornea samples at week 7. **(A)** H&E staining, **A)** collagen staining and **C-D)** vimentin staining. Scale bars: **(A)** 100 µm, **B-D)** 50 µm.

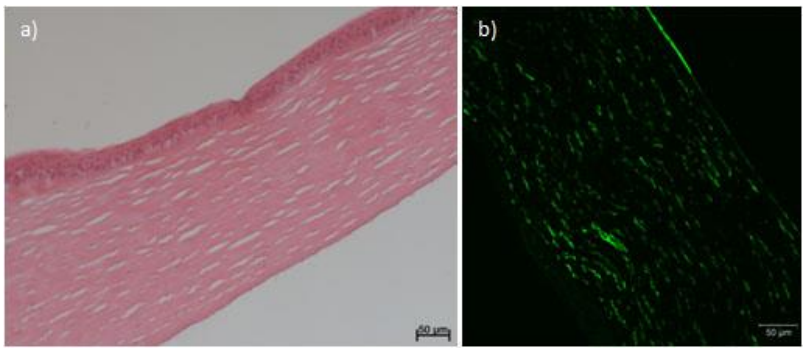

Figure 2.22 Histological and immunohistochemical analyses of native rabbit corneas **(A)** H&E staining, **(B)** Vimentin staining.

Comparison between anti-collagen I and anti-vimentin staining of KKRGD-PA injected and corneal pocket without injection groups revealed a similar healing process and no cell migration at week 7 (Figure 19-21), which further supports the importance of the type of bioactivity that is displayed on the peptide nanofibers on their regeneration induction capability. Although the fibronectin derived RGD sequence is a widely used bioactive, cell-adhesive peptide, the presentation of this sequence on PA nanofibers did not induce cellular migration of keratocytes into the injection site in the corneal regeneration model. The laminin-derived YIGSR sequence is another widely used cell adhesive peptide and was previously shown to enhance corneal regeneration when used together with a collagen-containing copolymer [197]. When this sequence was displayed on peptide nanofiber scaffolds, stromal regeneration and keratocyte migration were enhanced in the present study as well. Although RGD functionalized artificial scaffolds were previously shown to support corneal fibroblast activity [198], the RGD functionalized peptide nanofiber system did not induce similar activity in the present study, which suggests that the scaffold material itself also might affect the bioactivity of the signal sequences. Overall, the ease of injection of the PA solutions into the corneal pocket, as well as versatility of the peptide sequences that can be used in their design makes PA molecules attractive materials for corneal tissue regeneration.

Studies on the regeneration of cornea have generally focused on two approaches: one is *in vitro* production of cornea in culture, and the other is *in vivo* regeneration of the cornea via use of tissue engineered matrixes. In the

first approach, keratocytes and/or fibroblasts are directed to produce corneal ECM components in cell culture media. Gaudreault et al. [205] stimulated dermal fibroblasts by ascorbic acid to produce ECM and collagen. ECM layers were stacked together one above the other and further processed in cell culture to form the corneal stroma. The primary problem in this technique is that the time period to produce transplantable cornea was too long [205]. Carrier et al. [105] used a combination of human dermal fibroblasts and keratocytes in corneal stroma production to promote rapid and healthy epithelial healing. This approach enabled production of cultured corneal stroma with mechanical and microstructural properties similar to native human cornea [105]. Guo et al. [206] cultured human keratocytes and stimulated them to produce corneal ECM. Within 4 weeks, they produced 36-μm thick stroma similar to human corneal stroma [206]. Vrana et al. [207] inserted keratocytes into the porous matrix containing collagen and CS to produce corneal stroma, after which they implanted epithelial and endothelial layers. With this approach, they were able to produce all three layers of the cornea [207].

The second approach, which is *in vivo* regeneration of the cornea via use of tissue engineered matrices, uses ECM properties that direct cell proliferation and differentiation. Type 1 collagen matrix was the most commonly researched macromolecule for *in vivo* corneal regeneration. In cell culture, keratocytes could convert collagen type 1 matrix into lamellar stroma similar to human corneal stroma [208-209]. Recombinant human collagen type 1 and 3 (RHC1 and RHC3) containing ECM mimetics were implanted into animal corneas using lamellar keratoplasty techniques [210]. After 12 months' follow-up, both

RHC1 and RHC3 integrated into the animals' corneas, and the corneas sustained their optical clarity. Light microscopy and TEM revealed that corneal lamellar structure was formed similar to native cornea. Upon these findings, human study was started for 10 patients with keratoconus and stromal scarring was included in the study. Parallel to the animal studies, RHC integrated into the human corneas and corneas sustained their optical clarity. Keratocytes settled into the collagen matrix and converted it into lamellar corneal stroma [211]. In the present work, YIGSR peptide nanofiber scaffold promoted keratocyte migration into the scaffold, and the keratocytes converted the peptide nanofiber matrix into the lamellar corneal stroma. Preservation of the optical clarity of the animal corneas together with histological findings shows that peptide YIGSR-PA nanofiber scaffolds can achieve corneal stroma regeneration without any significant injury to the cornea.

In clinical practice, injectable peptide nanofiber scaffolds have several promising advantages over other corneal stromal regeneration approaches. Injectable matrices may give flexibility of applications in corneal tissues. They could be used to fill and regenerate a defect area of the cornea, especially in corneal diseases with stromal thinning, such as keratoconus and pellucid marginal degeneration. Addition of extra stromal tissue to the peripheral cornea may also reverse myopic refractive errors; conversely, addition to central cornea could reverse hypermetropic refractive errors.

2.4 CONCLUSION

This study investigated the potential of peptide nanofiber scaffolds decorated with bioactive laminin derived YIGSR and fibronectin RGD peptides for corneal regeneration. Chemical and physiological characterization studies indicated that all groups exhibited ECM mimicking nanofibrous morphology with β-sheet secondary structure, which was driven through self assembly of PA molecules. *In vitro* studies showed that PA nanofibers were biocompatible with the human stromal keratocyte cell line, HTK cells, and supported their adhesion and viability. In *in vitro* cell proliferation assays, laminin-mimetic YIGSR-PA nanofibers showed an enhanced effect on cell proliferation compared with other PA groups. The *in vivo* cornea damage model demonstrated that the YIGSR-PA injection to the damage site induced keratocyte migration and collagen I synthesis, which is an indication of corneal stroma regeneration. However, when presented on PA nanofibers, the fibronectin-derived RGD sequence, which is widely used for enhancing cell adhesion for various purposes, did not show a similar effect to YIGSR-PA. Although collagen I synthesis in the damage site was detected in the fibronectin mimetic peptide nanofiber injected samples and the corneal pocket without injection controls, there was a striking absence of cells in the damage area, which shows the importance of the type of bioactive epitope for specific applications. In conclusion, the laminin mimetic YIGSR functionalized peptide nanofiber system presents a promising scaffold for corneal stroma regeneration.

CHAPTER 3

IMPROVING PANCREATIC ISLET TRANSPLANTATION EFFICIENCY USING HEPARIN MIMETIC PEPTIDE AMPHIPHILE NANOFIBER GEL

Part of this thesis is published in the following article [212]; *Reprinted from Improving Pancreatic Islet in Vitro Functionality and Transplantation Efficiency by Using Heparin Mimetic Peptide Nanofiber Gels*.; *Uzunalli, G., Tumtas, Y., Delibasi, T., Yasa, O., Mercan, S., Guler, M.O., and Tekinay, A.B., Acta Biomaterialia, 22 (2015), 8–18, with permission from Elsevier*

3.1 INTRODUCTION

Diabetes mellitus is one of the most common diseases in the world and causes more than 200,000 death each year in the United States [213]. There are approximately 177 million diabetic patients worldwide and this number is expected to double by 2025 [214]. Diabetes is associated with several and serious complications, including cardiovascular, renal, ophthalmic, neurological, cerebrovascular, and peripheral vascular diseases [215-219].

Type 1 diabetes (T1D) is a chronic autoimmune disease and involves the destruction of or damage to the β-cells in the islets of Langerhans, resulting in insulin deficiency and hyperglycemia [220]. Previously it was thought that symptoms of T1D emerged during adolescence, however, it can also be diagnosed in adults [221]. An individual can be diagnosed as T1D when his/her blood glucose level is higher than 200 mg/dL and fasting blood glucose is higher than 126 mg/dL [222].

Since the discovery of the insulin hormone in 1921, insulin treatment has been the standard therapeutic approach to treat T1D. However, because of the fluctuation of the blood glucose levels of the patients throughout the day, insulin therapy alone was found to be insufficient for curing the disease, as acute morbidity and mortality as well as a series of chronic complications were observed after insulin treatment [223-224]. Although improvements in insulin delivery systems were proposed to provide strict control on blood glucose level, there are several limitations including poor patient compliance, risk of hypoglycemia and complications caused by using devices for insulin delivery [224]. Therefore, the therapeutic approaches that replace the physical

conditions of pancreas are needed. Islet transplantation has been used as a treatment for T1D to improve glycemic control in patients and rescue them from daily insulin injection [225]. This method is as effective as whole pancreas transplantation and less invasive [224]. After five years of transplantation, the rate of patients with relapsed T1D was 90% [226]. Although it is a promising method, there are several limitations such as insufficient number of donors and decreased islet viability during and after isolation [225]. Cellular stress and disruption of islets' original integrity during isolation limit the success of islet transplantations [227-228]. Pancreatic islets tend to form clusters and in these clusters, cells, which exist in the core of the islet die due to decreased oxygen and nutrient transport. Normally, islets have extensive intraislet vasculature to overcome these problems [229] This vasculature is damaged during the isolation procedure, and the damaged microvasculature only regenerates after 10 to 14 days following the transplantation [230-233]. However, low diffusion of nutrients and oxygen leads to deterioration of cells [234] including β-cells and leads to hypoxia and death [235].

Using alternative transplantation sites, supportive scaffolds and minimizing the immunological responses are being investigated in order to increase the islet viability and consequently long term normoglycemia. Until now, several alternative transplantation sites such as liver through the portal venous circulation [236], spleen, kidney [237], testis [238], anterior chamber of the eye [239], and greater omentum [240] have been tested to find an effective and less invasive healing strategy. Due to its self-healing potential, omentum was also used for revascularization of brain [241] and heart [242], and

regeneration of spinal cord [243]. It has several advantages compared to other transplantation sites which are 1) large transplantation area, 2) less direct contact with blood that prevent instant immunological response and higher blood pressure, and 3) not being a vital organ. On the other hand, it requires more islets for transplantation and enhanced blood vessel formation for transplantation efficiency [244].

During islet isolation procedure, enzyme treatment disrupts islet-matrix interactions, which results in extracellular matrix (ECM) degradation and cell apoptosis [228, 245]. Supporting the islets in *in vitro* conditions with matrices that contain ECM components like collagen and fibrin increases viability of the islets [246-248] which shows the importance of ECM scaffolds in providing a variable environment for islets.

In this study, peptide amphiphile (PA) nanofibers were used as a bioactive scaffold for islet transplantation. The PA molecules self-assemble into nanofibers due to intermolecular hydrogen bonding, electrostatic interaction between charged amino acids, and hydrophobic interactions [249-250]. PA nanofibers form a 3D network in aqueous environment, which resemble natural ECM and this network can be enriched with specific bioactive sequences to modulate cell-material interactions. PA nanofibers have previously been used as functional scaffolds for bone [189, 251], neural [157], and cornea [163] regeneration and can also be used as drug delivery agents [252].

Here, heparin mimetic peptide amphiphile (HM-PA) nanofibers were used as a new therapeutic approach for T1D to enhance the function of

pancreatic islets and to improve the islet transplantation efficiency. The HM-PA nanofibers induce capillary-like structure formation of endothelial cells *in vitro* and the PA scaffold applied with vascular endothelial growth factor (VEGF) and fibroblast growth factor 2 (FGF-2), induce angiogenesis, in cornea *in vivo* [253]. In this study, the HM-PA provides an ECM like environment to enhance angiogenesis, which in turn enhances islet viability and functionality both *in vitro* and *in vivo*.

3.2 MATERIALS & METHODS

3.2.1 Materials

ABCR Collagenase V and Streptozotocin (STZ) were purchased from Sigma-Aldrich**.** RPMI 1640, Hanks Balanced Salt Solution (HBSS), Fetal Bovine Serum (FBS), penicillin/ streptomycin/ amphotericin B and L-glutamine were purchased from Lonza. Rat-Mouse Insulin Assay and cell inserts were purchased from Milipore. All other materials were obtained from Invitrogen, Fisher and Merck. VEGF was purchased from R&D and human FGF-2 from Sigma-Aldrich. All chemicals were used as provided.

3.2.2 Synthesis of Peptide Amphiphile Molecules

Two peptide amphiphile molecules were synthesized by solid phase peptide synthesis method for this study. HM-PA (Lauryl-VVAGEGD(K-pbs)S-Am) and K-PA (Lauryl-VVAGK) were constructed on Rink Amide MBHA resin. Resins were swelled in DCM for 30 min and then washed with DMF three times. Removal of Fmoc protecting groups was performed by shaking 20% piperidine in DMF (v/v) for 20 min.

After washing steps with three times each in DMF-DCM-DMF, 2 mole equivalents of carboxylate group activated amino acids by 1.95 mole equivalents of HBTU and 3 mole equivalents of DIEA for 1 mole equivalent of functional sites on the solid resin were dissolved in DMF. Coupling for each amino acid addition step was set to be at least 2.5h. Confirmation of completion of each coupling was performed by Kaiser Test. Following Kaiser Test, capping of unreacted amine groups was done by treating with 10% acetic anhydride in DMF solution for 30 min. These steps were followed, until desired peptide chain was completed. For HM-PA synthesis, 4-methyltrityl group was removed from side chain of lysine by TFA/TIS/H_2O/DCM mixture (5:2.5:2.5:90 ratio) for 5 min and P-sulfobenzoicacid was added to the lysine's side chain. Cleavage of peptide amphiphile molecules from resin was performed by incubation with TFA, TIS and ddH_2O mixture (95:2.5:2.5) for 2 h. Excessive TFA and DCM were evaported by rotary evaporator at 40 °C. Peptide amphiphile molecules were stored at -20 ºC with ice-cold diethyl ether overnight for precipitation. Precipitated peptide and diethyl ether were transferred to a 50 mL falcon tube and centrifuged at 6000 rpm for 20 min. Supernatant was discharged and remaining diethyl ether was evaporated. Pellet was dissolved in ddH_2O and frozen at -80 °C overnight. Then PA was lyophilized to obtain a powder.

3.2.3 Purification of Peptide Amphiphile Molecules

Synthesized PA molecules purity was measured with Agilent 6530 quadruple time of flight (Q-TOF) mass spectrometer with electrospray ionization (ESI) source equipped with a reverse phase analytical high

performance liquid chromatography. Negatively charged HM-PA was characterized by 2.1 x 50 mm Agilent Zorbax Extend-C18 column in basic condition while positively charged K-PA was characterized by 4.6 x 100 mm Zorbax SB-C8 column in acidic condition. A gradient of water (0.1% formic acid or 0.1% NH_4OH) and acetonitrile (0.1% formic acid or 0.1% NH_4OH) was used. Purification of PAs was performed by using a reverse phase preparative high performance liquid chromatography (HPLC) (Agilent 1200 series) system by using Zorbax Extend-C18 21.2 x 150 mm column.

3.2.4 Physical, Mechanical and Chemical Characterization of Self assembled Nanofiber Network

3.2.4.1 Transmission Electron Microscopy

The morphology of self assembled PA nanostructure was characterized by transmission electron microscopy [29]. PA gels were prepared by mixing 1% (w/v) K-PA and 1% (w/v) HM-PA and the gel was diluted 100 times. Then, 10 µL of the PA gel was deposited on a Lacey carbon-coated 300-mesh copper grid and incubated for 3 min. Excess solution was removed by tissue paper and the sample was negatively stained with 2 wt % uranyl acetate and dried at RT. Images were visualized by a FEI Tecnai G2 F30 transmission electron microscope.

3.2.4.2 Atomic Force Microscopy (AFM)

PA solutions that were dissolved in ddH_2O were prepared by mixing 0.05 wt% HM-PA with K-PA at 1:1 volume ratio on a silicon wafer. After sample was dried at RT for 30 min, AFM images were taken via MFP-30 Asylum Research in tapping mode using appropriate cantilever. All images were taken with 1.0-

1.5 Hz scan rate and 1024×512 resolution. Tips with resonance frequency of 246 kHz were used.

3.2.4.3 Scanning Electron Microscopy

The three dimensional nanofibrous network of PA molecules was investigated using scanning electron microscopy. 1% w/v PA solutions were mixed with the volume ratio of 1:1 to achieve gel formation. Gels were incubated for 15 min for maturation. Dehydration was performed gradually with increasing concentrations of ethanol for 2 min each from 20% to 100%. Samples were dried in a critical point dryer (Tousimis, Autosamdri-815B, Series C critical point dryer) and coated with 8 nm of Au/Pd. Scanning electron microscopy imaging of the nanofiber networks were taken with an FEI Quanta 200 FEG scanning electron microscope under high vacuum.

3.2.4.4 Circular Dichroism (CD)

Secondary structure of PA molecules was investigated by CD analysis using JASCO J815 CD spectrapolarimetry. PA solutions were dissolved in deionized water at a concentration of 0.01% w/v and pH was adjusted to 7.4. The CD spectra of HM-PA, K-PA and HM-PA/K-PA (1:1 volume ratio) were obtained by scanning from 190 nm to 300 nm using a digital integration time of 1 s, a band width of 1 nm and with standard sensitivity. Values were converted to molar ellipticity by using the formula below:

$[\theta]$ (deg cm2 $dmol^{-1}$) = (ellipticity (mdeg) x (10^6) / pathlength (mm) x concentration (μM)

3.2.4.5 Oscillatory Rheology

Oscillatory rheology measurements of HM-PA/K-PA gel were performed with an Anton Paar Physica RM301 rheometer operating with a 25 mm parallel plate configuration at 25 ºC. 1 wt.% HM-PA and K-PA were loaded on the center of the lower plate with 300 µL total volume and incubated for 15 min before measurement. A gap distance of 0.3 mm was used with 100 - 0.1 rad/s angular frequency and 0.5% shear strain.

3.2.5 Animals

In vivo experiments were carried out with 3 months old Wistar male rats for both islet isolation and transplantation. Rats were maintained on *ad libitum* access to water and nutrition in a 12 h-12 h light-dark cycle except the day before transplantation. All procedures regarding animals were approved by Institutional Animal Care and Use Committee of Diskapi Yildirim Beyazit Training and Research Hospital.

3.2.6 Islet Isolation and Culture

Cell culture studies were carried out with isolated primary pancreatic islets. The pancreas islet isolation was done according to methods modified from other studies [201, 254]. Briefly, rats were anesthetized by an intraperitoneal injection of ketamycin (80 mg/kg) and xylazine (20 mg/kg). Then midline laparotomy was performed, and the common bile duct was cannulated. Following the injection of 7 mL of cold collagenase (Type V, 1 mg/mL) into the duct, the distended pancreas was removed and subjected to stationary digestion for 18 min at 37 ºC. HBSS supplemented with 10% FBS, 1% penicillin/ streptomycin/amphotericin B, and 1% L-glutamine was used for

washing. After digested pancreas was centrifuged, the pellet suspension was filtered by a steal sieve of 450 µm to remove islets from undigested tissue. Subsequently, the islets were purified by using Biocoll (Biochrome) 1100, 1077 and RPMI 1640 to create a gradient. Islets were counted and picked up under optical microscope via handpick method. Islet cells were cultured with 1% penicillin/streptomycin/amphotericin B and 1% L-glutamine supplemented RPMI 1640 at 37 °C under humidified atmosphere containing 5% CO_2.

3.2.6.1 Pancreatic Islet Viability

Viability was assessed by normalizing to DNA content using Alamar Blue Assay (Invitrogen) and FluoReporter Blue Fluorometric dsDNA Quantitation Kit (Invitrogen) by using 50 islets sized between 100-200 µm under microscope. After incubation of islets for 24 h with culture medium, eight experimental conditions were constituted: (1) media only as a control group; (2) media with HM-PA and K-PA; (3) media with HM-PA; (4) media with VEGF and FGF-2; (5) media with HM-PA, VEGF and FGF2; and (6) media with HM-PA, K-PA, VEGF and FGF2. RPMI 1640 with 1% L-glutamine and 1% penicillin/streptomycin/amphotericin B was used as culture media. PA solutions were added to the media at the final concentration of 0.1% w/v HM-PA and 0.1% w/v K-PA (1:1 volume ratio) and the growth factor amounts were determined as 100 ng. The experiment was performed at day 1, 3 and 7 (n=4). Before starting Alamar Blue Assay, islets were collected and transferred into tissue culture inserts (8 µm pore size, Millicell). Alamar Blue stock solution was diluted at 1:10 ratio with the culture medium and incubated with islets at 37 ºC with 5% CO_2 for 4h. At the end of the 4h, absorbance was monitored at 570

nm. The inserts with islets were kept at -80 ºC for DNA quantification. In order to quantify DNA amounts, islet samples were thawed at RT and 200 µL of ddH_2O was added into each well. Plates were incubated in a humidified incubator (37 ºC, 5% CO_2) for 1h, and then frozen at -80 ºC for 2 h to disrupt cell membrane. Afterwards, cells were thawed at RT again and Hoechst 33258 dye in TNE (10 mM Tris, 2 M NaCl, 1 mM EDTA, pH 7.4, containing 2 mM sodium azide) was added into wells with the volume of 200 µL/well. 200 µL from this solution was transferred to a 96 well plate and fluorescence was read at 360 nm and 460 nm by microplate reader. The ratio of viability and DNA was calculated by dividing the Alamar Blue Assay results by DNA Assay results.

3.2.6.2 Glucose Stimulated Insulin Release

Islets (10 islets each well) cultured on tissue culture inserts (8 µm pore size) (Millipore, Billerica, MA) for 24 h were processed for evaluation of glucose stimulated insulin release. Islets were washed with RPMI 1640 medium containing 3.3 mM glucose for 30 min to normalize the metabolism. Following the wash, islets were sequentially incubated in 3.3 mM glucose and 16.7 mM glucose containing media at 37 ºC, 5% CO_2 for 1h. Before medium changes, sera were collected and stored at -20 ºC. Experiments were carried out on days 1, 3 and 7. Glucose stimulation assay was performed via Rat/Mouse Insulin 96 Well Plate Assay, ELISA Kit, Millipore. Before the ELISA experiment, the 10x HRP wash buffer was diluted 1x with ddH_2O. Required number of strips was removed and wells were washed with 1x HRP wash buffer three times and tapped after each washing step. 20 µL assay buffer was added into the blank wells while 10 µL into samples, controls and standards wells. Standards

were run duplicated and 10 µL Rat Insulin standards were added in order of ascending concentration to the appropriate wells. QC1 and QC2 were added as 10 µL, respectively. Then, samples were added to the wells. After adding 80 µL of detection antibody into all wells, plate was covered with plate sealer and incubated at RT for 2h by shaking at 400-500 rpm. At the end of 2h, plate was tapped and washed with 1x HRP wash buffer three times. 100 µL enzyme solution was added into each well and plate was incubated at RT for 2 h by shaking 400-500 rpm. Wells were washed with 1x HRP buffer six times. Following the addition of 100 µL substrate solution, absorbance was measured at 370 nm at 5 min intervals. When absorbance was between 1.2 and 1.8, 100 µL stop solution was added and blue color turned to yellow. Then, absorbance at 450 nm and 590 nm were read within 5 min. Insulin release was quantified as a ratio of high glucose to low glucose state and presented as the stimulation index.

3.2.7 Transplantation

10 days before transplantation, 220 mg/kg STZ which was in citrate tampon (pH 4.5) was injected to rats intraperitoneally to induce diabetes. Blood glucose levels of the rats were measured using On Call Advanced Blood Glucose Monitoring System (Acon Laboratories Inc., CA USA). Animals were included in the study only if the blood glucose levels were greater than 300 mg/dL on consecutive days before transplantation. 2000 islets were transplanted into the omentum of each rat. Isolated islets with minimal volume of medium were mixed with HM-PA, and gelation was triggered with addition

of K-PA. The final concentrations of PA solutions in scaffold were 1% w/v HM-PA and 1% w/v K-PA at 1:1 volume ratio.

An intraperitoneal injection of ketamycin (80 mg/kg) and xylazine (10 mg/kg) were used as anesthetic agents. The abdominal region of rats were shaved and sterilized with Batticon. The greater omentum was reached by lower abdominal incision and it was spread onto the wet sterile gauze pad. Islets with PA gel were placed onto the omentum, and omentum was sewed with 3.0 PGLA (90% glycolide and 10% L-lactide) surgical sutures as a pouch model. After the procedure, animals were administered with 1000 mg/kg cefazolin subcutaneously. Recipient rats were classified as (i) control (untreated), (n=7), (ii) sham (n=7), (iii) PA (n=7), (iv) islet (n=7), (v) PA+islet groups (n=7).

PA gels without islets were transplanted to serve as negative control (PA group). Sham group animals were transplanted with neither PA nor islets. Healthy rats showing normal blood glucose levels were used as a positive control. Animals in the islet group were transplanted with only islets but no PA gel. Rats were allowed to eat and drink freely after the operation and routine controls were done throughout the study for infection.

3.2.8 Scaffold Function Assessment

After transplantation, non-fasting blood glucose levels and weight of the animals were measured three times a week for 28 days. Transplantation was considered to be functional only if the blood glucose levels of the recipients were less than 300 mg/dL. Intraperitoneal glucose tolerance test (IPGTT) was performed at 28 days after transplantation to measure the effect of glucose

challenges. After fasting overnight, rats were injected with glucose solution (2 g/kg) intraperitoneally after intraperitoneal injection of anesthetic agents; ketamycin (80 mg/kg) and xylazine (10 mg/kg). Blood glucose levels were measured from the tail vein at baseline (before injection) and 5, 10, 15, 30, 60, 90 and 120 min after injection.

3.2.9 Histological Analysis

At the end of the 28 days, rats were anesthetized and transcardially perfused with saline and formaline, respectively. Omentum and pancreas tissues were collected and fixed in formalin for approximately 18 h before being embedded into paraffin. Tissues were sectioned with a Leica microtome at 5 µm thickness. Sections were deparaffinized in xylene and rehydrated in serial ethanol series for hematoxylin & eosin (H&E) staining and Masson's trichrome staining according to the standard protocol. For immunohistochemistry experiments, sections were stained with anti-insulin (1:500; Sigma), anti-macrophage (1:300; Millipore) and anti-von Willebrand Factor (1:200; Abcam) antibodies. After primary antibody staining, horseradish peroxidase conjugated goat anti-mouse secondary antibody (1:500; Millipore) was used followed by 3,3'-diaminobenzidine [93] staining. All samples were mounted onto glass slides using xylene based mounting medium. Digital images were acquired via Zeiss Axio Scope A1. For vascular density quantification, each paraffin-embedded omentum tissue was serially sectioned and 5 matching slides were selected from each tissue for quantification with approximately 100 µm intervals. Images were acquired using a 20x objective.

3.2.10 Statistical Analysis

Statistical analyses were performed using two-way ANOVA or one-way ANOVA with Bonferonni multiple comparison test. The level of significance was set at $p<0.05$ (*, $p<0.05$; **, $p<0.01$; ***, $p<0.001$). Error bars indicate standard error of mean.

3.3 RESULTS

3.3.1 Heparin Mimetic PA Molecules Self-assemble Into Nanofibers

The HM-PA was functionalized with bioactive chemical groups to mimic heparin structure and function (Figure 3.1A). Non-bioactive positively charged K-PA was synthesized in order to induce nanofiber formation through charge neutralization after mixing with HM-PA (Figure 3.1B). All peptide molecules were characterized by liquid chromatography–mass spectrometry (LC–MS) and purified by preparative HPLC (Figure 3.2 and 3.3). β-sheet-driven nanofiber elongation was provided via the VVAG motif and analyzed by circular dichroism (CD) spectroscopy. CD results showed that β-sheet structure dominates HM-PA/K-PA mixture with a negative band at 218 nm and a positive band at 195 nm (Figure 3.4). Scanning electron microscopy image demonstrated formation of a porous nanofiber network when HM-PA and K-PA were mixed (Figure 3.5A). AFM and TEM images of PA molecules revealed that nanofibers were uniform in width and were *c.* 20–30 nm in diameter (Figure 3.5B-C).

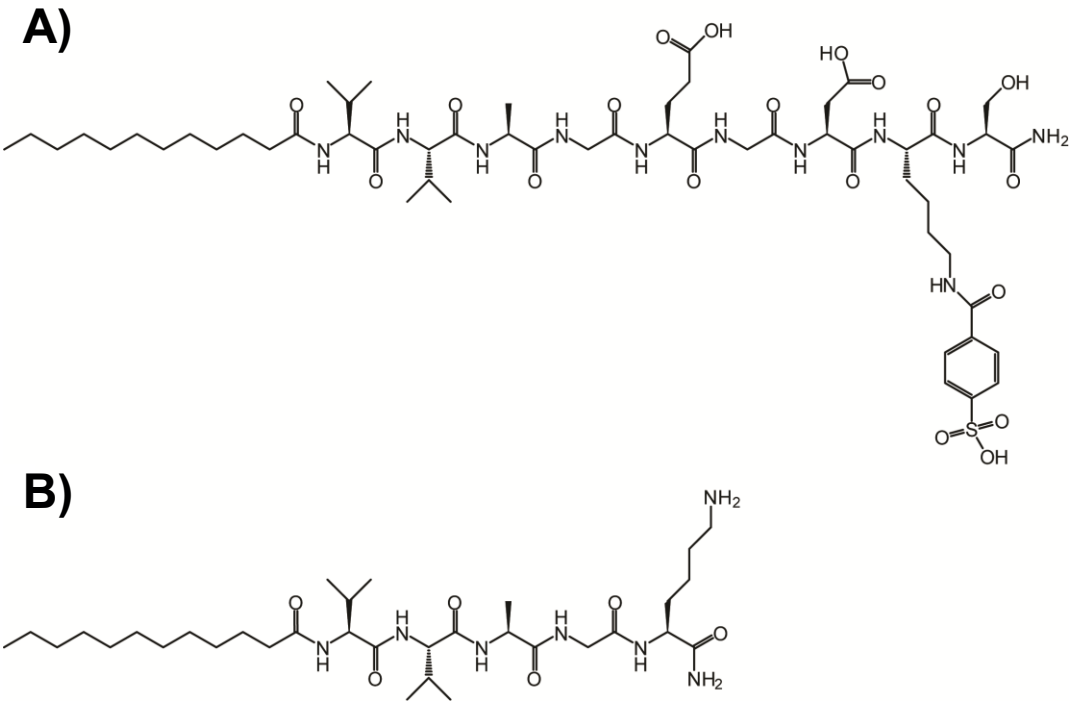

Figure 3.1 Chemical structures of peptide amphiphiles used in this study: **(A)** negatively charged HM-PA, and **(B)** positively charged K-PA.

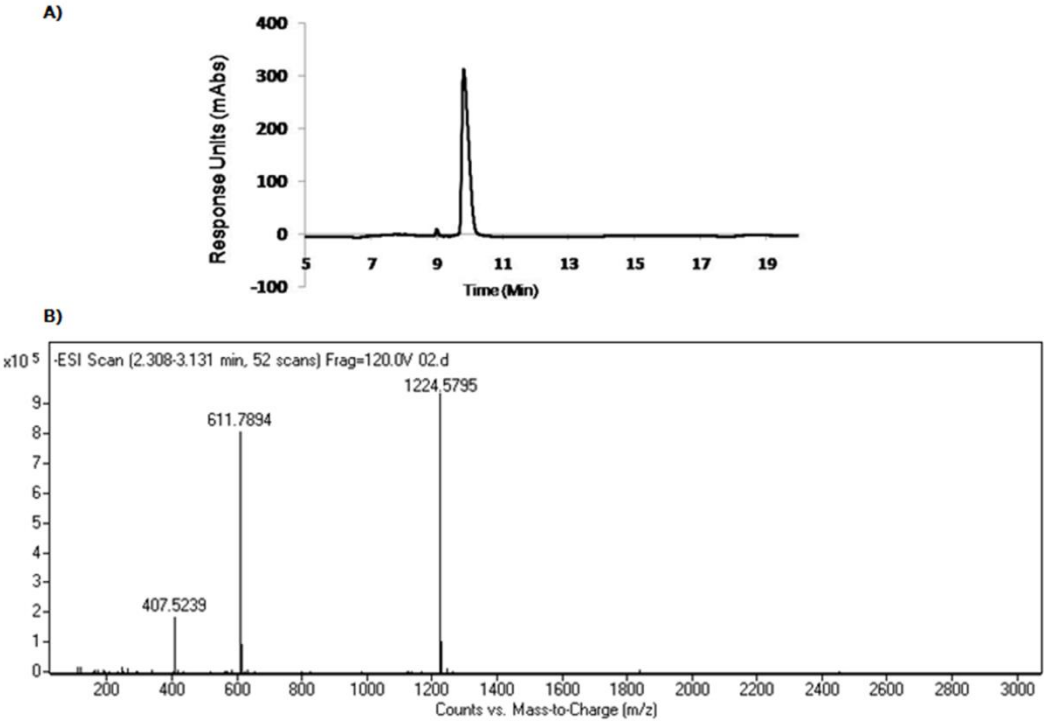

Figure 3.2 (A) HPLC chromatogram of purified Heparin-mimetic PA molecule at 220 nm. **(B)** Mass spectrometry analysis of Heparin-mimetic PA molecule. $[M-H]^-$ (observed)= 1224.59, $[M-H]^-$ (calculated)= 1224.58, $[M-2H]^{-2}/2$ (observed)= 611.76, $[M-2H]^{-2}/2$ (calculated)= 611.89.

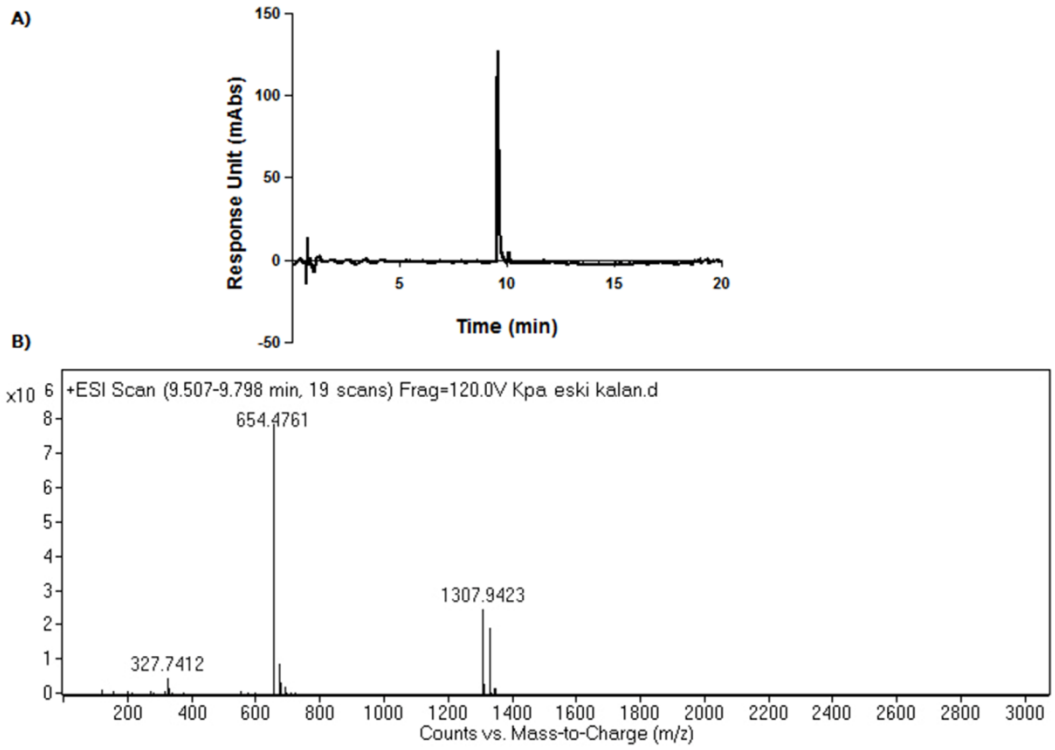

Figure 3.3 (A) HPLC chromatogram of purified K-PA molecule at 220 nm. **(B)** Mass spectrometry analysis of K-PA molecule. $[M+H]^+$ (observed)= 654.49, $[M+H]^+$ (calculated)= 654.49, $[2M+H]^+$ (observed)= 1307.98, $[2M+H]^+$ (calculated)= 1307.96.

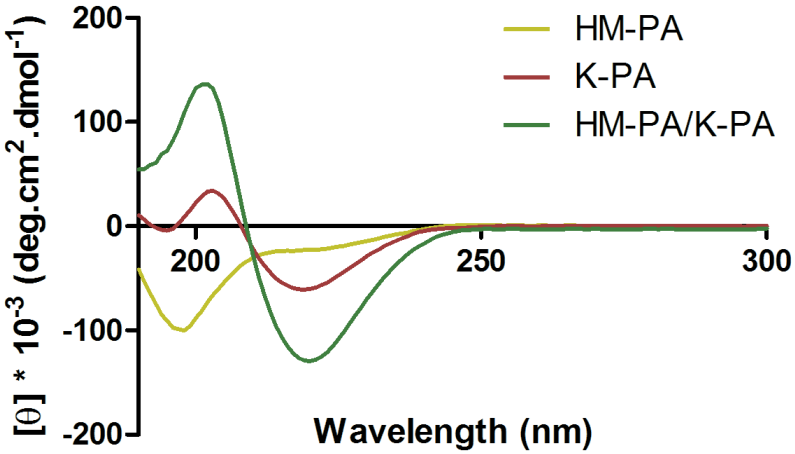

Figure 3.4 Circular dichroism spectra of the peptide amphiphile molecules. The PA nanofibers showed characteristic β-sheet structure at physiological pH.

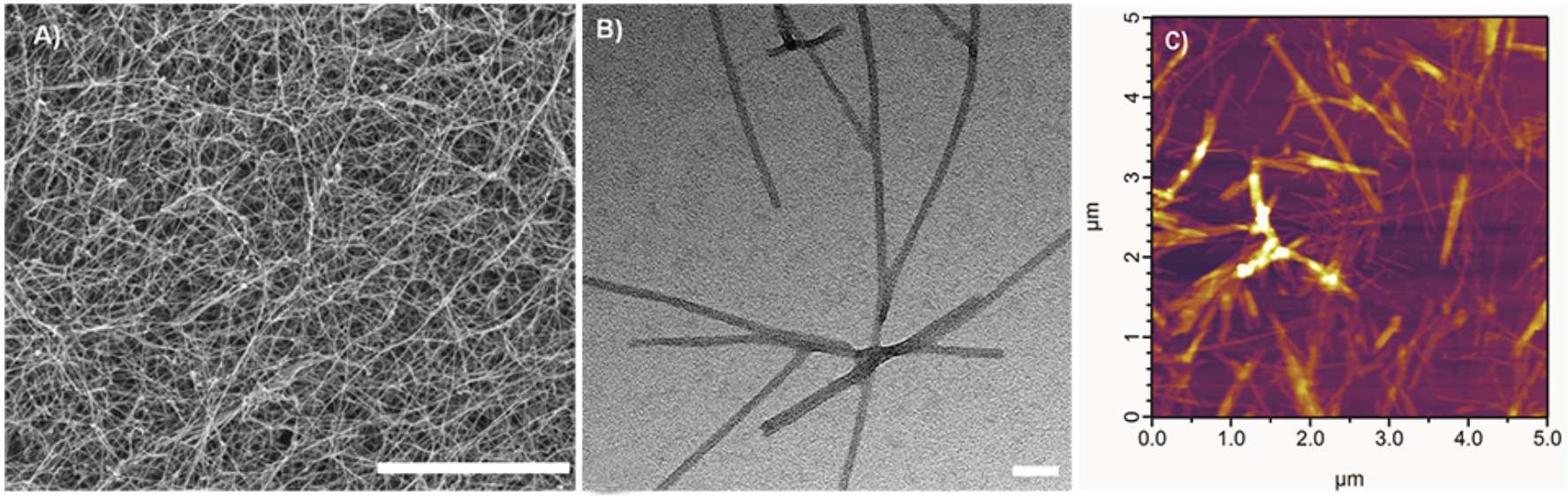

Figure 3.5 Characterization of peptide amphiphile nanofiber and scaffolds at pH 7.4 by using: **(A)** Scanning electron microscopy, **(B)** Transmission electron microscopy, and **(C)** Atomic force microscopy. Scale bars are 5 µm **(A)** and 50 nm **(B)**.

3.3.2 HM-PA Improves Function of Islets *In Vitro*

A viability analysis was performed to investigate the effect of HM-PA on pancreatic islets. Viability of cultured islets sized between 100-200 μm in diameter was determined over a 7-day period using Alamar Blue assay. In a previous study, HM-PA was shown to have a high binding affinity to VEGF, and FGF-2 [253]. Since FBS contains high amounts of growth factors [255], evaluation of islet viability and function was performed in serum-free conditions 100 ng of FGF-2 and VEGF were added to culture media where indicated, in order to assess the effect of growth factor supplementation. During 7 days of culture, although islets tended to cluster in other groups, islets cultured with HM-PA/K-PA nanofibers did not form clusters (Figure 3.6). Viability measurements indicated that HM-PA/K-PA combinations with and without growth factors showed higher viability at day 1 and day 3 (Figure 3.7). However, day 7 results were similar between all experimental groups.

It is known that increased cellular viability or activity does not indicate enhanced functionality because of the tendency of islets to lose their insulin release capabilities [256]. Thus, insulin release capacities of cultured islets in response to different glucose concentrations were measured with an ultrasensitive rat insulin ELISA (Figure 3.8). After 1 day of culture, HM-PA and the combination of HM-PA and growth factors had 5.7 ($p<0.001$) and 4.9 ($p<0.01$) times greater glucose stimulation indices (GSI), respectively, compared to the freshly isolated islets (Figure 3.8A). At day 3, though all experimental groups displayed decreased value of GSI compared to day 1, islets cultured with HM-PA/K-PA and GFs had highest GSI (not statistically

significant) (Figure 3.8B). However, after 7 days, islets cultured with HM-PA/K-PA and GFs showed a GSI of 0.98 which was similar to freshly isolated islets (1.25) (Figure 3.8C).

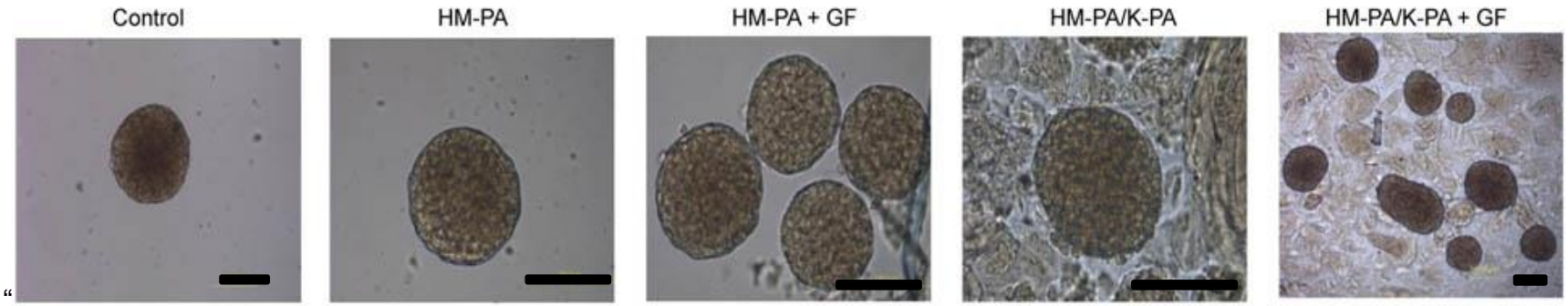

Figure 3.6 Morphology of pancreatic islets cultured with HM-PA, HM-PA with growth factors (GF), HM-PA/K-PA, HM-PA/K-PA growth factors at day 7. Scale bars are 100 µm. (GF = VEGF + FGF-2).

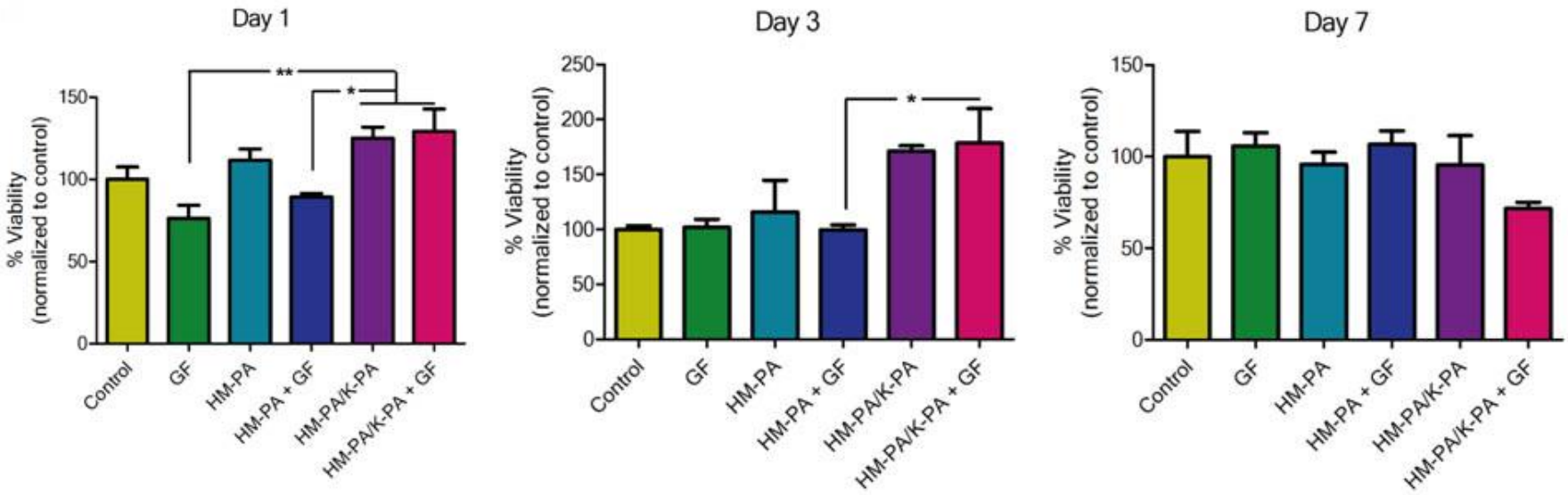

Figure 3.7 Viability analysis of the islets seeded on different PA hydrogels with or without growth factor (GF) by using the Alamar blue assay at **(A)** day 1, **(B)** day 3 and **(C)** day 7 (GF = VEGF + FGF-2).

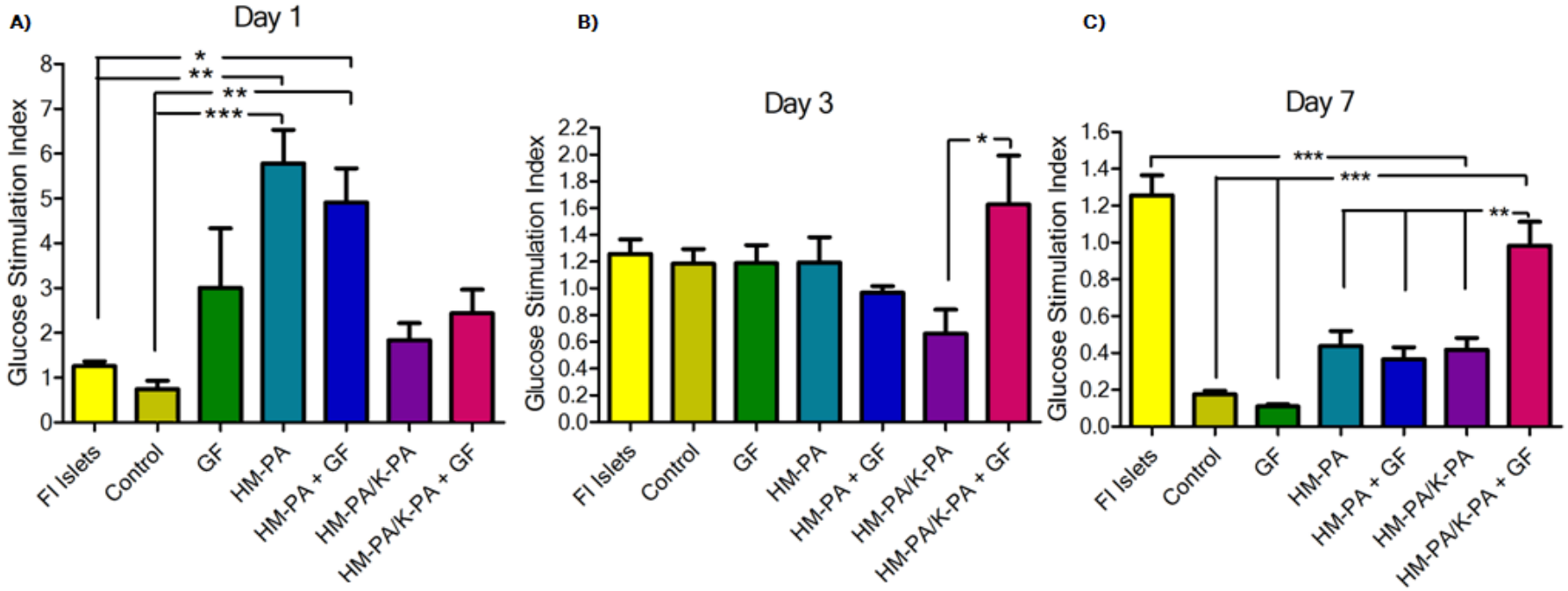

Figure 3.8 Results of glucose stimulation test at **(A)** day 1, **(B)** day 3, and **(C)** day 7. Islets cultured with HM-PA/K-PA nanofiber containing media preserved their insulin secretion capability for 7 days better than other groups (GF = VEGF + FGF-2).

3.3.3 Transplantation within Bioactive PA Scaffold Improves Glucose Responsiveness of the Transplanted Islets

Islets with or without PA gel were transplanted into the omentum of STZ-induced diabetic rats under general anesthesia. For transplantation, the omentum was reached through the abdominal cavity with a small incision. Islets with or without PA gel scaffold were placed onto it, and finally they were sewed together as a pouch (Figure 3.9 A-D). No complications were observed during and after the surgery. Blood glucose levels of recipient rats (n=7) are shown in Figure 3.10. When islets were transplanted with PA scaffold, 2 out of 7 recipients maintained normal glucose level and 4 out of 7 had blood glucose levels less than 270 mg/dL over the course of 28 days. “Only islets” group showed higher blood glucose levels than “islets with PA scaffold” group. Weight of the animals in all experimental groups did not show significant change during 28 days (Figure 3.11).

To investigate the glucose responsiveness of animals transplanted with islets and PA scaffold, we performed intraperitoneal glucose tolerance test (Figure 3.12). The blood glucose level was increased at 90 min after glucose administration, followed by a decrease after that point for both “control” and “islets transplanted with PA scaffold” groups. However, the other experimental groups did not show this blood glucose level pattern.

Although blood glucose levels typically start decreasing within 30 min in IPGT tests, no such trend was observed in our experimental groups, except for a very slight decrease in the control group. This was probably caused by the

administration of general anesthetics ketamycin and xylazine, which are known to interfere with IPGTT results [257].

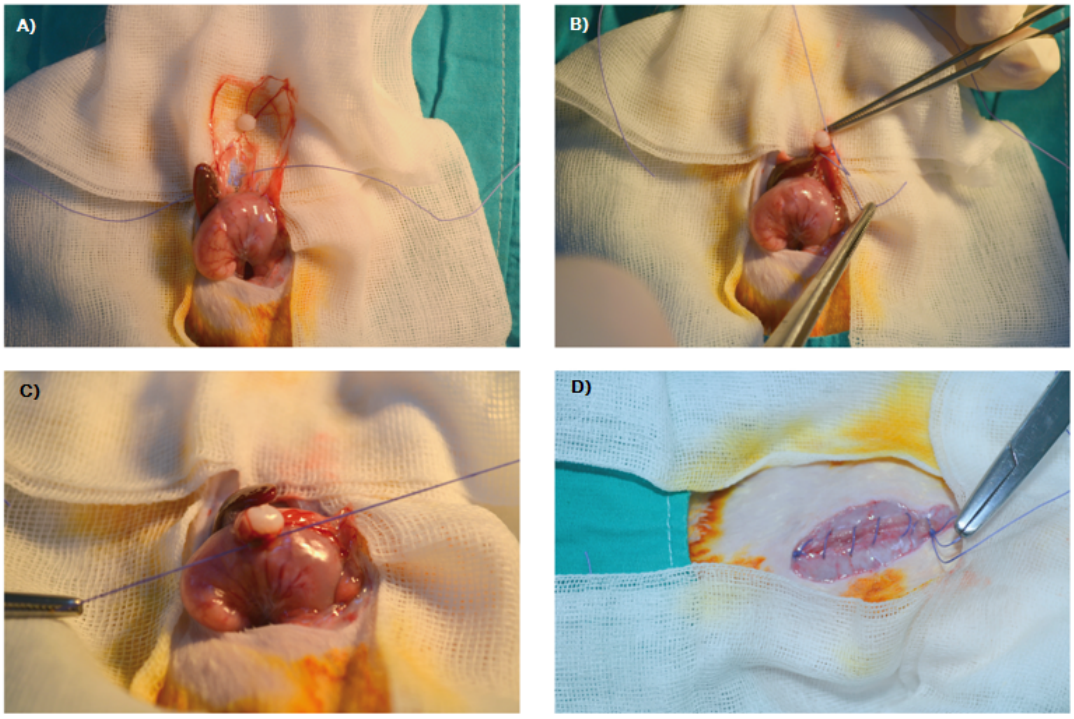

Figure 3.9 Technique used to implant peptide amphiphile gel into the omentum of rats. The greater omentum was spread onto a sterile gauze pad and cargo (unless it was sham) containing PA gel, islet or their combination was placed onto it **(A)**. The omentum was sutured like a pouch without disturbing the transplanted cargo **(B)**. The Omentum and stomach were placed back into the abdomen **(C)** and the abdomen was sutured **(D)**.

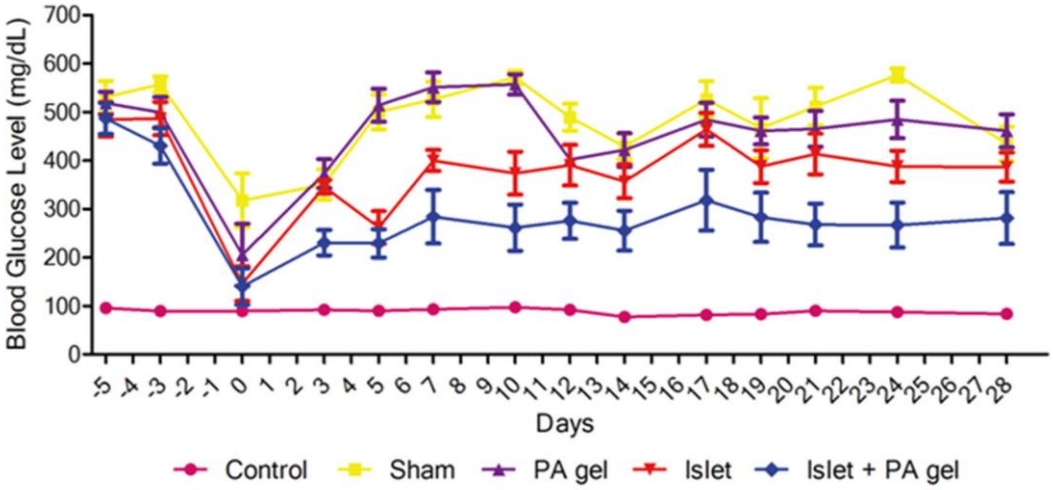

Figure 3.10 Blood glucose levels were measured 5 days before and throughout 28 days after transplantation. (Day 0; transplantation day).

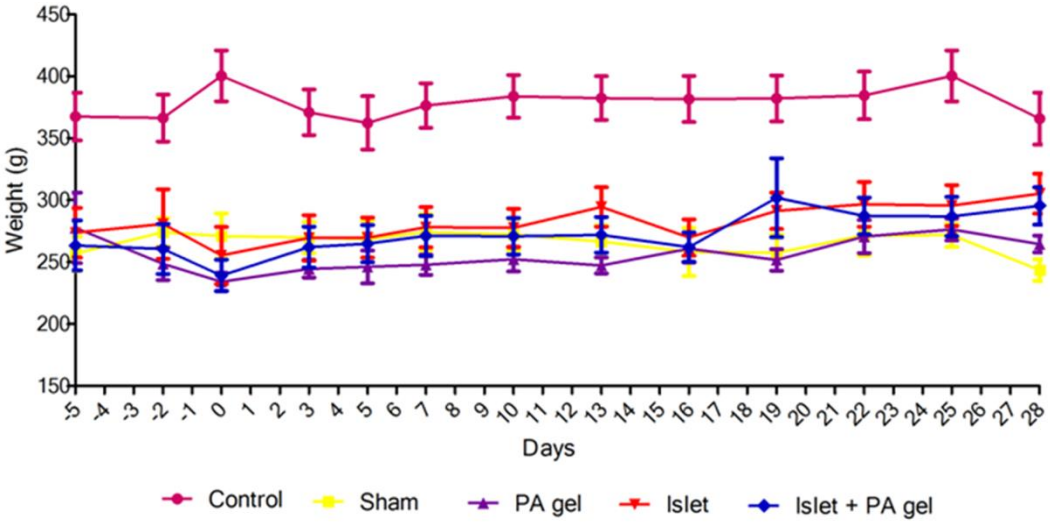

Figure 3.11 Change of weight of animals during 28 days.

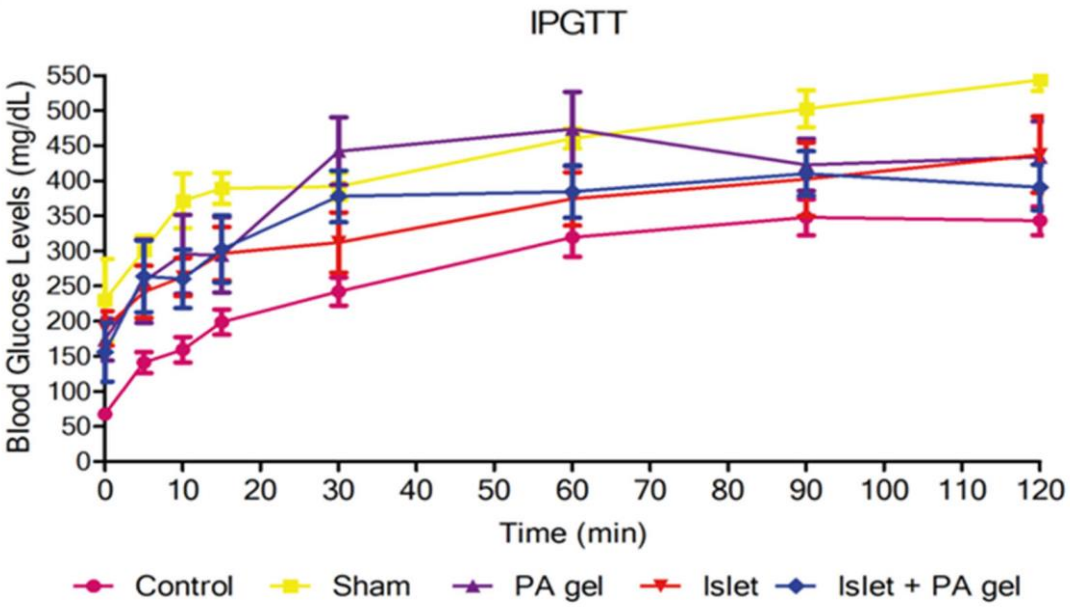

Figure 3.12 Intraperitoneal glucose tolerance test (IPGTT) at the end of 28 days.

3.3.4 PA Scaffold Supports Islet Integrity and Enhance Vascular Density of the Transplantation Site

In order to monitor morphology of the transplanted islets, **H&E** and Masson's Trichrome stainings were carried out on omentum sections. H&E staining revealed that "peptide gel only" transplanted group showed regular omentum morphology and some peptide gel was still observable in the omentum (Figure 3.13 A-B) although most of the gel was degraded. The transplanted islets were observed to be more intact and had normal morphology in the group where islets were transplanted with PA gel, compared to only islet group (Figure 3.13 C-D). This result shows that PA gel helps islets to maintain their integrity. Masson's trichrome staining suggests that collagen is present in the islets belonging to "only PA", "only islet" and "islets in PA gel"

groups, indicating fibroblast action around the transplantation site (Figure 3.14 A-D).

Immunohistochemical stainings showed that viable islets at the transplantation site were positive for insulin, indicating that they were still functioning, and islets transplanted with PA gel were more intact (Figure 3.15). Immunological response was visualized with macrophage staining. Macrophage presence was observed to be more extensive around the islets in “only islet” group compared to the “islets in PA gel group” (Figure 3.16).

In order to observe blood vessels in omenta, anti-von Willebrand Factor staining was performed, as a vascular endothelial cell marker (Figure 3.17). Newly formed blood vessels within the PA gel and islets were observed in “PA only”, “islet only” and “islets in PA gel” groups (Figure 3.17 B-D). We also assessed the number of intraomental vascularization with 10 images of per section and in a total of 5 sections from the omentum of each animal (Figure 3.17 E). This assessment revealed “only PA” and “islets in PA gel” groups had significantly more intraomental vessel number than other groups. Additionally, there was a significant difference between sham group and groups containing PA ($p<0.001$), which demonstrate that PA itself promotes vascularization. The absence of statistical difference between “sham” and “only islet” groups and presence of statistically significant difference between “only islet” and “islet with PA groups” ($p<0.05$) proved the fact that increased vascularization was induced by HM-PA.

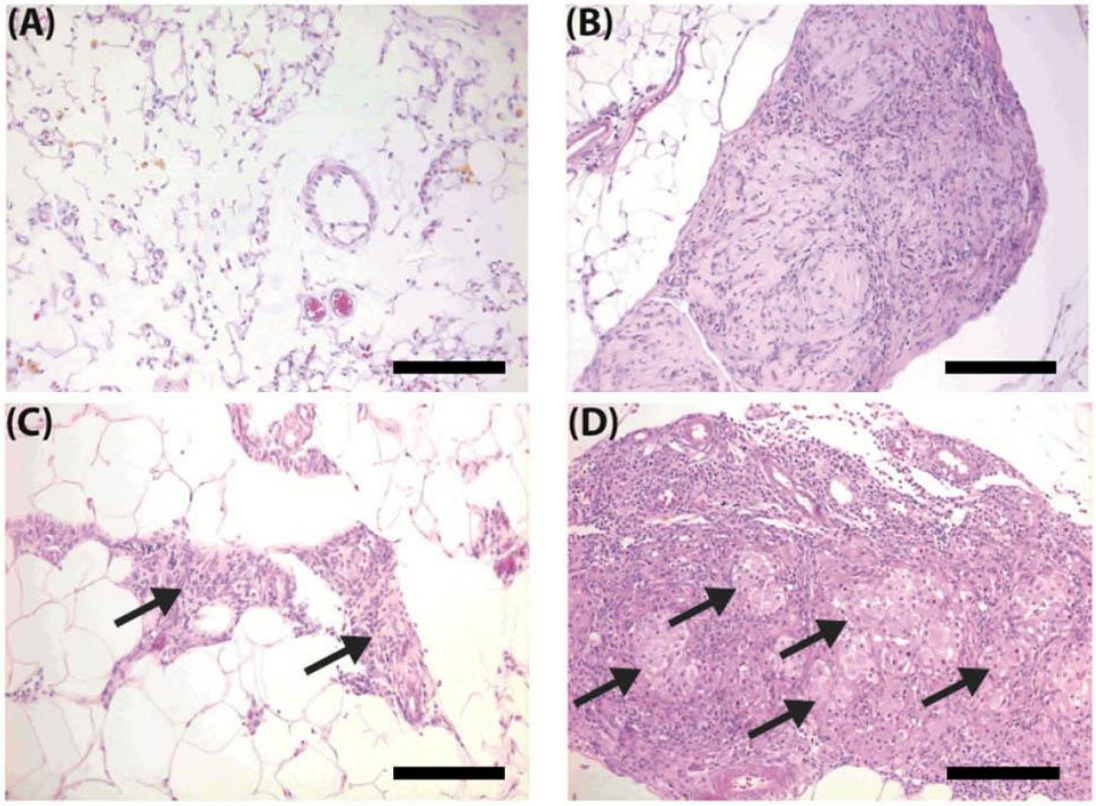

Figure 3.13 H&E staining of **(A)** Sham, **(B)** PA hydrogel, **(C)** Islet, and **(D)** Islet + PA hydrogel groups. Islets transplanted with PA gel conserved their morphology and integrity on post-transplantation day 28. All images were taken at 200X magnification. Scale bars are 100 μm.

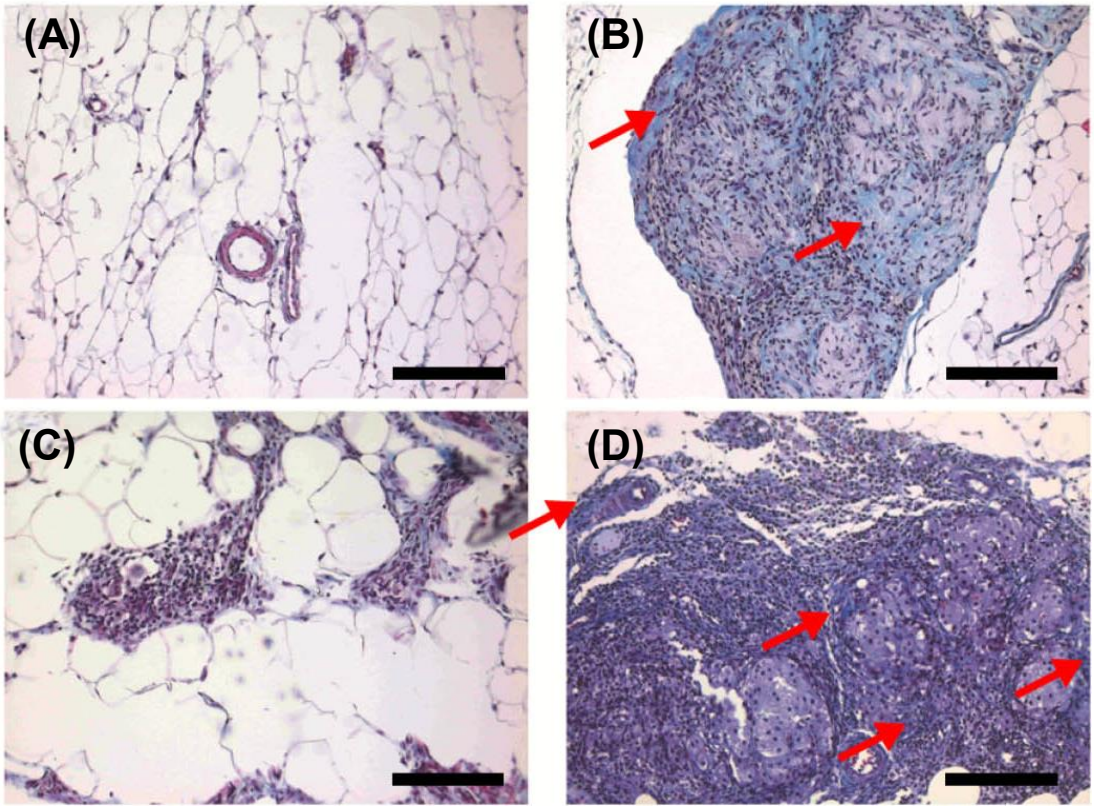

Figure 3.14 Masson's trichrome staining of **(A)** Sham, **(B)** PA hydrogel, **(C)** Islet, and **(D)** Islet + PA hydrogel groups. Staining showed collagen expression around the transplantation site on post-transplantation day 28. Arrows show transplanted islets. All images were taken at 200X magnification. Scale bars are 100 μm.

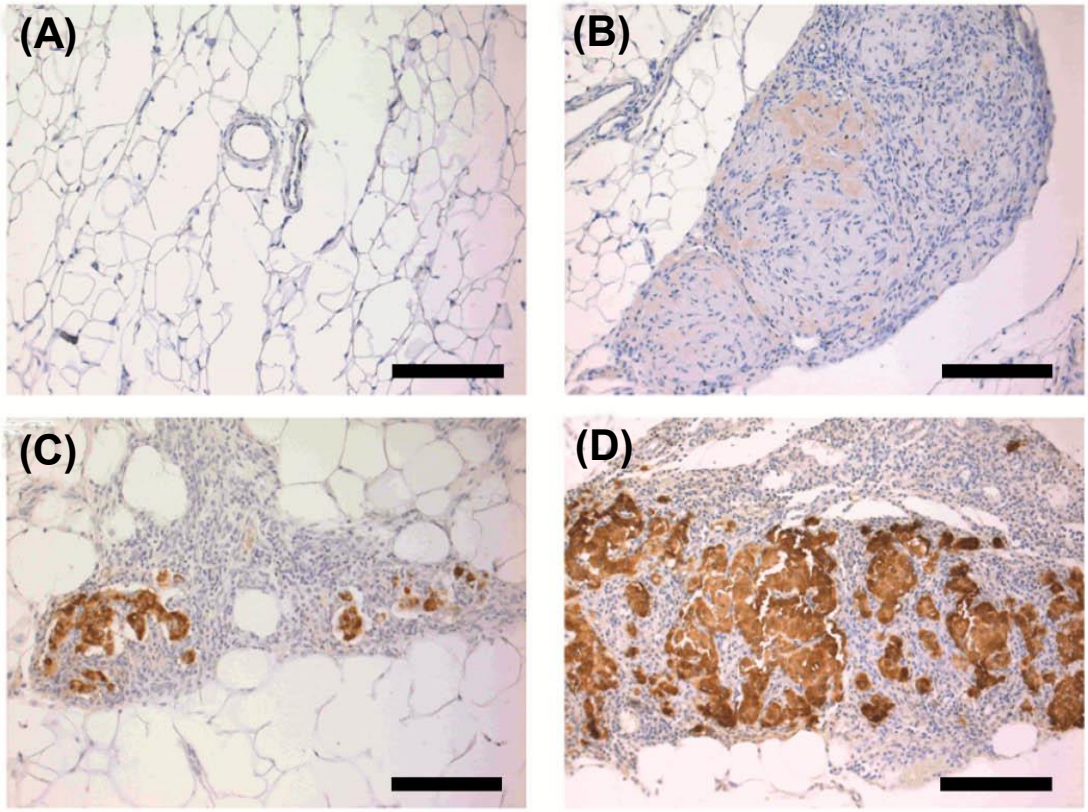

Figure 3.15 Immunohistological staining of **(A)** Sham, **(B)** PA hydrogel, **(C)** Islet, and **(D)** Islet + PA hydrogel groups using anti-insulin antibody. All images were taken at 200X magnification. Scale bars are 100 μm.

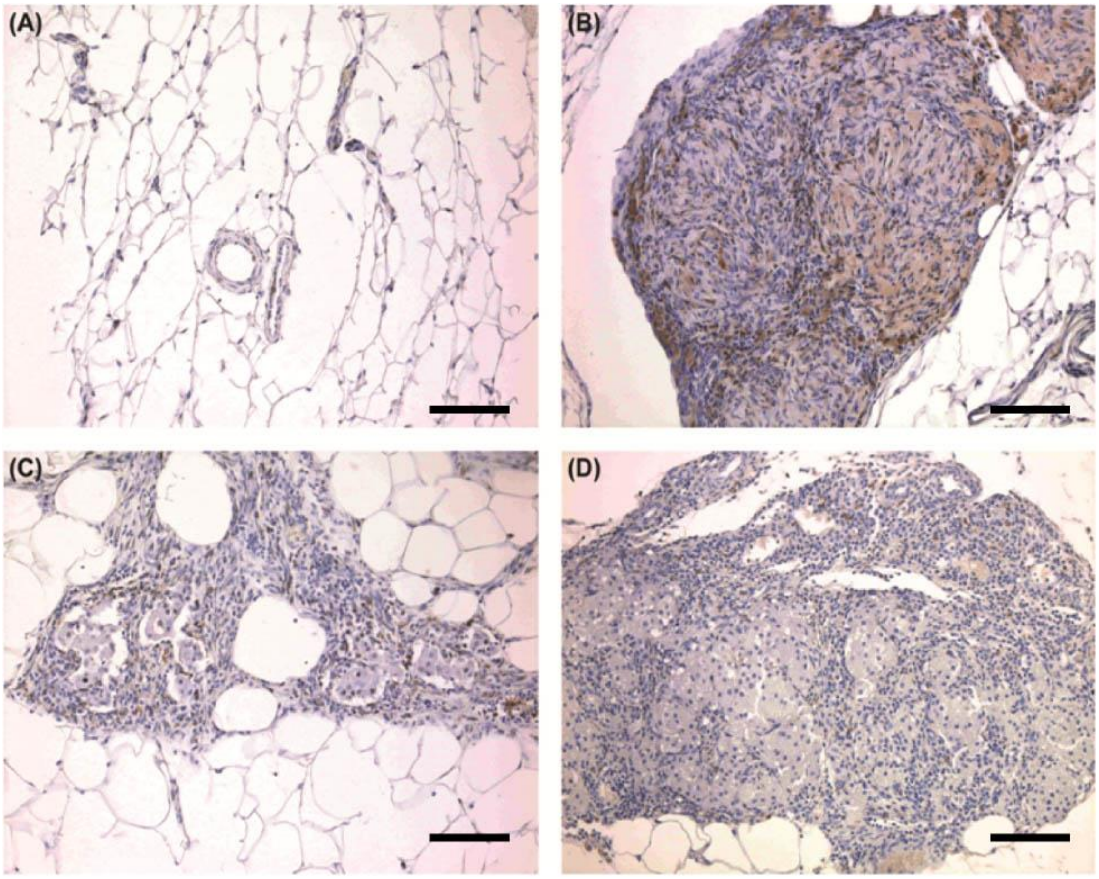

Figure 3.16 Immunohistochemical staining of macrophages in omenta. Representative sections obtained from **(A)** Sham, **(B)** PA hydrogel, **(C)** Islet, and **(D)** Islet + PA hydrogel groups. All images were taken at 200X magnification. Scale bars are 100 µm.

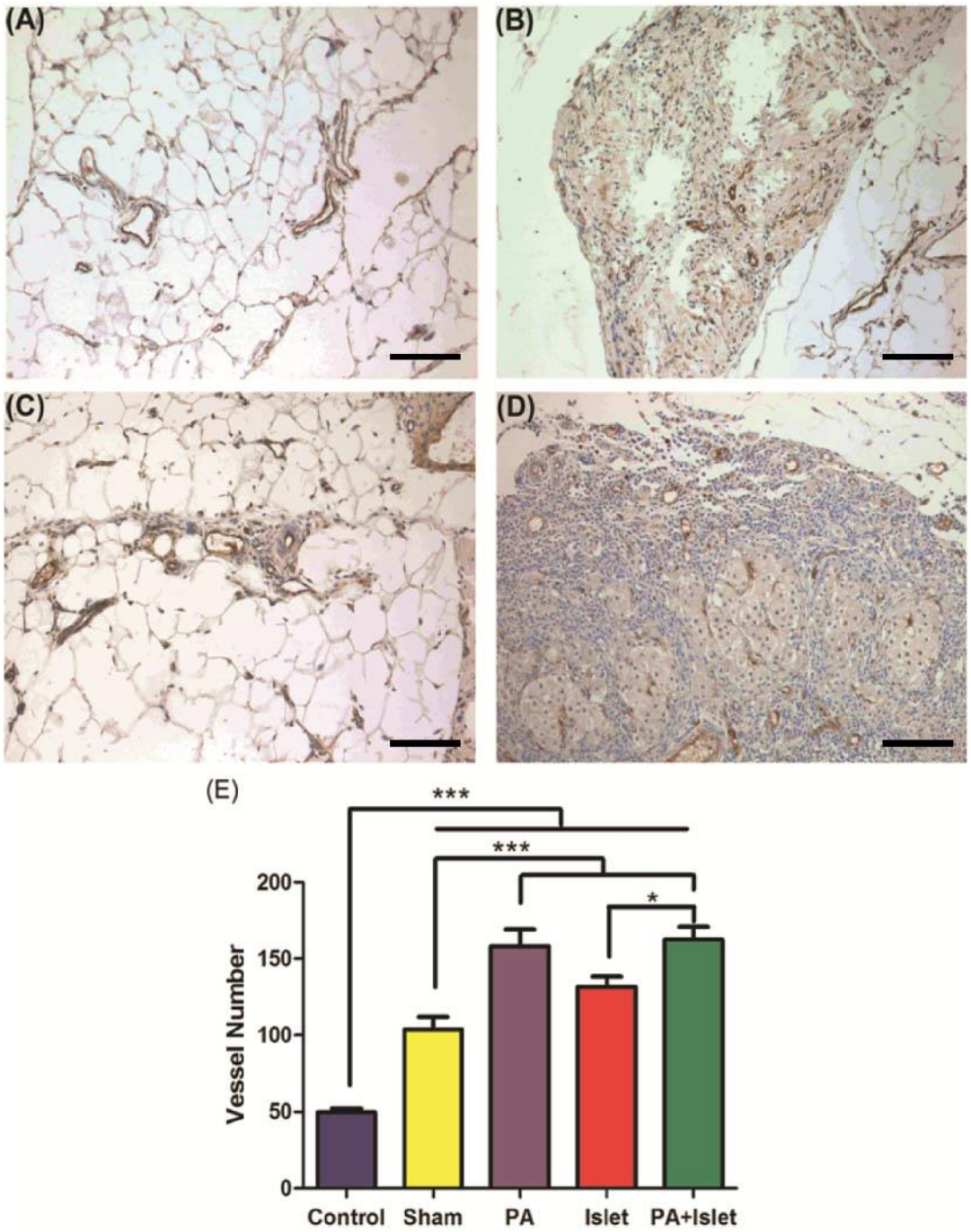

Figure 3.17 Immunohistochemical staining of blood vessels by using anti-von Willebrand Factor in the omenta and quantification of blood vessels. Representative sections obtained from **(A)** sham, **(B)** PA hydrogel, **(C**) islet, **(D)** islet+PA hydrogel groups, and **(E)** average blood vessel number. All images were taken at 200X magnification. Scale bars are 100 µm.

3.4 DISCUSSION

Islet transplantation is currently the most promising therapeutic method for diabetes treatment. Angiogenesis is crucial for viability and functionality of islets after transplantation. In this study, we utilized a bioactive peptide nanofiber system for enhancing viability and functionality of islets *in vitro* and *in vivo*. These nanofibers are formed through self-assembly of short peptide amphiphile molecules (HM-PA) that were designed to mimic heparin, since heparin is important in angiogenesis and growth factor binding. HM-PA was previously shown to enhance angiogenesis *in vitro* and *in vivo* through its interactions with heparin-binding proangiogenic growth factors and their receptors [258]. In this work, we used a positively charged peptide amphiphile, K-PA, which is designed to induce nanofiber formation when mixed with negatively charged HM-PA via electrostatic interactions and hydrophobic collapse at physiological pH [154]. Secondary structure characterization proved that β-sheets drive the nanofiber formation (Figure 3.4) [259].

Pancreatic islets are normally surrounded by ECM elements to provide mechanical support and cellular signaling in the normal pancreas. Because it affects the metabolic activity, it is important to preserve the morphology and integrity of the islets in *in vitro* conditions prior to the transplantation process[260]. Moreover, vascular network integrity and cell-matrix interactions are diminished during isolation, resulting in a decrease in metabolic function [261]. Thus, scaffold and materials that can enhance islet viability and function prior to and during transplantation process will be extremely valuable for the success of diabetes therapy. While designing materials to mimic the natural

ECM, it is important to consider not only to provide cells the necessary mechanical support, but also to have enough porosity to be able to make them reach required components in microenvironment. The natural nanofibers comprising the ECM network are formed by glycosaminoglycans and other fibrous and non-fibrous biomolecules [262]. In this study, we utilized glycosaminoglycan mimetic peptide nanofiber scaffolds to provide the required support and retain islet shape without causing any toxic effect (Figure 3.7). In this way, cultured islets maintained their glucose-responsive insulin secretion capability to an extent comparable to freshly isolated islets. We observed increased viability of cultured islets at days 1 and 3 when kept in the HM-PA/K-PA combinations. The similarity between all experimental groups at day 7 could have been caused by culturing in serum-free media, since all in vitro experiments were performed in serum-free conditions to eliminate external effects of serum, which contains several growth factors, proteins and transcription factors (Figure 3.8) [256, 263]. However, although islets showed similar viability profiles between groups at day 7, the islets cultured in HM-PA/K-PA nanofiber containing media showed significant enhancement of functionality compared to other groups, assessed by glucose stimulation assay. The surprising similarity between the responses of islets cultured in HM-PA/K-PA nanofiber containing media for 7 days and freshly isolated islets shows the effectiveness of this nanofiber system for *in vitro* preservation of pancreatic islets. Previously, it was shown that bioactive scaffolds such as collagen, fibrin or fibronectin increase the insulin secretion of islets [135, 246]. In addition, when growth factor cocktails are added into the system, islets can

maintain their spherical morphology and give highest insulin secretion [247]. It is also known that islet damage reflects as diminishing of insulin. Bennet et al. showed that when islets are cultured with heparin, the islet damage was reduced [264]. The success of our day 7 results may arise because our system has both heparin mimetic bioactive peptide scaffold and growth factors. Encouraged by these *in vitro* findings, our heparin mimetic gel system was analyzed for their effectiveness as a scaffold system for islet transplantation *in vivo*.

The omental pouch model (Figure 3.9) was used for transplantation [265], since, transplantation of islets to omental site both protects them from high blood pressure and provides large transplantation volume [244]. After transplantation, islets transplanted within HM-PA decreased blood glucose levels more than “only islet” transplanted group (Figure 3.10). Furthermore, intraperitoneal blood glucose tolerance test performed 28 days after transplantation revealed that “islets transplanted with PA gel” display similar pattern with healthy control group; however, this pattern was not observed in sham group and “islet only” group (Figure 3.11).

Morphological analysis of the integrity of islets by H&E staining showed that “islets with PA gel” group preserved their original shape, while “only islet” group did not. Correlation between morphological integrity and functionality was previously shown and the morphological integrity of the transplanted islets might have contributed to better glucose responsiveness of the “islets with PA gel” group [260].

Insulin secretion was shown by immunohistochemical staining that has proved functionality of the islets both in “only islet” and “islet with PA gel” groups, however, strikingly insulin secretion was enhanced in “islets transplanted with PA gel” compared to “islet only group” (Figure 3.15). This result also supports correlation between preservation of integrity and enhanced functionality, which was assessed by insulin secretion of the islets that was provided by PA gel.

In healthy individuals, islets of Langerhans are surrounded by a collagen matrix [258, 260]. Enhanced collagen deposition after transplantation due to PA gel regardless to islet existence was observed with immunohistochemistry analyses. Collagen deposition might trigger formation of extracellular matrix composition for the islets similar to natural microenvironment after transplantation and therefore enhance transplantation efficiency (Figure 3.16 B, D). Macrophage staining showed that there was relatively less macrophage concentration around islets with PA gel compared to only islet group (Figure 3.17). Reduced macrophage infiltration after surgery might prevent excess cell death, help to maintain islet integrity and functionality retain the insulin secretory capacity, and lower blood glucose levels for a longer period. Implantation of the PA alone resulted in a more intense immune response (macrophage infiltration) than transplantation of islets in PA gel or transplantation of islets only. This might have resulted because the release of various cytokines from injured islets prevents macrophage recruitment to the transplantation site [52, 92, 266-268].

Anti-von Willebrand staining was used to demonstrate vascularization inside and around the islets, and in the omentum when PA gel was applied or not (Figure 3.17 B-D). After counting blood vessels for all animals in all groups, it was clarified that PA gel also promotes vascularization *in vivo* (Figure 3.17 E). The significant difference between vessel number in only islets and islets with PA gel groups can be resulted from the ability of HM-PA to bind growth factors, concentrate them, and serve to the cells in excess amount as previously shown [253, 255]. In islet transplantation, number of blood vessels in transplantation site is an important issue. In order to increase transplantation efficiency, get faster response in case of elevated glucose concentration, and supply enough oxygen and nutrients to the islets, the blood vessel number needs to be high in the transplantation sides. Mammadov et al. previously showed that HM-PA enhances tube formation by endothelial cells *in vitro* compared to Matrigel® [255]. That provides an explanation for our *in vivo* vascularization result which examines vessel numbers and their relativity to both control and sham groups. With PA gel system, it was shown that vascularization in the omenta of animals can be increased; and when this system is used with islets in transplantation operation for T1D treatment, it increases the efficiency and stabilizes blood glucose level more effectively compared to bare islet transplantation.

3.5 CONCLUSIONS

In order to increase the islet transplantation efficiency, it is important to maintain required environment for survival and function of islets both *in vitro* and *in vivo*. Herein, we presented a bioactive peptide amphiphile nanofiber gel

platform for islet culture and transplantation. Chemical and physiological characterization studies of PAs showed that they can be used as synthetic ECM mimicking agents with their nanofibrous structures. Our results demonstrated that PA gel provided a potent environment, diffusion and mechanical support for viability and function of islets. Under serum-free condition, PA gel with VEGF and FGF-2 provided GSI of fresh isolated islets even after the 7 days of culture. These findings indicate that PA gel can be used for long-term culture of islets until the transplantation.

Furthermore, *in vivo* results show that islet transplanted with PA scaffold reduced the blood glucose level of STZ-induced diabetic rats when compared to the only islet transplantation group. This finding showed that this supportive and bioactive scaffold can increase the transplantation efficiency. The histological analyses also proved longtime insulin secretion from the islets transplanted with HM-PA gel and increased vessel numbers in groups which contain HM-PA gel. Blood vessel quantification clearly indicated that bioactive PA scaffold triggers angiogenesis without any external stimuli. This result can be explained by HM-PA-triggered angiogenesis both *in vitro* and *in vivo* due to affinity of this supramolecule to the growth factors which are key elements of angiogenesis and its ability to increase the local concentrations of them. The overall findings imply that HM-PA scaffold is a promising strategy for both islet culture and transplantation.

CHAPTER 4

ANGIOGENIC HEPARIN-MIMETIC PEPTIDE NANOFIBER GEL IMPROVES THE REGENERATIVE HEALING OF ACUTE WOUNDS

4.1 INTRODUCTION

Lacerations, crushes, punctures and other types of trauma may cause long-lasting wound injuries in patients of any age. Wounds are defined as any break in tissue integrity that results in damage to tissue structure and functionality. The integrity of the damaged tissue should be recovered in a rapid process to prevent infection and loss of body fluids and provide homeostasis [269]. A complex process, called wound healing, occurs in all tissue types through a similar set of signaling cascades and cell-cell and cell-matrix interactions [270]. In addition to facilitating the recovery process, wound healing also encompasses the reversion of cell-proliferation signals required to prevent the excessive amplification of repair-associated responses [271].

Wound healing is a series of overlapping events and contains a variety of cellular activities, including homeostasis, inflammation, proliferation (angiogenesis, granulation, re-epithelialization) and remodeling [269, 272]. Immediately after injury, degranulated platelets and serum from damaged blood vessels release a plethora of growth factors and cytokines to promote cellular activation for tissue regeneration [273]. Blood clot formation occurs as a result of the interactions between aggregated platelets, cross-linked fibrin and some ECM elements such as fibronectin, vitronectin, and thrombospondin [274-275]. Apart from being a barrier to the external effects such as pressure and infection, the blood clot also serves as a provisional matrix for cell migration and proliferation at the injury site [270]. Release of platelet-derived growth factor (PDGF) and TGF-β in particular triggers the migration of neutrophils, macrophages, smooth muscle cells and fibroblasts towards the

wound bed [271, 276]. Cells in the inflammation phase are responsible for sterilizing the area and secreting the growth factors and cytokines that are required to initiate the proliferation phase. This phase encompasses a set of events that partially restore tissue function and structure through the re-establishment of a new epithelial layer by keratinocytes and the filling of the injury site with a vascular network- and collagen-rich granulation tissue. During the proliferation phase, fibroblasts are the predominant cell type and are responsible for collagen deposition. However, the secretion of abundant amounts of collagen can cause fibrosis while the lack of collagen production results in a loose wound structure [277]. Angiogenesis promotes the formation of massive blood vessels at the wounded site and allows the transmission of oxygen, nutrients, growth factors and cytokines to cells, thereby facilitating their metabolic activities. Following the initial phase of wound closure, the remodeling phase starts to form a mature scar, which lasts 6 to 12 months [278]. In addition, collagen type III (which is the predominant collagen at early stages of wound healing) is gradually replaced by collagen I [279], and the blood vessels are resorbed [280]. Nonetheless, the mature scar does not exhibit the structure and tensile strength of healthy skin even after the healing process is fully completed [274].

Blood vessel formation is one of the crucial steps in wound healing, as it is necessary to restore the cellular supplies of oxygen and nutrients. Lack of vascularization may therefore create delays in wound healing [274]. This complex process is carried out through both angiogenesis (extension of

existing blood vessels) and neovascularization (*de novo* formation of new blood vessels) [269].

Wounding causes hypoxia and triggers the release of FGF-2 and VEGF from macrophages and epidermal cells, respectively [281]. These growth factors stimulate endothelial cells to secrete plasminogen activator, which converts plasminogen to plasmin, and procollagenase, which activates collagenase for the degradation of the basement membrane. Endothelial cells also migrate from the degraded basement membrane and form new blood vessels. Immediately after wounding, the permeability of existing blood vessels to endothelial cells is increased by histamin, VEGF, nitric oxide and angiopoetin [282], allowing endothelial cells to localize into the perivascular space. Endothelial cell migration is also promoted by collagen degradation through the activity of matrix metalloproteinase-2, which is activated by FGF-2-induced integrin [283]. In addition, heparan sulfate proteoglycans in the ECM participate in blood vessel formation by binding to these angiogenic growth factors [284-286]. Since they carry functional groups (such as hydroxyls, carboxyls and sulfates), these proteoglycans also serve as an additional source of VEGF and FGF-2 and protect them from degradation [287]. Zhou *et al.* showed that the absence of heparan sulfate causes impaired wound healing [288]. Moreover, peptide amphiphile scaffolds decorated with heparin-binding groups were shown to promote angiogenesis through enhancing the interactions of growth factors with their receptors [191, 289].

Peptide amphiphile molecules are next generation materials that activate cellular responses through their bioactive peptide epitopes and structures.

These hydrocarbon chains bear amino acid sequences that are able to form nanofibrous structures through self-assembly mechanisms, and can physically mimic the extracellular matrix [290]. Self-assembling peptide amphiphiles are promising scaffolds due to their biocompatible and biodegradable features, which have been utilized to enhance neural [157], bone [251], cornea [163] and cartilage [188] regeneration.

In this study, we describe the potential of a heparin mimetic peptide amphiphile (HM-PA) hydrogel system to facilitate skin injury repair in an acute wound model. HM-PA nanofibers have the ability to trigger formation of capillary-like structures in endothelial cell culture even in the absence of external angiogenic growth factors and heparin molecules. In addition, the scaffold induces angiogenesis in cornea, which normally lacks blood vessels [253]. HM-PA fibers also bind to heparin-binding growth factors such as VEGF and FGF-2, which are key growth factors in angiogenesis. This effect increases the local concentrations of these molecules and promotes angiogenesis until the PA scaffold is degraded [255]. Here, the HM-PA scaffold was tested on a full-thickness rat acute wound model to determine whether its angiogenesis-promoting properties are effective in facilitating wound repair. The scaffold is able to enhance the healing by triggering the newly formed blood vessels at the injury site. The structural regeneration of the wounded area was quantified through wound closure; granulation tissue, epithelial tissue formation and angiogenesis assays to investigate the effect of HM-PA treatment on the regeneration process. HM-PA treated wounds were shown to have a well organized granulation tissue. In addition, higher blood vessel

densities and re-epithelization rates were observed following HM-PA treatment, while granulation tissue formation decreased on day 14 post wounding, suggesting that the peptide matrix is able to increase the rate of wound repair.

4.2 MATERIALS & METHOD

4.2.1 Materials

9-Fluorenylmethoxycarbonyl (Fmoc) and other protected amino acids, lauric acid, [4-[α-(2',4'-dimethoxyphenyl) Fmoc-amino methyl] phenoxy] acetomidonorleucyl-MBHA resin (Rink amide MBHA resin), 2-(1H-Benzotriazol-1-yl)-1,1,3,3- tetramethyluronium hexafluorophosphate (HBTU), and diisopropylethylamine (DIEA) were purchased from Merck. Alginate was purchased from NU-DERM® Alginate (Systagenix). All chemicals were used as provided.

4.2.2 Synthesis and Purification of Peptide Amphiphile Molecules

In this project, heparin mimetic peptide amphiphile was used as a bioactive molecule while E-PA was used control PA molecule. Positively charged K-PA was chosen to trigger the gel formation. Synthesis of HM-PA and K-PA was described in chapter 3 part 3.3.2 and E-PA synthesis was explained in detail in chapter 2 part 2.3.2. In addition, their characterization via LC-MS and purification via HPLC were also described in the parts that were mentioned above.

4.2.3 Physical and Mechanical Characterization of Self-assembled Nanofiber Networks

4.2.3.1 Scanning Electron Microscopy

Nanofibrous network of HM-PA/K-PA and E-PA/K-PA mixtures were observed with FEI Quanta 200 FEG SCANNİNG ELECRTON MİCROSCOPY device under high vacuum. Before imaging, 1 wt.% of PA solutions were prepared in 0.25 M sucrose solution. A volume ratio of 1:1 was used for the mixtures. After 15 min incubation of mixtures for gel system maturation, samples were treated with 20%, 40%, 60%, 80% and 100% ethanol series for 2 min per incubation, respectively. Samples were kept in 100% ethanol until critical point drying. The basic principle behind it is replacing the liquids in sample with CO_2 to maintain the morphology of samples. After critical point drying, samples were coated with 6 nm of Au/Pd.

4.2.3.2 Oscillatory Rheology

Mechanical characterizations of HM-PA/K-PA and E-PA/K-PA gels were measured with oscillatory rheometry. Anton Paar Physica RM301 was used with a 25 mm parallel plate at RT. Peptide mixtures were prepared on the centre of the lower plate of the device. Prior to measurement, they were incubated for 15 min for maturation of gel system. 300 µL total volume of 1 wt% HM-PA/K-PA or E-PA/K-PA was used. Gap distance was determined as 0.3 mm and angular frequency was adjusted between 100 - 0.1 rad/s with 0.5% shear strain.

4.2.4 Wound Healing Animal Model

In order to create an *in vivo* model, 3-month-old (200-250 g) Wistar rats were used (n=8). All procedures concerning animals were approved by the Institutional Animal Care and Use Committee of Diskapi Yildirim Beyazit Training and Research Hospital. Rats were maintained on *ad libitum* access to water and nutrition in a 12 h-12 h light-dark cycle.

HM-PA/K-PA combination was used as a bioactive group while E-PA/K-PA combination was the PA gel control group. As negative control 0.25 M sucrose solution was applied. PA solutions were prepared within 0.25 M sucrose solution to preserve the osmotic balance. Final concentrations were determined as 1 wt %.

As mentioned in chapter 3 part 3.2.7, rats were anesthetized with injection of ketamycin (80 mg/kg) and xylazine (10 mg/kg), intraperitonally. Under deep anesthesia, dorsums of rats were sterilized with an antiseptic and hair removal was done with a clipper for surgery. 6 mm circular biopsy punch was used for full thickness excisional wounds. In order to apply all experimental groups in each animal (HM-PA/K-PA, E-PA/K-PA, control), starting from the ear of each animal 3 wounds were opened with 2 cm intervals. Wounds and the surrounding area were cleaned. Prior to use PA solutions were sterilized under UV light for 30 min. PA solutions were applied immediately after wound creation to prevent drying of the wound and re-applied at day 1.

When wounds are on the mobile areas, the healing can be affected. Therefore, in order to prevent the local differences that might be occurred during the experiment, PA and control applications were distributed evenly across distal, median and proximal wounds. Alginate (Nu-derm) was used as wound dressing material right after PA gel application. To keep the PA gels, sucrose and alginate on the wounded area, dorsal part of the animals was covered with a non-woven, elastic, adhesive bandage. During the experiment, rats were fed on commercial pellets and water *ad libitum* and routine control for infection was performed.

Wound boundaries were traced and wound areas were measured using Image J software (NIH, USA) at days 3, 7, 10 and 14 following the operation. Rats were euthanized at 7 and 14 days following the operation and the wounds and their surrounding areas were excised. Wound area closure was calculated by using the following formula:

Wound area reduction (%) = wound area at day t / wound area day 0 X 100

4.2.5. Histological Analyses

Skin tissues of sacrificed rats were collected, fixed in formalin, embedded in paraffin and cut in 5 µm sections using a Leica microtome. According to the standard protocol of Hematoxylin & Eosin (H&E) and Masson's trichrome stainings, xylene and serial ethanol were applied to the samples for deparaffinization and rehydration, respectively. For immunohistochemistry experiments, sections were stained primarily with anti-von Willebrand Factor (1:400; Abcam) antibody and secondarily with horseradish peroxidase

conjugated goat anti-mouse secondary antibody (1:500; Millipore). Antibody staining was followed by 3,3'-diaminobenzidine (DAB) staining and hematoxylin counterstaining. Mounting was performed for all samples using a xylene based mounting medium. Digital images were acquired using a Zeiss Axio Scope A1 microscope. Granulation tissue areas of the samples were measured with Image J. Blood vessel numbers were quantified from sections stained with anti-von Willebrand factor antibody. Re-epithelization was quantified by measuring the distance between left and right wound edges; total re-epithelized tissue area was taken as the sum of new epithelium produced at the left and right edges of the wound. Images were acquired using 10x or 20x objectives and analyzed with Image J.

4.2.6 Statistical Analysis

Statistical analyses were performed using GraphPad Prism 5. One-way ANOVA with Bonferonni multiple comparison test was employed to determine statistical differences between groups. The level of significance was set at $p<0.05$. Error bars indicate standard error of mean.

4.3 RESULTS

HM-PA (bioactive peptide, Lauryl-VVAGEGDK(pbs)S-Am) (Figure 4.1), E-PA (negatively-charged non-bioactive peptide, Lauryl-VVAGE-OH) (Figure 4.2) and K-PA (positively-charged non-bioactive peptide, Lauryl-VVAGK-Am) (Figure 4.3) form nanofibrous structures through self-assembly. E-PA was used as a control molecule, while K-PA was used to trigger gel formation

through charge neutralization. All PA molecules were prepared in sucrose solution at physiological pH. The characterization and purification of PA molecules was performed by liquid chromatography–mass spectrometry (LC–MS), while their purification was performed by preparative HPLC (Figure 4.4 - 4.6). The ECM-like architectures of both HM-PA/K-PA and E-PA/K-PA combinations were investigated with scanning electron microscopy (Figure 4.7 A and B). HM-PA/K-PA and E-PA/K-PA scaffolds showed hydrogel properties according to oscillatory rheology measurements, as their storage moduli (G´) are higher than loss moduli (G´´) (Figure 4.8)

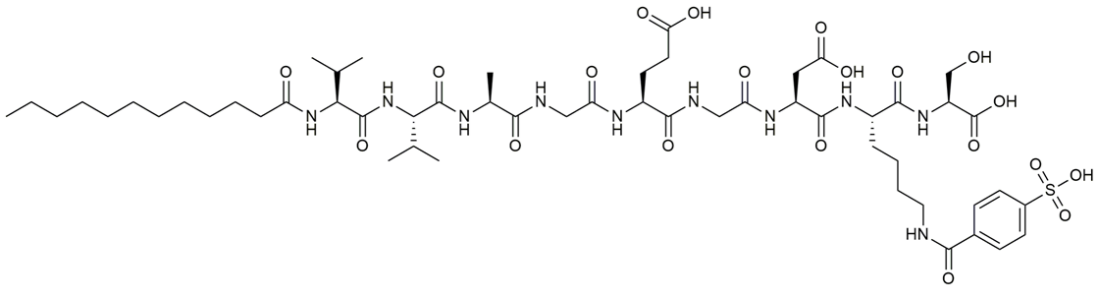

Figure 4.1 Chemical structure of heparin mimetic PA molecule (HM-PA).

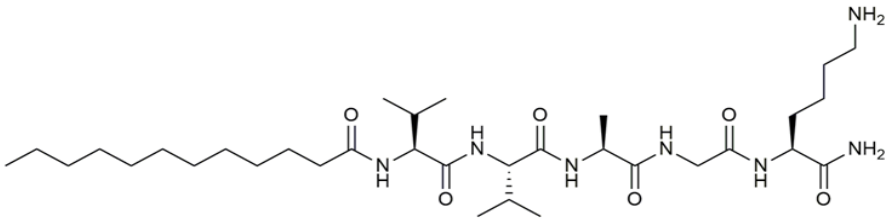

Figure 4.2 Chemical structure of K-PA molecule.

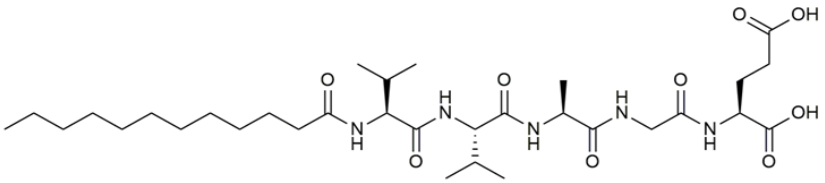

Figure 4.3 Chemical structure of E-PA molecule.

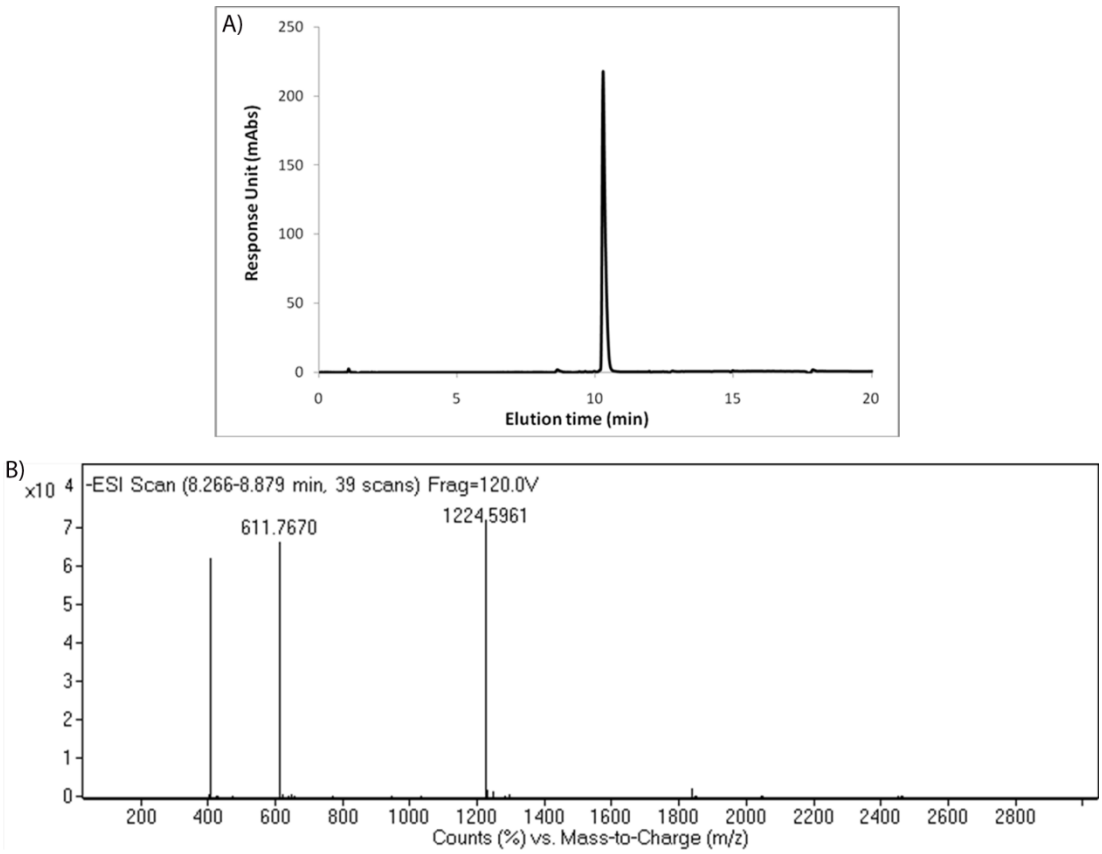

Figure 4.4 Purification and characterization of HM-PA. **(A)** HPLC chromatogram of purified heparin-mimetic PA molecule at 220 nm. **(B)** Mass spectrometry analysis of heparin-mimetic PA molecule; $[M-H]^-$ (observed)= 1224.59, $[M-H]^-$ (calculated)= 1224.58, $[M-2H]^{-2}/2$ (observed)= 611.76, $[M-2H]^{-2}/2$ (calculated)= 611.89.

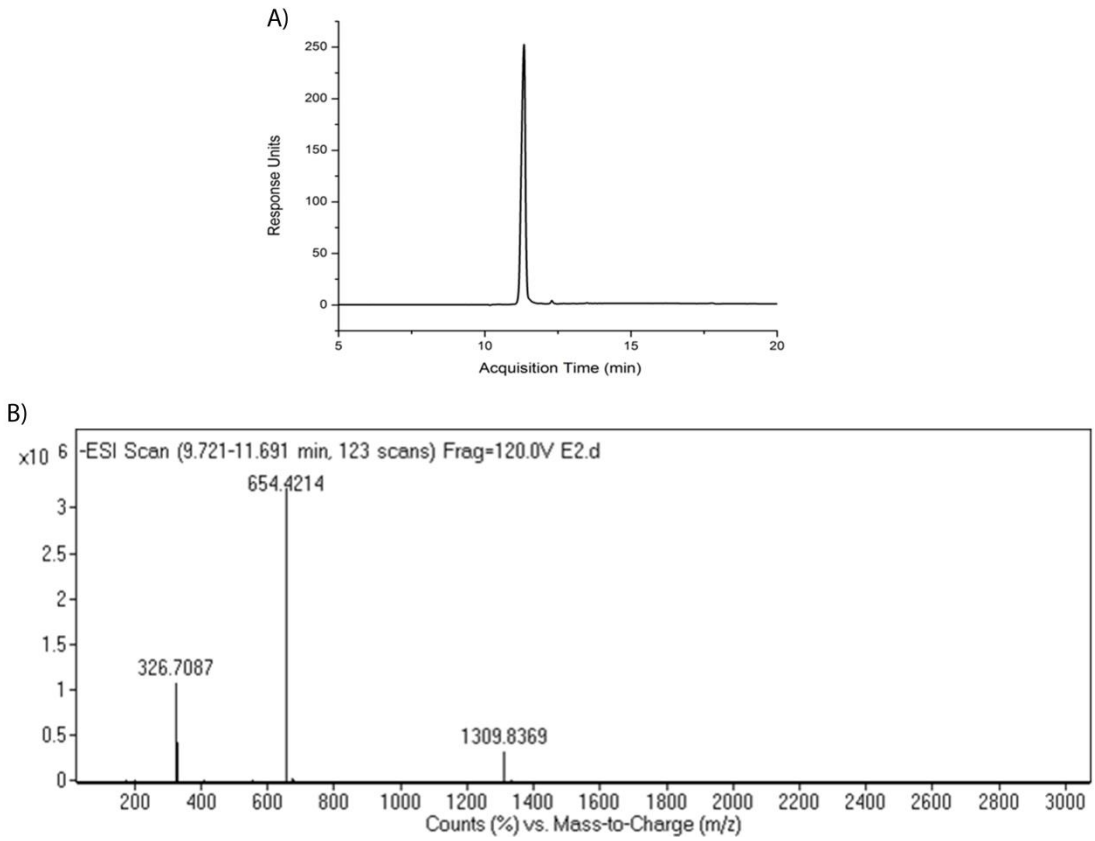

Figure 4.5 Purification and characterization of E-PA. **(A**) HPLC chromatogram of purified E-PA molecule at 220 nm. **(B)** Mass spectrometry analysis of E-PA molecule. $[M-H]^-$ (observed)= 654.42, $[M-H]^-$ (calculated): 654.42, $[M-2H]^{-2}/2$ (observed)= 326.70, $[M-2H]^{-2}/2$ (calculated)= 326.71, $[2M-H]^-$ (observed)= 1309.83, $[2M-H]^-$ (calculated)= 1309.84.

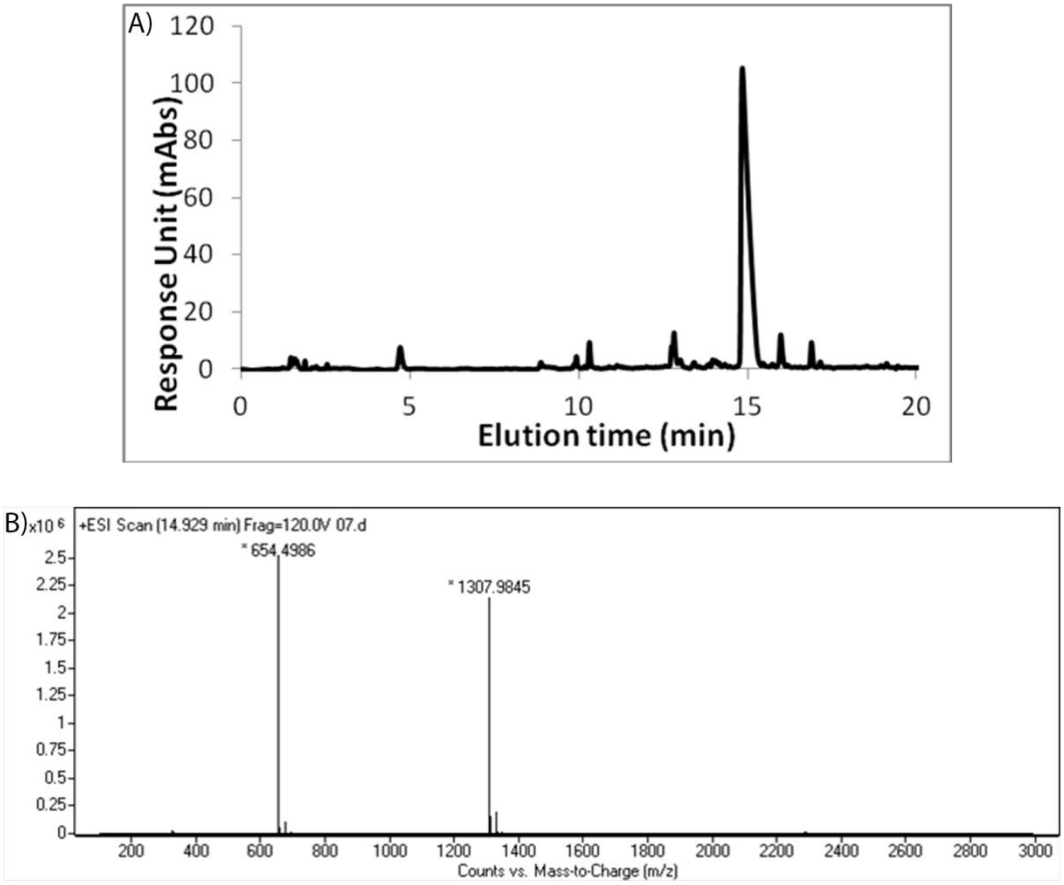

Figure 4.6 Purification and characterization of K-PA. **(A)** HPLC chromatogram of purified K-PA molecule at 220 nm. **(B)** Mass spectrometry analysis of K-PA molecule. $[M+H]^+$ (observed)= 654.49, $[M+H]^+$ (calculated)= 654.49, $[2M+H]^+$ (observed)= 1307.98, $[2M+H]^+$ (calculated)= 1307.96.

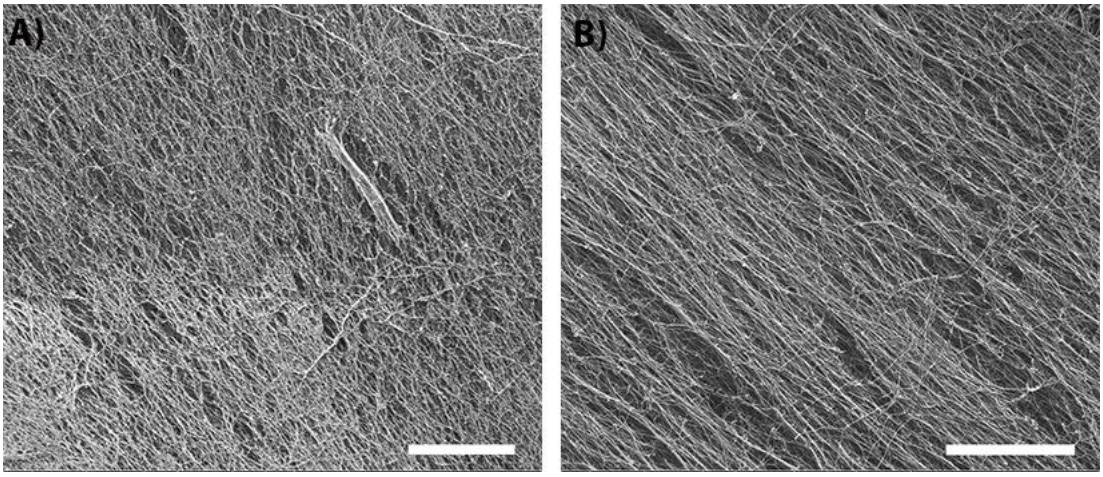

Figure 4.7 Scanning electron microscopy images of **(A)** HM-PA/K-PA and **(B)** E-PA/K-PA reveal the ECM-like morphology of the scaffolds. Scale bars are 5 µm.

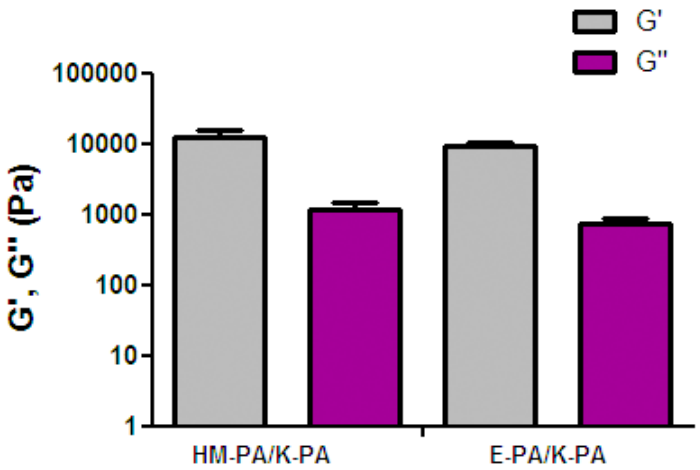

Figure 4.8 Rheology results showed that HM-PA/K-PA and E-PA/K-PA combinations formed gels and that their mechanical properties were similar.

In this study, full-thickness excision wounds were used as an acute wound model, and wounds were treated with bioactive and control PA gels immediately following and 24 h after injury. Wounds were observed daily during the experimental period and no infections were observed (Figure 4.9).

In order to prevent the wound site effect, applications were distributed across all three wounds in each rat. Wound area evaluations were performed at day 3, 7, 10 and 14. Although wound healing proceeded even after day 10 of post-wounding in HM-PA/K-PA applied wounds, healing peaked at day 10 in sucrose and E-PA/K-PA applied wounds. Recovery rates of HM-PA/K-PA, sucrose and E-PA/K-PA treated wounds reached 93%, 79% and 86% at the end of the experimental period, respectively (Figure 4.10). However, there was no significant difference in wound closure rates between wound locations, except between E-PA/K-PA and HM-PA/K-PA at day 3 in the proximal wound area (Figure 4.11- 4.14).

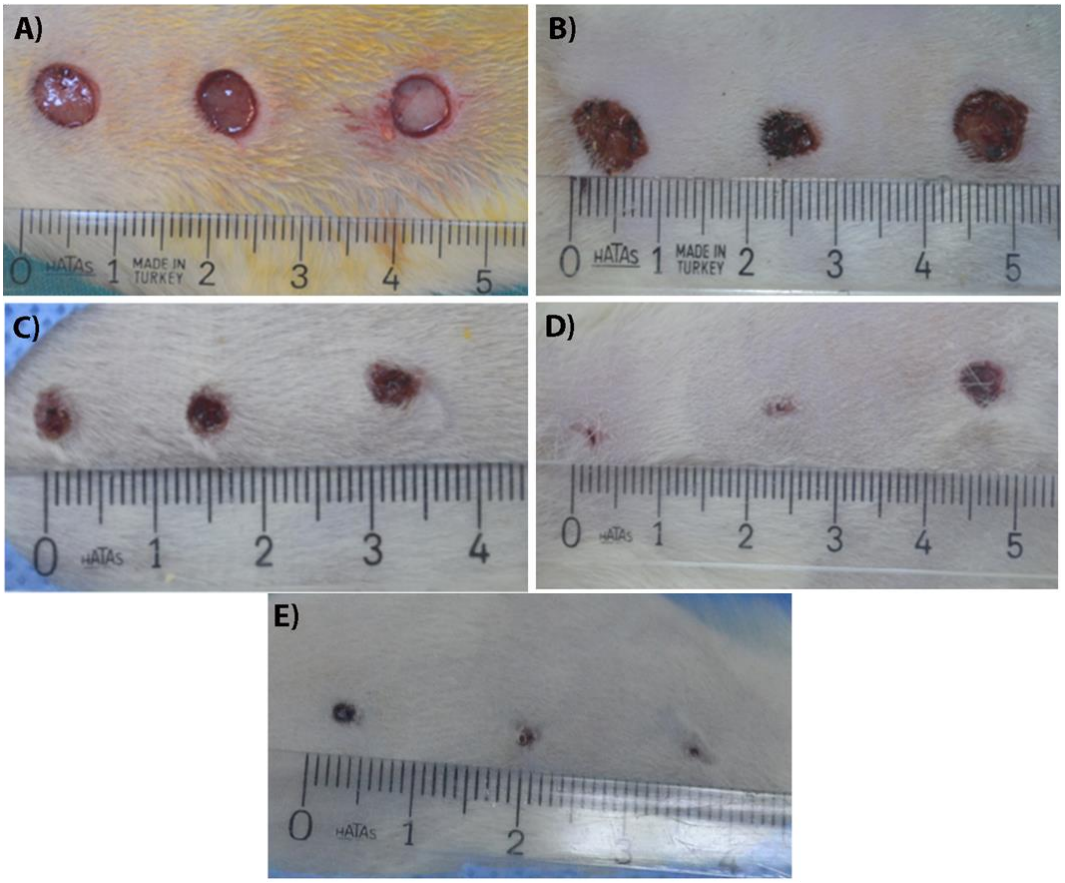

Figure 4.9 Representative images of wounds following hydrogel applications **(A)** Day 0, **(B)** Day 3, **(C)** Day 7, **(D)** Day 10 and **(E)** Day 14.

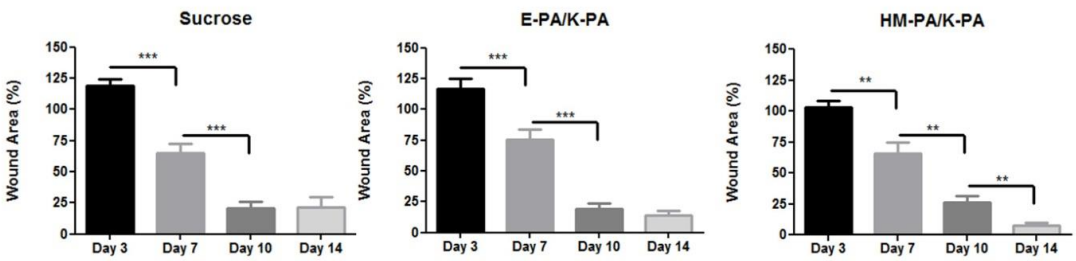

Figure 4.10 Wound areas of **(A)** sucrose, **(B)** E-PA/K-PA and **(C)** HM-PA/K-PA treated wounds at days 3, 7, 10 and 14. Data are expressed as means ± SEM, *p<0.05.

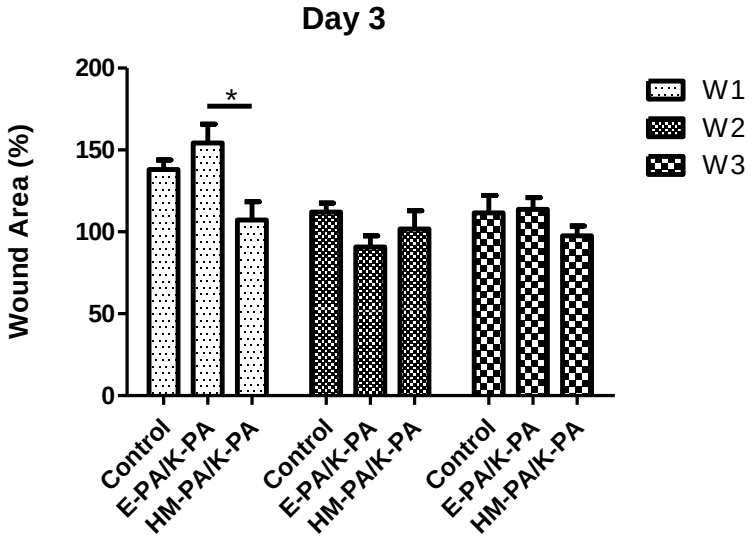

Figure 4.11 Wound area (%) according to the location of wounds in control, E-PA/K-PA and HM-PA/K-PA treated groups on day 3. Data are expressed as means ± SEM, *p<0.05. (W1: distal, W2: median, W3: proximal wounds).

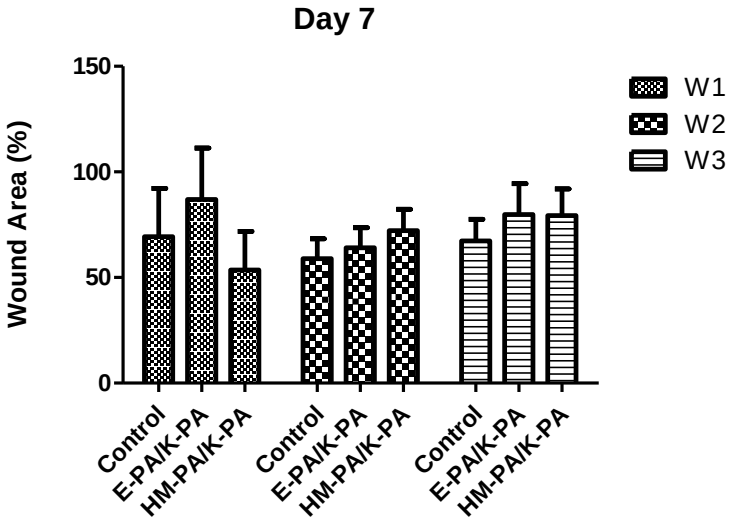

Figure 4.12 Wound area (%) according to the location of wounds in control, E-PA/K-PA and HM-PA/K-PA treated groups on day 7. Data are expressed as means ± SEM. (W1: distal, W2: median, W3: proximal wounds).

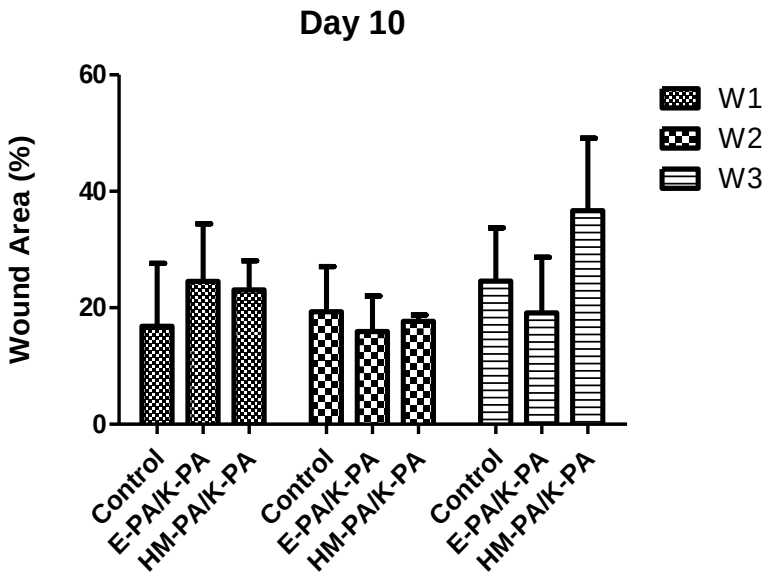

Figure 4.13 Wound area (%) according to the location of wounds in control, E-PA/K-PA and HM-PA/K-PA treated groups on day 10. Data are expressed as means ± SEM. (W1: distal, W2: median, W3: proximal wounds).

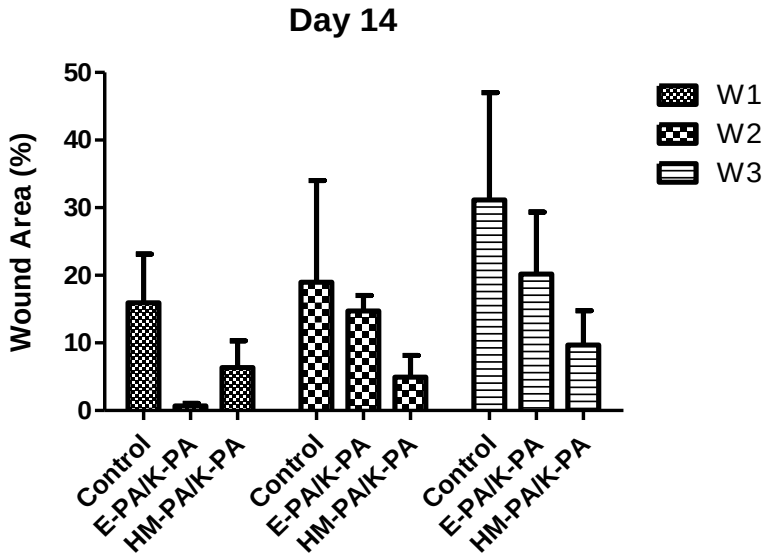

Figure 4.14 Wound area (%) according to the location of wounds in control, E-PA/K-PA and HM-PA/K-PA treated groups on day 14. Data are expressed as means ± SEM. (W1: distal, W2: median, W3: proximal wounds).

The proliferation phase of wound healing peaks at seven days after injury and consists of granulation tissue formation, re-epithelization and angiogenesis. Consequently, histological evaluations of wound samples were performed with H&E and Masson's trichrome staining 7 and 14 days post-injury. Stainings suggested that a well-organized, collagen-rich granulation tissue formed in HM-PA treated groups on day 7. In addition, there was less edematous area in the HM-PA treated granulation tissue compared to controls (Figure 4.15–4.17). Although the granulation tissue also appeared to be mature and had a homogenous, thick and well-organized structure in control groups at day 14, HM-PA/K-PA applied samples showed a relatively thick, basket-weave network of collagen fibers with an increased number of rete ridges, suggesting that the proliferation phase had been completed and the resolution phase was well under way (Figure 4.18-4.20). Sucrose and E-PA/K-PA applied samples, in contrast, had granulation tissues with poorly organized collagen fibers.

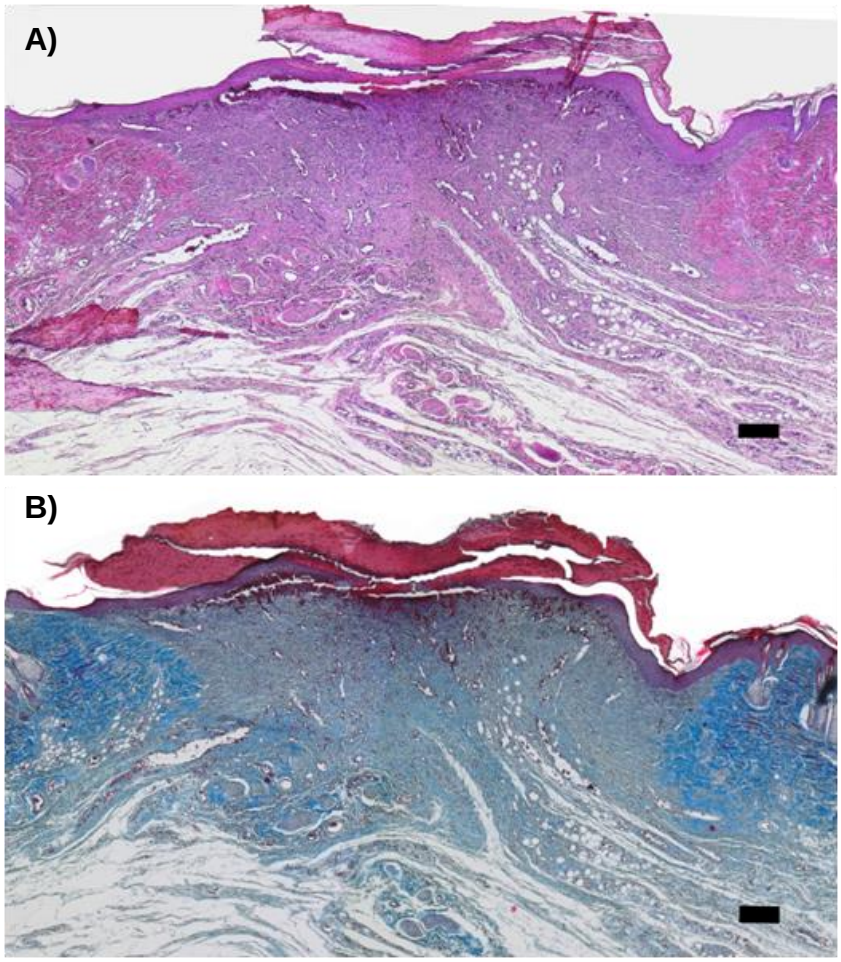

Figure 4.15 (A) H&E and **(B)** Masson's Trichrome staining (lower panel) of control group at day 7. Scale bars are 200 μm.

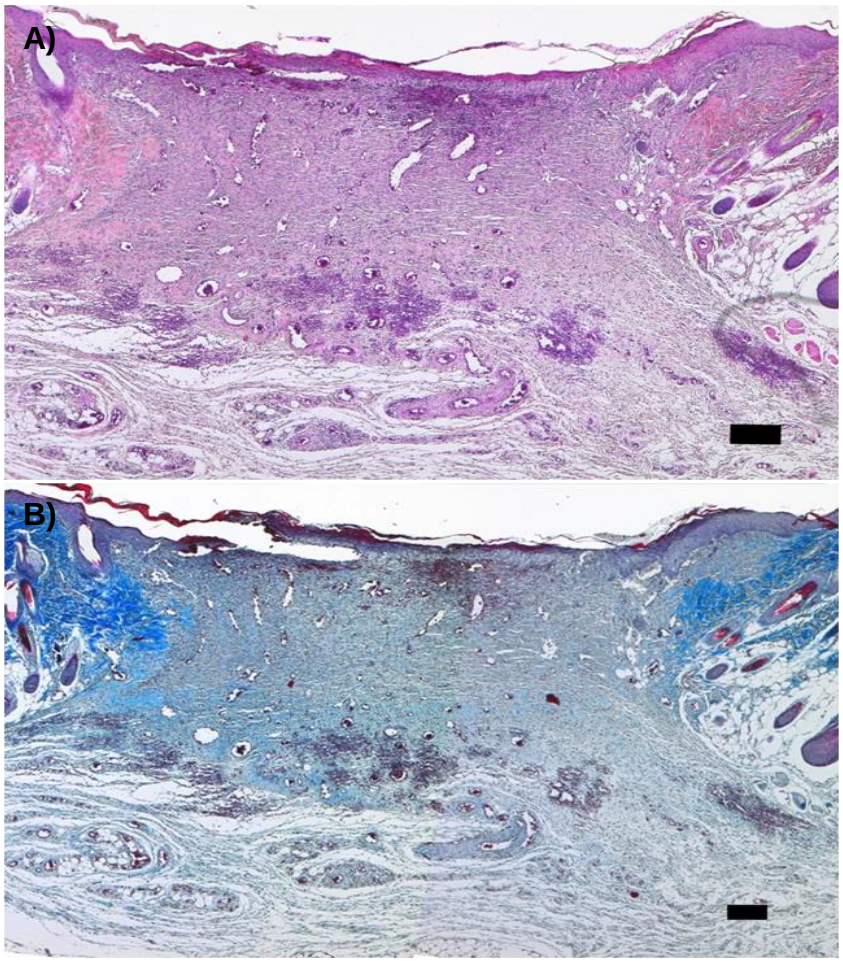

Figure 4.16 (A) H&E and **(B)** Masson's Trichrome staining (lower panel) of E-PA/K-PA application at day 7. Scale bars are 200 µm.

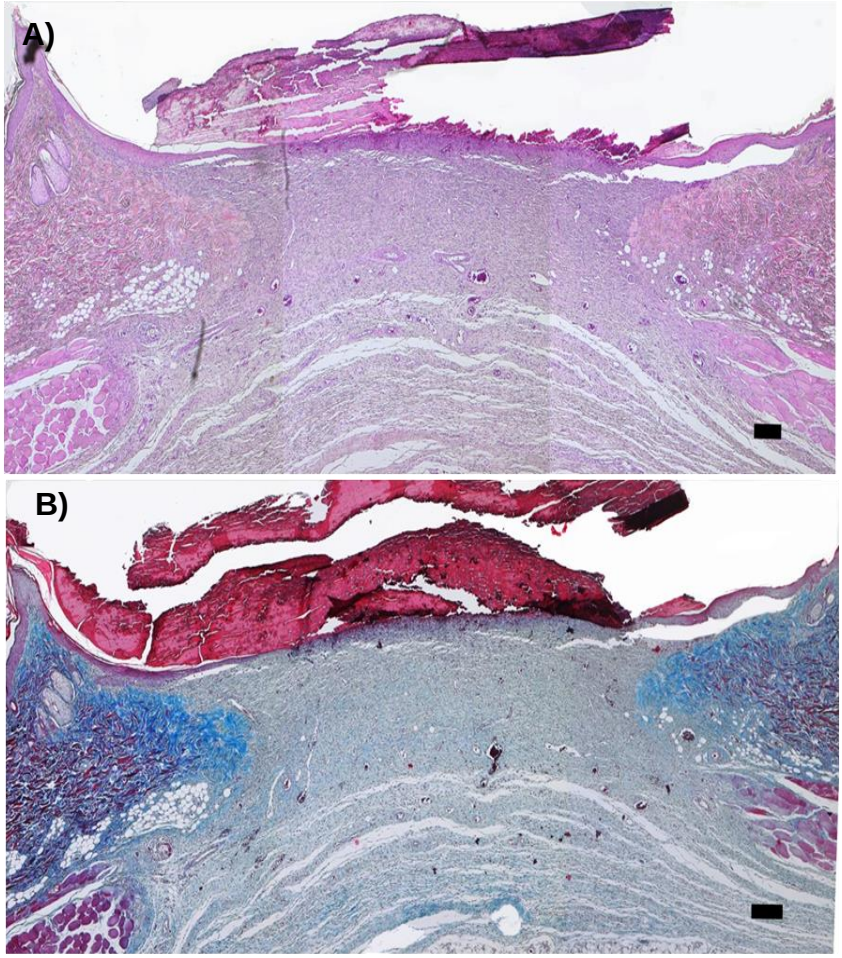

Figure 4.17 (A) H&E and **(B)** Masson's Trichrome staining (lower panel) of HM-PA/K-PA application at day 7. Scale bars are 200 µm.

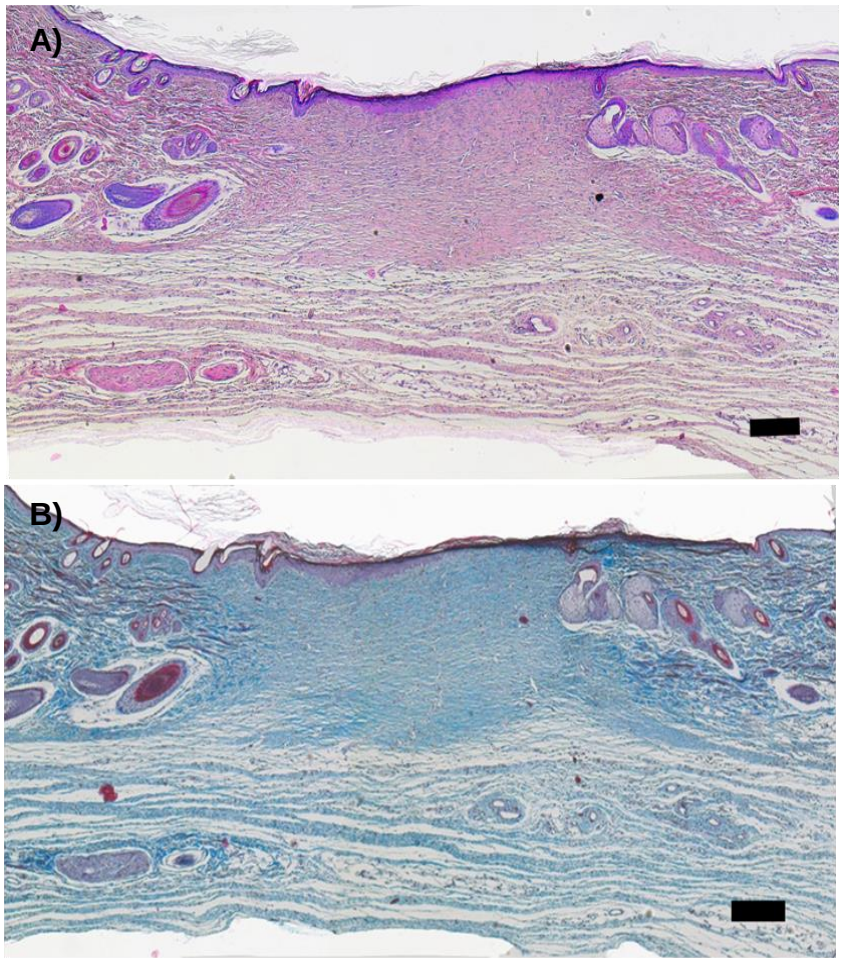

Figure 4.18 (A) H&E and **(B)** Masson's Trichrome staining (lower panel) of control group at day 14. Scale bars are 200 µm.

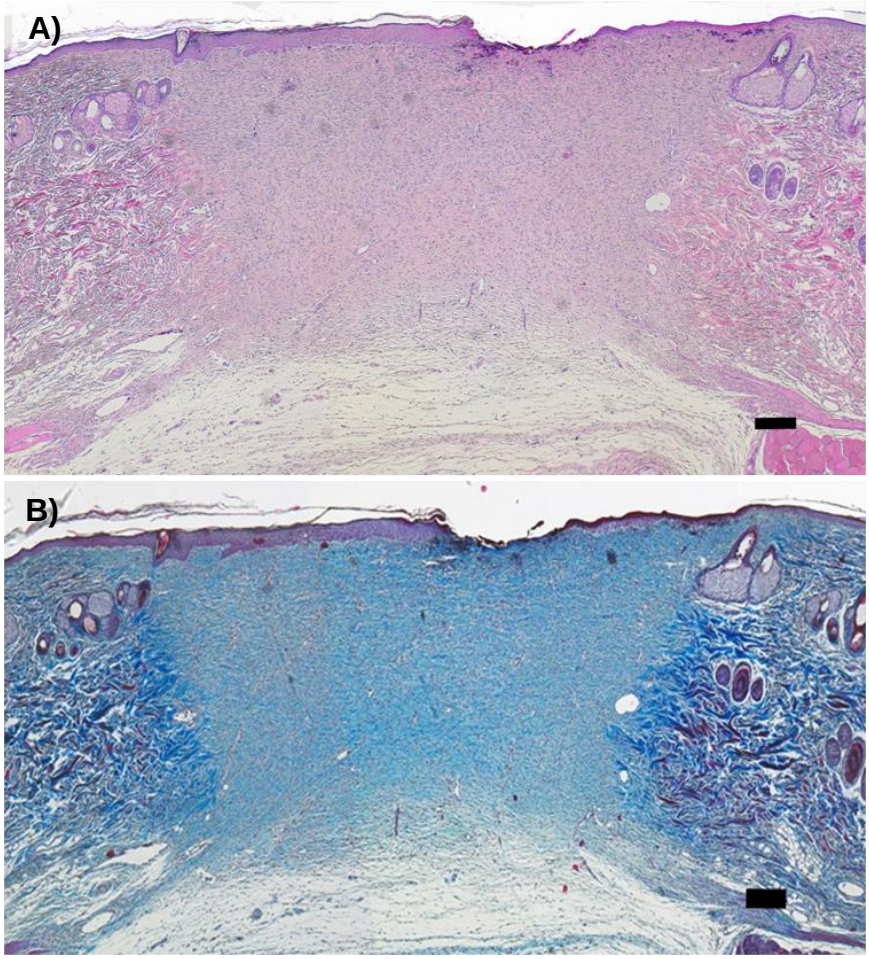

Figure 4.19 (A) H&E and **(B)** Masson's Trichrome staining (lower panel) of E-PA/K-PA application at day 14. Scale bars are 200 µm.

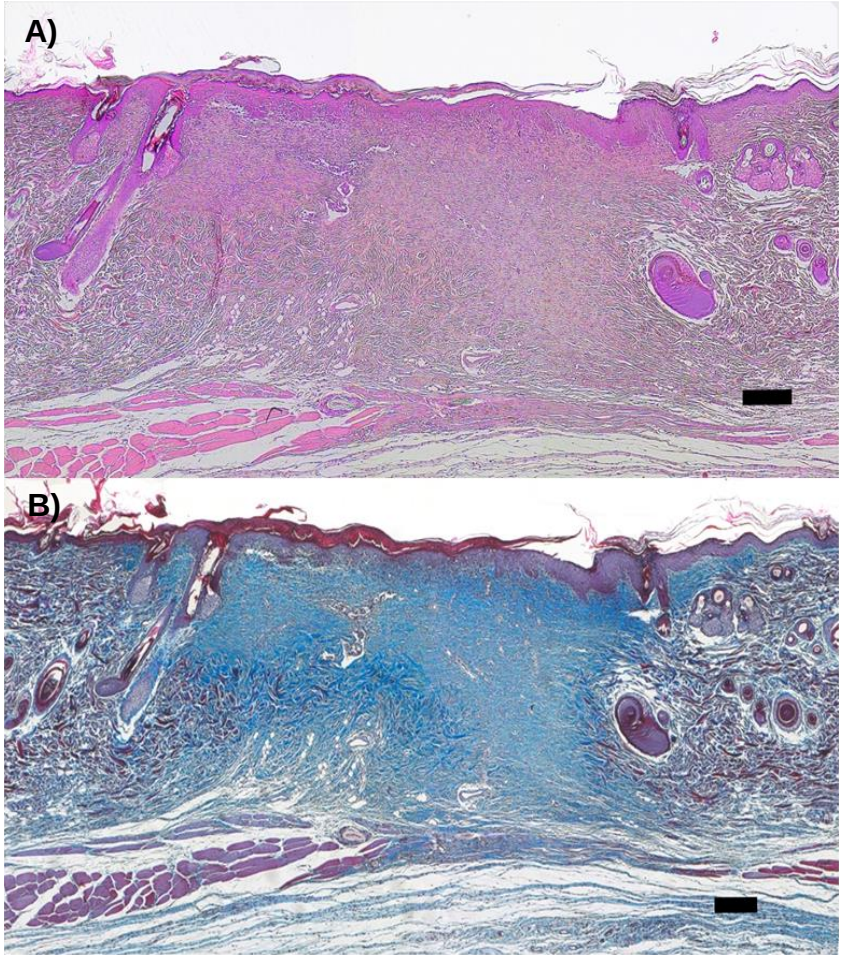

Figure 4.20 (A) H&E and **(B)** Masson's Trichrome staining (lower panel) of HM-PA/K-PA application at day 14. Scale bars are 200 µm.

Although no significant differences were observed in the granulation tissues of all experimental groups at day 7**,** the remodeling of granulation tissue was significantly enhanced at day 14 in HM-PA/K-PA samples compared to controls (Figure 4.21). Granulation tissue is an important element for the migration of keratinocytes to the wound area, since it provides a matrix conductive to this process. As such, re-epithelization was measured from the wound edges to the centre. Although wounds were fully covered with newly

formed epithelial tissue at day 14 (data not shown), HM-PA/K-PA applied samples showed increased re-epithelialization compared to the controls (Figure 4.22). Skin appendages were observed to form in all HM-PA/K-PA treated wounds, while control treatments included animals lacking skin appendage formation (Figure 4.23). In order to understand the angiogenic responses associated with the bioactive scaffold, newly formed blood vessels were stained with anti-von Willebrand Factor for all experimental groups (Figure 4.24 a-c). Vascularization was also assessed quantitatively for day 7 and 14 (Figure 4.24 d-e). The results demonstrated that HM-PA/K-PA promoted vascularization at day 7, although no significant difference was found between the experimental groups at day 14.

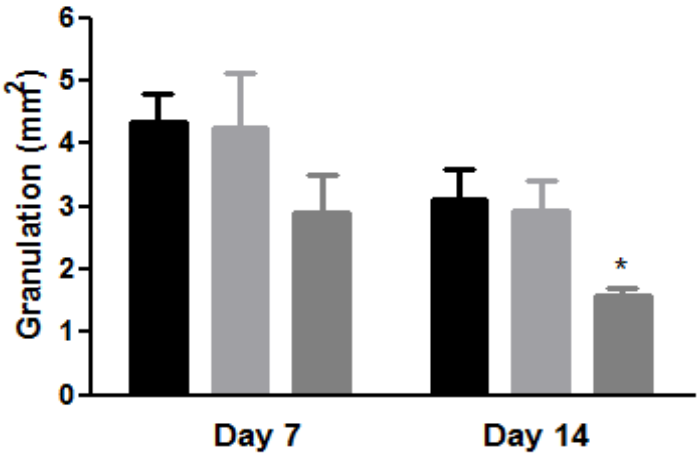

Figure 4.21 Quantitative analysis of granulation tissue of wound tissues at day 7 and 14. Data are expressed as means ± SEM, *p<0.05.

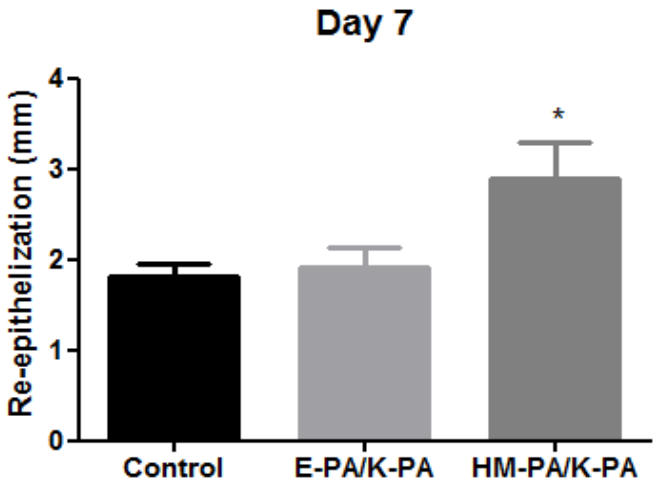

Figure 4.22 Quantitative analysis of re-epithelialization of wound tissues at day 7 and 14. Data are expressed as means ± SEM, *p<0.05.

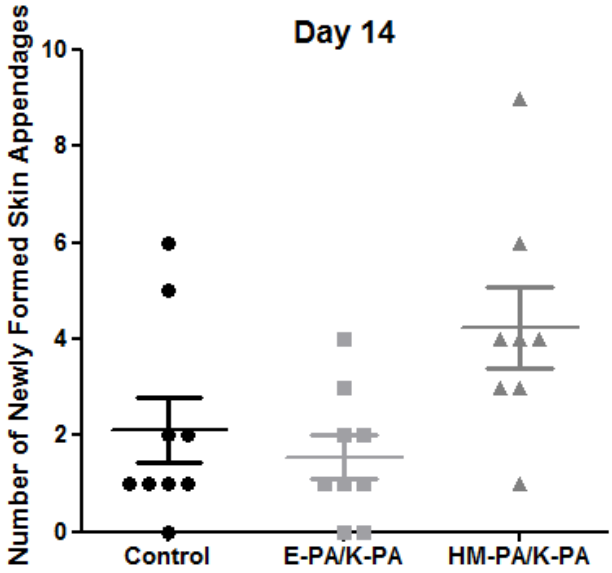

Figure 4.23 Quantitative analysis of skin appendages of wound tissues at day 14. Data are expressed as means ± SEM. *p< 0.05.

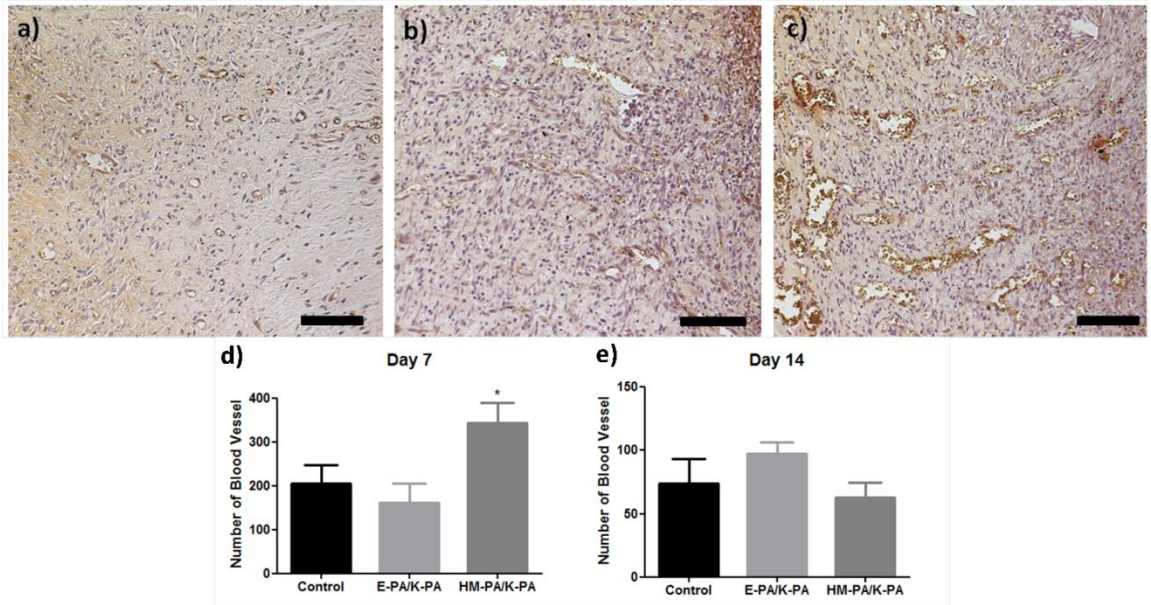

Figure 4.24 Staining of blood vessels by anti-von Willebrand Factor **(A-C)** and quantification of blood vessels at day 7 and 14 **(D-E)**. Representative sections obtained from **(A)** Control, **(B)** E-PA/K-PA and **(C)** HM-PA/K-PA at day 7 200X magnification. Scale bars are 100 µm. Data are expressed as means ± SEM. *p<0.05.

4.4 DISCUSSION

Wound healing still remains as one of the most prominent public health issues, because adult mammalian skin heats through scar formation instead of regaining its normal function [291]. Consequently, the functionality of adult tissues is decreased following every injury. Although using skin substitutes is the gold standard; even these materials suffer from reduced vascularization, scarring, mechanical and handling properties, low biocompatibility and high costs of production. Therefore, it is important to produce a novel approach that allows skin to gain its structural and functional properties without scar formation [291]. Hydrogel-based scaffolds are a promising strategy for the regeneration

of a broad range of wounds, and may also be applicable for skin tissue [292-294].

In this study, we utilized a bioactive peptide scaffold system to promote the wound healing process. HM-PA molecules mimic the heparin molecule and its functional groups, and have been reported to promote angiogenesis by increasing the local concentration of angiogenic growth factors, including VEGF and FGF-2, under *in vitro* and *in vivo* conditions [253, 255]. PA molecules are composed of amino acid sequences attached to a hydrocarbon chain, and may self assemble into nanofibrous structures through electrostatic stabilization, β-sheet driving units and hydrophobic collapse [153-154, 295]. This allows them to form nanofibers of c. 20–30 nm diameters [163]. Since the valine amino acid has a tendency to form β-sheet structures, the VVAG motif was chosen to trigger β-sheet formation [296]. The wound healing process requires a scaffold with good mechanical properties, the ability to serve as a barrier to protect the injuredd area, and high porosity for gas permeability. PA nanofibers fit all these criteria, as they exhibit biodegradable properties and form porous structures.

Although there were no significant differences in wound dosing rates between experimental groups, HM-PA applied wounds continued to heal 10 days after the wounding, while healing ceased in control groups after day 10 (Figure 4.10). The main challenge of wound healing is to promote regeneration instead of scarring. General charateristics of skin scars include fibrotic tissue, an altered collagen organization, reduced epidermal appendages and a smooth appearance [276]. Therefore, we investigated the tissues at day 7 and

14 post wounding, which are the points where proliferation peaks and remodeling starts, to see whether HM-PA treatment decreased tissue formation. Our histological analyses showed that HM-PA/K-PA treated wounds had decreased granulation tissue at day 14, and closely resembled to original tissue (Figure 4.15 - 4.20). The amount of newly formed epithelium increased at day 7 when wounds were treated with HM-PA/K-PA (Figure 4.22), and the healing process was largely completed at day 14 (data not shown). In addition, skin appendage formation was more complete in HM-PA/K-PA treated samples compared to the controls. It is known that skin appendages can generally be regenerated in partial thickness wound, but not in full thickness wounds [297]. Although it is known that Wnt signaling triggers *de novo* hair follicle production from epidermal progenitor cells [298], skin appendages are nevertheless reduced in wounded tissue [275, 278] which is one of the results of decreased rete ridge formation in wounds compared to the healthy skin [299]. However, HM-PA/K-PA application increased the rete ridges (Figure 4.20, black arrows), and thereby improved skin appendage formation.

These improvements can be derived from the increased number of new blood vessels within the granulation area at day 7 (Figure 6). Angiogenesis is one of the main issues in wound healing, especially for maintaining the long-term survival of skin grafts, as it is difficult to facilitate the rapid revascularization of the wound site [300]. FGF-2 is involved in scarless healing and is released from injured endothelial cells [283]. The lack of FGF-2 was shown to stop angiogenesis in wounded areas [301]. VEGF is another key growth factor in angiogenesis, and was shown to promote wound healing even

in the diabetic wound healing model [302]. In addition to these growth factors, hepatocyte growth factor (HGF) is another important molecule in angiogenesis, and plays a role in epithelial layer organization [303-306]. Apart from the high binding affinity of HM-PA to VEGF and FGF-2, it also shows affinity to HGF [255]. Therefore, it seems likely that the increased healing capacity of HM-PA/K-PA treated wounds is a result of GF induction capacity of the peptide matrix. In addition, angiogenesis was observed to be decreased at day 14 in HM-PA/K-PA treated wounds, which may further improve the quality of scar tissue, as fetal wounds heal without scarring and some studies have suggested that decreased angiogenesis can cause scarless healing [291, 294], and the peptide hyrdogels are biodegraded within a week.

4.5 CONCLUSION

Here, we evaluated the therapeutic potential of heparin mimetic peptide amphiphile scaffolds using rat full thickness wound model. The structural and mechanical characterization of PA molecules indicated that PA scaffolds exhibited morphologies similar to the ECM. HM-PA/K-PA, E-PA/K-PA and sucrose combinations did not show significant differences in wound closure rates. However, wounds treated with HM-PA/K-PA had advanced regeneration and organization; and these results correlated with a significant decrease in granulation tissue area at day 14 for this group. In addition, re-epithelization had increased at day 7 and the organization of wounded tissue improved in HM-PA/K-PA treated wounds, which also exhibited an increasing trend of skin appendage and rete ridge formations. While HM-PA/K-PA treated wounds presented an increased angiogenesis response at day 7, blood vessels were

observed to have resolved by day 14. This effect may suggest that the remodeling process has advanced rapidly in bioactive scaffold-treated wounds compared to controls. As scarless wound healing is a key element for restoring tissue functionality, heparin mimetic peptide nanofibers may potentially be employed as a novel therapeutic approach for regenerative wound healing with minimal scar formation.

CHAPTER 5

CONCLUSION AND FUTURE PERSPECTIVES

Mankind has long sought for a means of perfectly preserving and maintaining his mortal coil, and countless natural materials were used as cure-alls against diseases and injuries across time. Tissue engineering and regenerative medicine perhaps represent the modern equivalent of these endeavors, and have made it possible to realize, at least in part, some of these age-old goals. As advances in applied medicine have substantially increased human life expectancies, the necessity of finding a conclusive cure for aging is now greater than ever. Although much effort has been spent on the development of new materials and their applications, it is nevertheless challenging to meet the strict metabolic demands of tissues and organs. Consequently, I have aimed to develop materials that are simple in structure but complex in function, so as to minimize the potential side effects of scaffolds utilized in regenerative medicine. Peptide amphiphile molecules, which are the focus of my studies, provide tissues with an extracellular matrix-like 3D environment. In addition, they bear crucial biological signals to improve the regeneration process by directing cellular behavior. Beyond these features, these molecules are able to self-assemble and form nanofibrous structures in the absence of initiator molecules and without the formation of a cross-linked matrix, and their amino acid-based composition allows the integration of bioactive peptide motifs into their sequence. As such, they serve as an ideal scaffold system that is both biocompatible and biodegradable.

In the first study, we described a method for corneal stroma regeneration through the use of peptide amphiphile scaffold systems bearing laminin- or fibronectin-derived bioactive sequences. Ocular injuries can disrupt the

corneal transparency and are the second cause of blindness in the world. Cornea exhibits only a limited capacity for regeneration, and surgical methods such as excimer laser photorefractive keratectomy or laser-assisted *in situ* keratomileusis are associated with safety and permanency issues. Corneal transplantation is one of the most effective solutions but comes with its own set of problems, foremost among which is the scarcity of suitable donors. In this thesis, we have demonstrated that a bioactive and injectable gel system can be utilized to trigger the regeneration of keratocyte cells. Our YIGSR-decorated PA nanofibers represent a biocompatible system for the cultivation of keratocyte cells; supporting their adhesion, proliferation and collagen secretion. Although the fibronectin-derived KKRGD-PA scaffold exhibited biocompatibility, it was not a suitable platform for cell proliferation and adhesion. As such, we expected YIGSR-PA to facilitate the effective healing of corneal defects in a rabbit model. While negatively-charged PA molecules have been utilized for charge neutralization in *in vitro* studies, the corneal stroma is anion-rich by itself (primarily due to its GAG content) and does not require a neutralization agent for gelation. As such, positively charged PA solutions were injected directly into the stromal pocket. Similar to as our *in vitro* results, YIGSR-PA triggered keratocyte migration to the damaged site, and the site was filled up with collagen I. While KKRGD-PA did not affect cellular migration, its presence was nevertheless associated with an increase in collagen I compared to control. Overall, our laminin-mimetic PA nanofiber system appears to be suitable for stroma regeneration due to its bioactive properties and ease of handling. As the pig cornea is similar to humans, the

YIGSR-PA scaffold might also be used in the pig model and, if successful, can be subsequently utilized in clinical trials.

In the second study, we investigated the ability of a heparin-mimetic peptide amphiphile hydrogel system to increase the survival of pancreatic islets under culture and transplantation conditions. As an incurable disease, type 1 diabetes is associated with great economic and social burdens. Although insulin can be externally administered to control patients' blood glucose levels, pancreatic islet transplantation is the most convenient approach to ensure lifelong normoglycemia. However, during pancreatic islet isolation, the surrounding vascular network is damaged and the survival of the isolated islets in compromised. Pancreatic islets are cell clusters that consist of 3000-4000 cells each, and damage to their vascular network can cause cell loss especially in the core area. This situation decreases the survival of isolated pancreatic islets until transplantation. Moreover, the establishment of vascular formations immediately after transplantation is vital to keep the islets viable and functional. The PA scaffold used in this study has been proven to trigger angiogenesis under both *in vitro* and *in vivo* conditions by binding to angiogenic growth factors. The bioactive scaffold preserves islet viability when administered in tandem with additional angiogenic growth factors including VEGF and FGF-2, allowing islets to exhibit insulin production capacities comparable to freshly isolated islets even after seven days of culture. We also expected to see similar results *in vivo* and utilized an omental transplantation model to further characterize the effects of the heparin-mimetic scaffold. Omentum tissue was chosen as the transplantation site due to its self-healing

potential, large area for transplantation and status as a non-vital organ. Our transplantation results indicated that the co-administration of PA scaffolds decreases post-transplantation blood glucose levels in the STZ-induced diabetic rat model. In addition, histological analyses suggest that the PA scaffold provides structural support to the islets in the omental pouch, and transplanted islets were found to be functional for up to 28 days. It also should be underlined that HM-PA scaffold application increases the blood vessels in the omentum, thereby contributing to islet survival. Our results overall suggest that the affinity of HM-PA to angiogenic growth factors may have a key role in its ability to increase islet functionality under both *in vitro* and *in vivo* conditions. However, our system could not surpass the immune response problem. As a further study, an immune suppressive treatment can be added to the system or an immune-privileged site can be chosen for transplantation to overcome the problem.

In the last study, I investigated the effects of a heparin-mimetic peptide amphiphile hydrogel system on acute wound healing. Acute wounds are caused by injuries, traumas or surgical incisions, and heal rapidly if the individual does not suffer from certain systemic diseases. As bacterial infection and local loss of tissue integrity are both major dangers to many organisms, it is evolutionarily advantageous to rapidly facilitate the closure of wounds even if the repaired tissue is not fully functional. As such, wound repair typically culminates in the formation of scars, which do not fully restore the previous function, structure and physical appearance of the injured tissue. In this study, we used the previously discussed HM-PA scaffold system to reduce scar

formation following full-thickness skin injuries. This system was chosen because of its ability to trigger angiogenesis, which is well-recognized as a crucial step of the repair process and strongly associated with scarless skin regeneration. HM-PA treated wounds were found to exhibit improved collagen organization, a higher rate of re-epithelization and a greater number of blood vessels compared to control. Granulation tissue and angiogenesis decreased by day 14, and the histological organization of wounded tissues were similar to normal skin, exhibiting an increased number of skin appendages. Therefore, we may conclude that HM-PA increases the healing capacity of acute wounds. However, wound closure was not faster than that observed in control; as such, repeated applications of HM-PA can be utilized in future studies to improve wound closure rates.

Bibliography

[1] Brockes JP, Kumar A. Comparative aspects of animal regeneration. Annual review of cell and developmental biology 2008;24:525-49.
[2] Polezhaev LV. Loss and Restoration of Regenerative Capacity in Tissues and Organs of Animals: Harvard University Press; 1972.
[3] Bely AE, Nyberg KG. Evolution of animal regeneration: re-emergence of a field. Trends in ecology & evolution 2010;25:161-70.
[4] Brockes JP. Amphibian limb regeneration: rebuilding a complex structure. Science 1997;276:81-7.
[5] Sanan A, Haines SJ. Repairing holes in the head: a history of cranioplasty. Neurosurgery 1997;40:588-603.
[6] Shah AM, Jung H, Skirboll S. Materials used in cranioplasty: a history and analysis. Neurosurgical focus 2014;36:E19-E.
[7] Griffith LG, Naughton G. Tissue engineering--current challenges and expanding opportunities. Science (New York, NY) 2002;295:1009-14.
[8] Hollister SJ. Porous scaffold design for tissue engineering. Nature materials 2005;4:518-24.
[9] Place ES, Evans ND, Stevens MM. Complexity in biomaterials for tissue engineering. Nature materials 2009;8:457-70.
[10] Dvir T, Timko BP, Kohane DS, Langer R. Nanotechnological strategies for engineering complex tissues. Nature nanotechnology 2011;6:13-22.
[11] Langer R, Vacanti JP. Tissue engineering. Science (New York, NY) 1993;260:920-6.
[12] Mano JF, Silva GA, Azevedo HS, Malafaya PB, Sousa RA, Silva SS, et al. Natural origin biodegradable systems in tissue engineering and regenerative medicine: present status and some moving trends. Journal of the Royal Society, Interface / the Royal Society 2007;4:999-1030.
[13] Stock UA, Vacanti JP. Tissue engineering: current state and prospects. Annual review of medicine 2001;52:443-51.
[14] Patience C, Takeuchi Y, Weiss RA. Infection of human cells by an endogenous retrovirus of pigs. Nature medicine 1997;3:282-6.
[15] Pollak RA. A human dermal replacement for the treatment of diabetic foot ulcers. WOUNDS-A … 1997.
[16] Ryan EA, Lakey JR, Rajotte RV, Korbutt GS, Kin T, Imes S, et al. Clinical outcomes and insulin secretion after islet transplantation with the Edmonton protocol. Diabetes 2001;50:710-9.
[17] Chowdhury JR, Fox IJ. Hepatocyte transplantation for the treatment of human disease. Semin Liver Dis 1999.
[18] Ikada Y. Challenges in tissue engineering. Journal of the Royal Society, Interface / the Royal Society 2006;3:589-601.
[19] Thomson JA. Embryonic Stem Cell Lines Derived from Human Blastocysts. Science 1998;282:1145-7.
[20] Reubinoff BE, Itsykson P, Turetsky T, Pera MF, Reinhartz E, Itzik A, et al. Neural progenitors from human embryonic stem cells. Nature biotechnology 2001;19:1134-40.
[21] Levenberg S, Golub JS, Amit M, Itskovitz-Eldor J, Langer R. Endothelial cells derived from human embryonic stem cells. Proceedings of the National Academy of Sciences of the United States of America 2002;99:4391-6.
[22] Assady S, Maor G, Amit M, Itskovitz-Eldor J, Skorecki KL, Tzukerman M. Insulin production by human embryonic stem cells. Diabetes 2001;50:1691-7.

[23] Itskovitz-Eldor J, Schuldiner M, Karsenti D, Eden A, Yanuka O, Amit M, et al. Differentiation of human embryonic stem cells into embryoid bodies compromising the three embryonic germ layers. Molecular medicine (Cambridge, Mass) 2000;6:88-95.
[24] Kim JB, Sebastiano V, Wu G, Araúzo-Bravo MJ, Sasse P, Gentile L, et al. Oct4-induced pluripotency in adult neural stem cells. Cell 2009;136:411-9.
[25] Takahashi K, Tanabe K, Ohnuki M, Narita M, Ichisaka T, Tomoda K, et al. Induction of pluripotent stem cells from adult human fibroblasts by defined factors. Cell 2007;131:861-72.
[26] Takahashi K, Yamanaka S. Induction of pluripotent stem cells from mouse embryonic and adult fibroblast cultures by defined factors. Cell 2006;126:663-76.
[27] Wernig M, Meissner A, Foreman R, Brambrink T, Ku M, Hochedlinger K, et al. In vitro reprogramming of fibroblasts into a pluripotent ES-cell-like state. Nature 2007;448:318-24.
[28] Weissman IL. Stem cells: units of development, units of regeneration, and units in evolution. Cell 2000;100:157-68.
[29] Kocher AA, Schuster MD, Szabolcs MJ. Neovascularization of ischemic myocardium by human bone-marrow–derived angioblasts prevents cardiomyocyte apoptosis, reduces remodeling and improves. Nature medicine 2001.
[30] Wakitani S, Saito T, Caplan AI. Myogenic cells derived from rat bone marrow mesenchymal stem cells exposed to 5-azacytidine. Muscle & nerve 1995.
[31] Lagasse E, Connors H, Al-Dhalimy M, Reitsma M, Dohse M, Osborne L, et al. Purified hematopoietic stem cells can differentiate into hepatocytes in vivo. Nature medicine 2000;6:1229-34.
[32] Song L, Young NJ, Webb NE, Tuan RS. Origin and characterization of multipotential mesenchymal stem cells derived from adult human trabecular bone. Stem cells and development 2005;14:712-21.
[33] Dodson MV, Hausman GJ, Guan L, Du M, Rasmussen TP, Poulos SP, et al. Skeletal muscle stem cells from animals I. Basic cell biology. International journal of biological sciences 2010;6:465-74.
[34] Belicchi M, Pisati F, Lopa R, Porretti L, Fortunato F, Sironi M, et al. Human skin-derived stem cells migrate throughout forebrain and differentiate into astrocytes after injection into adult mouse brain. Journal of neuroscience research 2004;77:475-86.
[35] Feng J, Mantesso A, Sharpe PT. Perivascular cells as mesenchymal stem cells. Expert opinion on biological therapy 2010;10:1441-51.
[36] Shi M, Ishikawa M, Kamei N, Nakasa T, Adachi N, Deie M, et al. Acceleration of skeletal muscle regeneration in a rat skeletal muscle injury model by local injection of human peripheral blood-derived CD133-positive cells. Stem cells (Dayton, Ohio) 2009;27:949-60.
[37] Miura M, Gronthos S, Zhao M, Lu B, Fisher LW, Robey PG, et al. SHED: stem cells from human exfoliated deciduous teeth. Proceedings of the National Academy of Sciences of the United States of America 2003;100:5807-12.
[38] Kotobuki N, Hirose M, Takakura Y, Ohgushi H. Cultured autologous human cells for hard tissue regeneration: preparation and characterization of mesenchymal stem cells from bone marrow. Artificial organs 2004;28:33-9.
[39] Estes BT, Diekman BO, Gimble JM, Guilak F. Isolation of adipose-derived stem cells and their induction to a chondrogenic phenotype. Nature protocols 2010;5:1294-311.
[40] Estes BT, Guilak F. Three-dimensional culture systems to induce chondrogenesis of adipose-derived stem cells. Methods in molecular biology (Clifton, NJ) 2011;702:201-17.
[41] Brayfield CA, Marra KG, Rubin JP. Adipose tissue regeneration. Current stem cell research & therapy 2010;5:116-21.
[42] Dragoo JL, Samimi B. Tissue-engineered cartilage and bone using stem cells from human infrapatellar fat pads. Journal of Bone & … 2003.

[43] Rehman J, Traktuev D, Li J, Merfeld-Clauss S, Temm-Grove CJ, Bovenkerk JE, et al. Secretion of angiogenic and antiapoptotic factors by human adipose stromal cells. Circulation 2004;109:1292-8.
[44] Safford KM, Safford SD, Gimble JM, Shetty AK, Rice HE. Characterization of neuronal/glial differentiation of murine adipose-derived adult stromal cells. Experimental neurology 2004;187:319-28.
[45] Louët S. Reagent safety issues surface for cell/tissue therapies. Nature biotechnology 2004;22:253-4.
[46] McKay WF, Peckham SM, Badura JM. A comprehensive clinical review of recombinant human bone morphogenetic protein-2 (INFUSE Bone Graft). International orthopaedics 2007;31:729-34.
[47] Mann BK, Schmedlen RH, West JL. Tethered-TGF-beta increases extracellular matrix production of vascular smooth muscle cells. Biomaterials 2001;22:439-44.
[48] Raman R, Sasisekharan V, Sasisekharan R. Structural insights into biological roles of protein-glycosaminoglycan interactions. Chemistry & biology 2005;12:267-77.
[49] Tayalia P, Mooney DJ. Controlled growth factor delivery for tissue engineering. Advanced materials (Deerfield Beach, Fla) 2009;21:3269-85.
[50] Gama CI, Tully SE, Sotogaku N, Clark PM, Rawat M, Vaidehi N, et al. Sulfation patterns of glycosaminoglycans encode molecular recognition and activity. Nature chemical biology 2006;2:467-73.
[51] Pellegrini L, Burke DF, von Delft F, Mulloy B, Blundell TL. Crystal structure of fibroblast growth factor receptor ectodomain bound to ligand and heparin. Nature 2000;407:1029-34.
[52] Liu L-S, Ng C-K, Thompson AY, Poser JW, Spiro RC. Hyaluronate-heparin conjugate gels for the delivery of basic fibroblast growth factor (FGF-2). Journal of biomedical materials research 2002;62:128-35.
[53] Murugan R, Ramakrishna S. Design strategies of tissue engineering scaffolds with controlled fiber orientation. Tissue engineering 2007;13:1845-66.
[54] Berthiaume F, Maguire TJ, Yarmush ML. Tissue engineering and regenerative medicine: history, progress, and challenges. Annual review of chemical and biomolecular engineering 2011;2:403-30.
[55] Mecham RP. Overview of extracellular matrix. Current protocols in cell biology / editorial board, Juan S Bonifacino [et al] 2001;Chapter 10:Unit 10.1-Unit .1.
[56] Mouw JK, Ou G, Weaver VM. Extracellular matrix assembly: a multiscale deconstruction. Nature reviews Molecular cell biology 2014;15:771-85.
[57] Lutolf MP, Hubbell JA. Synthetic biomaterials as instructive extracellular microenvironments for morphogenesis in tissue engineering. Nature biotechnology 2005;23:47-55.
[58] Frantz C, Stewart KM, Weaver VM. The extracellular matrix at a glance. Journal of cell science 2010;123:4195-200.
[59] Gordon MK, Hahn RA. Collagens. Cell and tissue research 2010;339:247-57.
[60] Ricard-Blum S, Ruggiero F. The collagen superfamily: from the extracellular matrix to the cell membrane. Pathologie-biologie 2005;53:430-42.
[61] Chen CW, Tsai YH, Deng WP, Shih SN, Fang CL, Burch JG, et al. Type I and II collagen regulation of chondrogenic differentiation by mesenchymal progenitor cells. Journal of orthopaedic research : official publication of the Orthopaedic Research Society 2005;23:446-53.
[62] Rozario T, DeSimone DW. The extracellular matrix in development and morphogenesis: a dynamic view. Developmental biology 2010.
[63] Singh P, Carraher C, Schwarzbauer JE. Assembly of fibronectin extracellular matrix. Annual review of cell and developmental biology 2010;26:397-419.

[64] Houseman BT, Mrksich M. The microenvironment of immobilized Arg-Gly-Asp peptides is an important determinant of cell adhesion. Biomaterials 2001;22:943-55.
[65] Takahashi S, Leiss M, Moser M, Ohashi T, Kitao T, Heckmann D, et al. The RGD motif in fibronectin is essential for development but dispensable for fibril assembly. The Journal of cell biology 2007;178:167-78.
[66] Bentzinger CF, Wang YX, von Maltzahn J, Soleimani VD, Yin H, Rudnicki MA. Fibronectin regulates Wnt7a signaling and satellite cell expansion. Cell stem cell 2013;12:75-87.
[67] Lu P, Takai K, Weaver VM, Werb Z. Extracellular matrix degradation and remodeling in development and disease. Cold Spring Harbor perspectives in biology 2011;3:a005058--a-.
[68] Singh P, Schwarzbauer JE. Fibronectin and stem cell differentiation–lessons from chondrogenesis. Journal of cell science 2012.
[69] Schwarzbauer J. Basement membrane: Putting up the barriers. Current Biology 1999;9:R242-R4.
[70] Aumailley M, Bruckner-Tuderman L, Carter WG, Deutzmann R, Edgar D, Ekblom P, et al. A simplified laminin nomenclature. Matrix Biology 2005;24:326-32.
[71] Graf J, Iwamoto Y, Sasaki M, Martin GR, Kleinman HK, Robey FA, et al. Identification of an amino acid sequence in laminin mediating cell attachment, chemotaxis, and receptor binding. Cell 1987;48:989-96.
[72] Iwamoto Y, Robey FA, Graf J, Sasaki M, Kleinman HK, Yamada Y, et al. YIGSR, a synthetic laminin pentapeptide, inhibits experimental metastasis formation. Science 1987;238:1132-4.
[73] Grant DS, Tashiro K-I, Segui-Real B, Yamada Y, Martin GR, Kleinman HK. Two different laminin domains mediate the differentiation of human endothelial cells into capillary-like structures in vitro. Cell 1989;58:933-43.
[74] Kibbey MC, Grant DS, Kleinman HK. Role of the SIKVAV Site of Laminin in Promotion of Angiogenesis and Tumor Growth: An In Vivo Matrigel Model. JNCI Journal of the National Cancer Institute 1992;84:1633-8.
[75] Tashiro K, Sephel GC, Weeks B, Sasaki M, Martin GR, Kleinman HK, et al. A synthetic peptide containing the IKVAV sequence from the A chain of laminin mediates cell attachment, migration, and neurite outgrowth. J Biol Chem 1989;264:16174-82.
[76] Bornstein P. Diversity of function is inherent in matricellular proteins: an appraisal of thrombospondin 1. The Journal of cell biology 1995;130:503-6.
[77] Iozzo RV, Murdoch AD. Proteoglycans of the extracellular environment: clues from the gene and protein side offer novel perspectives in molecular diversity and function. FASEB journal : official publication of the Federation of American Societies for Experimental Biology 1996;10:598-614.
[78] Schaefer L, Schaefer RM. Proteoglycans: from structural compounds to signaling molecules. Cell and tissue research 2010;339:237-46.
[79] Badylak SF. The extracellular matrix as a scaffold for tissue reconstruction. Seminars in cell & developmental biology 2002;13:377-83.
[80] Iozzo RV, San Antonio JD. Heparan sulfate proteoglycans: heavy hitters in the angiogenesis arena. The Journal of clinical investigation 2001;108:349-55.
[81] Sugahara K, Mikami T, Uyama T, Mizuguchi S, Nomura K, Kitagawa H. Recent advances in the structural biology of chondroitin sulfate and dermatan sulfate. Current opinion in structural biology 2003;13:612-20.
[82] Carulli D, Laabs T, Geller HM, Fawcett JW. Chondroitin sulfate proteoglycans in neural development and regeneration. Current opinion in neurobiology 2005;15:116-20.
[83] Lin X. Functions of heparan sulfate proteoglycans in cell signaling during development. Development (Cambridge, England) 2004;131:6009-21.

[84] Casu B, Guerrini M, Torri G. Structural and conformational aspects of the anticoagulant and anti-thrombotic activity of heparin and dermatan sulfate. Current pharmaceutical design 2004;10:939-49.
[85] Brown BN, Valentin JE, Stewart-Akers AM, McCabe GP, Badylak SF. Macrophage phenotype and remodeling outcomes in response to biologic scaffolds with and without a cellular component. Biomaterials 2009;30:1482-91.
[86] Hutmacher DW. Scaffolds in tissue engineering bone and cartilage. Biomaterials 2000;21:2529-43.
[87] Collins MN, Birkinshaw C. Hyaluronic acid based scaffolds for tissue engineering--a review. Carbohydrate polymers 2013;92:1262-79.
[88] O'Brien FJ. Biomaterials & scaffolds for tissue engineering. Materials Today 2011;14:88-95.
[89] Nair LS, Laurencin CT. Biodegradable polymers as biomaterials. Progress in Polymer Science 2007;32:762-98.
[90] Barnes CP, Pemble CW, Brand DD, Simpson DG, Bowlin GL. Cross-linking electrospun type II collagen tissue engineering scaffolds with carbodiimide in ethanol. Tissue engineering 2007;13:1593-605.
[91] Atala A. Tissue engineering and regenerative medicine: concepts for clinical application. Rejuvenation research 2004;7:15-31.
[92] Chen G, Ushida T, Tateishi T. A biodegradable hybrid sponge nested with collagen microsponges. Journal of biomedical materials research 2000;51:273-9.
[93] Knight CG, Morton LF, Peachey AR, Tuckwell DS, Farndale RW, Barnes MJ. The collagen-binding A-domains of integrins alpha(1)beta(1) and alpha(2)beta(1) recognize the same specific amino acid sequence, GFOGER, in native (triple-helical) collagens. The Journal of biological chemistry 2000;275:35-40.
[94] Konitsiotis AD, Raynal N, Bihan D, Hohenester E, Farndale RW, Leitinger B. Characterization of high affinity binding motifs for the discoidin domain receptor DDR2 in collagen. The Journal of biological chemistry 2008;283:6861-8.
[95] Pierschbacher MD, Ruoslahti E. Cell attachment activity of fibronectin can be duplicated by small synthetic fragments of the molecule. Nature 1984;309:30-3.
[96] Fiedler LR, Schönherr E, Waddington R, Niland S, Seidler DG, Aeschlimann D, et al. Decorin regulates endothelial cell motility on collagen I through activation of insulin-like growth factor I receptor and modulation of alpha2beta1 integrin activity. The Journal of biological chemistry 2008;283:17406-15.
[97] Gingras M, Beaulieu M-M, Gagnon V, Durham HD, Berthod F. In vitro study of axonal migration and myelination of motor neurons in a three-dimensional tissue-engineered model. Glia 2008;56:354-64.
[98] Harley BA, Lynn AK, Wissner-Gross Z, Bonfield W, Yannas IV, Gibson LJ. Design of a multiphase osteochondral scaffold. II. Fabrication of a mineralized collagen-glycosaminoglycan scaffold. Journal of biomedical materials research Part A 2010;92:1066-77.
[99] Wolf K, Müller R, Borgmann S, Bröcker E-B, Friedl P. Amoeboid shape change and contact guidance: T-lymphocyte crawling through fibrillar collagen is independent of matrix remodeling by MMPs and other proteases. Blood 2003;102:3262-9.
[100] Tedder ME, Liao J, Weed B, Stabler C, Zhang H, Simionescu A, et al. Stabilized collagen scaffolds for heart valve tissue engineering. Tissue engineering Part A 2009;15:1257-68.
[101] L'Heureux N, Pâquet S, Labbé R, Germain L, Auger FA. A completely biological tissue-engineered human blood vessel. FASEB journal : official publication of the Federation of American Societies for Experimental Biology 1998;12:47-56.

[102] Edmonds M. Apligraf in the treatment of neuropathic diabetic foot ulcers. The international journal of lower extremity wounds 2009;8:11-8.
[103] Jean J, Lapointe M, Soucy J, Pouliot R. Development of an in vitro psoriatic skin model by tissue engineering. Journal of dermatological science 2009;53:19-25.
[104] Régnier M, Staquet MJ, Schmitt D, Schmidt R. Integration of Langerhans cells into a pigmented reconstructed human epidermis. The Journal of investigative dermatology 1997;109:510-2.
[105] Carrier P, Deschambeault A, Talbot M, Giasson CJ, Auger FA, Guérin SL, et al. Characterization of wound reepithelialization using a new human tissue-engineered corneal wound healing model. Investigative ophthalmology & visual science 2008;49:1376-85.
[106] Dravida S, Gaddipati S, Griffith M, Merrett K, Lakshmi Madhira S, Sangwan VS, et al. A biomimetic scaffold for culturing limbal stem cells: a promising alternative for clinical transplantation. Journal of tissue engineering and regenerative medicine 2008;2:263-71.
[107] Grueterich M, Espana EM, Tseng SCG. Ex vivo expansion of limbal epithelial stem cells: amniotic membrane serving as a stem cell niche. Survey of Ophthalmology 2003;48:631-46.
[108] Bouhout S, Perron E, Gauvin R, Bernard G, Ouellet G, Cattan V, et al. In vitro reconstruction of an autologous, watertight, and resistant vesical equivalent. Tissue engineering Part A 2010;16:1539-48.
[109] Boeriu CG, Springer J, Kooy FK, van den Broek LAM, Eggink G. Production Methods for Hyaluronan. International Journal of Carbohydrate Chemistry 2013;2013:1-14.
[110] Hascall VC. Hyaluronan, a common thread. Glycoconjugate journal 2000.
[111] Freymann U, Endres M, Neumann K, Scholman HJ, Morawietz L, Kaps C. Expanded human meniscus-derived cells in 3-D polymer-hyaluronan scaffolds for meniscus repair. Acta biomaterialia 2012;8:677-85.
[112] Tan H, Chu CR, Payne KA, Marra KG. Injectable in situ forming biodegradable chitosan-hyaluronic acid based hydrogels for cartilage tissue engineering. Biomaterials 2009;30:2499-506.
[113] Toh WS, Lim TC, Kurisawa M, Spector M. Modulation of mesenchymal stem cell chondrogenesis in a tunable hyaluronic acid hydrogel microenvironment. Biomaterials 2012;33:3835-45.
[114] Park JK, Shim J-H, Kang KS, Yeom J, Jung HS, Kim JY, et al. Solid Free-Form Fabrication of Tissue-Engineering Scaffolds with a Poly(lactic-co-glycolic acid) Grafted Hyaluronic Acid Conjugate Encapsulating an Intact Bone Morphogenetic Protein-2/Poly(ethylene glycol) Complex. Advanced Functional Materials 2011;21:2906-12.
[115] Ananthanarayanan B, Kim Y, Kumar S. Elucidating the mechanobiology of malignant brain tumors using a brain matrix-mimetic hyaluronic acid hydrogel platform. Biomaterials 2011;32:7913-23.
[116] Faga A, Nicoletti G, Brenta F, Scevola S, Abatangelo G, Brun P. Hyaluronic acid three-dimensional scaffold for surgical revision of retracting scars: a human experimental study. International wound journal 2013;10:329-35.
[117] Kogan G, Soltés L, Stern R, Gemeiner P. Hyaluronic acid: a natural biopolymer with a broad range of biomedical and industrial applications. Biotechnology letters 2007;29:17-25.
[118] Fagien S, Cassuto D. Reconstituted injectable hyaluronic acid: expanded applications in facial aesthetics and additional thoughts on the mechanism of action in cosmetic medicine. Plastic and reconstructive surgery 2012;130:208-17.
[119] Percival E MRH. Algal polysaccharides. Academic Press; 1990. p. 523-47.
[120] Stevens M. A rapid-curing alginate gel system: utility in periosteum-derived cartilage tissue engineering. Biomaterials 2004;25:887-94.

[121] Kuo CK, Ma PX. Ionically crosslinked alginate hydrogels as scaffolds for tissue engineering: Part 1. Structure, gelation rate and mechanical properties. Biomaterials 2001;22:511-21.
[122] Hubbell JA. Materials as morphogenetic guides in tissue engineering. Current Opinion in Biotechnology 2003;14:551-8.
[123] Boontheekul T, Kong HJ, Mooney DJ. Controlling alginate gel degradation utilizing partial oxidation and bimodal molecular weight distribution. Biomaterials 2005.
[124] Opara EC, McQuilling JP, Farney AC. Microencapsulation of pancreatic islets for use in a bioartificial pancreas. Methods in molecular biology (Clifton, NJ) 2013;1001:261-6.
[125] Smidsrod O, Skjakbrk G. Alginate as immobilization matrix for cells. Trends in Biotechnology 1990;8:71-8.
[126] Cole SM, Garbe JE. Alginate hydrogel foam wound dressing. Google Patents; 1990.
[127] Rao SB, Sharma CP. Use of chitosan as a biomaterial: studies on its safety and hemostatic potential. Journal of biomedical materials research 1997;34:21-8.
[128] Croisier F, Jérôme C. Chitosan-based biomaterials for tissue engineering. European Polymer Journal 2013;49:780-92.
[129] Francis Suh JK, Matthew HWT. Application of chitosan-based polysaccharide biomaterials in cartilage tissue engineering: a review. Biomaterials 2000;21:2589-98.
[130] Azad AK, Sermsintham N, Chandrkrachang S, Stevens WF. Chitosan membrane as a wound-healing dressing: characterization and clinical application. Journal of biomedical materials research Part B, Applied biomaterials 2004;69:216-22.
[131] Ao Q, Fung C-K, Tsui AY-P, Cai S, Zuo H-C, Chan Y-S, et al. The regeneration of transected sciatic nerves of adult rats using chitosan nerve conduits seeded with bone marrow stromal cell-derived Schwann cells. Biomaterials 2011;32:787-96.
[132] Pashuck ET, Stevens MM. Designing regenerative biomaterial therapies for the clinic. Science translational medicine 2012;4:160sr4-sr4.
[133] Calonder C, Matthew HWT, Van Tassel PR. Adsorbed layers of oriented fibronectin: a strategy to control cell-surface interactions. Journal of biomedical materials research Part A 2005;75:316-23.
[134] Perka C, Spitzer RS, Lindenhayn K, Sittinger M, Schultz O. Matrix-mixed culture: new methodology for chondrocyte culture and preparation of cartilage transplants. Journal of biomedical materials research 2000;49:305-11.
[135] Wang Y, Kim U-J, Blasioli DJ, Kim H-J, Kaplan DL. In vitro cartilage tissue engineering with 3D porous aqueous-derived silk scaffolds and mesenchymal stem cells. Biomaterials 2005;26:7082-94.
[136] Balgude AP, Yu X, Szymanski A, Bellamkonda RV. Agarose gel stiffness determines rate of DRG neurite extension in 3D cultures. Biomaterials 2001;22:1077-84.
[137] Lévesque SG, Lim RM, Shoichet MS. Macroporous interconnected dextran scaffolds of controlled porosity for tissue-engineering applications. Biomaterials 2005;26:7436-46.
[138] Magnusson JP, Saeed AO, Fernández-Trillo F, Alexander C. Synthetic polymers for biopharmaceutical delivery. Polym Chem 2011;2:48-59.
[139] Oh SH, Kang SG, Kim ES, Cho SH, Lee JH. Fabrication and characterization of hydrophilic poly(lactic-co-glycolic acid)/poly(vinyl alcohol) blend cell scaffolds by melt-molding particulate-leaching method. Biomaterials 2003;24:4011-21.
[140] Williams DF. Biocompatibility of clinical implant materials, 2. cilt1981.
[141] Santerre JP, Woodhouse K, Laroche G, Labow RS. Understanding the biodegradation of polyurethanes: from classical implants to tissue engineering materials. Biomaterials 2005.
[142] Jain JP, Chitkara D, Kumar N. Polyanhydrides as localized drug delivery carrier: an update. Expert opinion on drug delivery 2008;5:889-907.

[143] Guo B, Ma PX. Synthetic biodegradable functional polymers for tissue engineering: a brief review. Science China Chemistry 2014;57:490-500.
[144] Sreejalekshmi KG, Nair PD. Biomimeticity in tissue engineering scaffolds through synthetic peptide modifications-altering chemistry for enhanced biological response. Journal of biomedical materials research Part A 2011;96:477-91.
[145] Lee KY, Mooney DJ. Hydrogels for tissue engineering. Chemical reviews 2001;101:1869-79.
[146] Ovsianikov A, Deiwick A, Van Vlierberghe S, Dubruel P, Möller L, Dräger G, et al. Laser fabrication of three-dimensional CAD scaffolds from photosensitive gelatin for applications in tissue engineering. Biomacromolecules 2011;12:851-8.
[147] Cruise GM, Hegre OD, Lamberti FV, Hager SR, Hill R, Scharp DS, et al. In vitro and in vivo performance of porcine islets encapsulated in interfacially photopolymerized poly(ethylene glycol) diacrylate membranes. Cell transplantation;8:293-306.
[148] Bryant SJ, Anseth KS. The effects of scaffold thickness on tissue engineered cartilage in photocrosslinked poly (ethylene oxide) hydrogels. Biomaterials 2001.
[149] Burdick JA, Anseth KS. Photoencapsulation of osteoblasts in injectable RGD-modified PEG hydrogels for bone tissue engineering. Biomaterials 2002;23:4315-23.
[150] Bohl KS, West JL. Nitric oxide-generating polymers reduce platelet adhesion and smooth muscle cell proliferation. Biomaterials 2000;21:2273-8.
[151] Aida T, Meijer EW, Stupp SI. Functional supramolecular polymers. Science (New York, NY) 2012;335:813-7.
[152] Monnard P-A, Deamer DW. Membrane self-assembly processes: steps toward the first cellular life. The Anatomical record 2002;268:196-207.
[153] Hartgerink JD, Beniash E, Stupp SI. Peptide-amphiphile nanofibers: a versatile scaffold for the preparation of self-assembling materials. Proceedings of the National Academy of Sciences of the United States of America 2002;99:5133-8.
[154] Niece KL, Hartgerink JD, Donners JJJM, Stupp SI. Self-assembly combining two bioactive peptide-amphiphile molecules into nanofibers by electrostatic attraction. Journal of the American Chemical Society 2003;125:7146-7.
[155] Rudra JS, Sun T, Bird KC, Daniels MD, Gasiorowski JZ, Chong AS, et al. Modulating adaptive immune responses to peptide self-assemblies. ACS nano 2012;6:1557-64.
[156] Ustun S, Tombuloglu A, Kilinc M, Guler MO, Tekinay AB. Growth and differentiation of prechondrogenic cells on bioactive self-assembled peptide nanofibers. Biomacromolecules 2013;14:17-26.
[157] Mammadov B, Mammadov R, Guler MO, Tekinay AB. Cooperative effect of heparan sulfate and laminin mimetic peptide nanofibers on the promotion of neurite outgrowth. Acta biomaterialia 2012;8:2077-86.
[158] Lin Y-D, Luo C-Y, Hu Y-N, Yeh M-L, Hsueh Y-C, Chang M-Y, et al. Instructive nanofiber scaffolds with VEGF create a microenvironment for arteriogenesis and cardiac repair. Science translational medicine 2012;4:146ra09-ra09.
[159] Ceylan H, Kocabey S, Unal Gulsuner H, Balcik OS, Guler MO, Tekinay AB. Bone-like mineral nucleating peptide nanofibers induce differentiation of human mesenchymal stem cells into mature osteoblasts. Biomacromolecules 2014;15:2407-18.
[160] Bulut S, Erkal TS, Toksoz S, Tekinay AB, Tekinay T, Guler MO. Slow release and delivery of antisense oligonucleotide drug by self-assembled peptide amphiphile nanofibers. Biomacromolecules 2011;12:3007-14.
[161] Sever M, Mammadov B, Guler MO, Tekinay AB. Tenascin-C mimetic Peptide nanofibers direct stem cell differentiation to osteogenic lineage. Biomacromolecules 2014;15:4480-7.
[162] Matson JB, Newcomb CJ, Bitton R, Stupp SI. Nanostructure-templated control of drug release from peptide amphiphile nanofiber gels. Soft Matter 2012;8:3586-95.

[163] Uzunalli G, Soran Z, Erkal TS, Dagdas YS, Dinc E, Hondur AM, et al. Bioactive self-assembled peptide nanofibers for corneal stroma regeneration. Acta biomaterialia 2014;10:1156-66.
[164] Griffith M. Functional Human Corneal Equivalents Constructed from Cell Lines. Science 1999;286:2169-72.
[165] Pinnamaneni N, Funderburgh JL. Concise review: Stem cells in the corneal stroma. Stem cells (Dayton, Ohio) 2012;30:1059-63.
[166] Daniels JT, Dart JKG, Tuft SJ, Khaw PT. Corneal stem cells in review. Wound Repair and Regeneration 2001;9:483-94.
[167] Litwin KL, Moreira H, Ohadi C, McDonnell PJ. Changes in corneal curvature at different excimer laser ablative depths. American journal of ophthalmology 1991;111:382-4.
[168] Jue B, Maurice DM. The mechanical properties of the rabbit and human cornea. Journal of biomechanics 1986;19:847-53.
[169] Whitcher JP, Srinivasan M, Upadhyay MP. Corneal blindness: a global perspective. Bulletin of the World Health Organization 2001;79:214-21.
[170] Whitcher JP, Srinivasan M, Upadhyay MP. Prevention of corneal ulceration in the developing world. International ophthalmology clinics 2002;42:71-7.
[171] Hay ED, Meier S. Stimulation of corneal differentiation by interaction between cell surface and extracellular matrix. Developmental biology 1976;52:141-57.
[172] Hanna C, Bicknell DS, O'Brien JE. Cell turnover in the adult human eye. Archives of ophthalmology (Chicago, Ill : 1960) 1961;65:695-8.
[173] Newsome DA, Gross J, Hassell JR. Human corneal stroma contains three distinct collagens. Investigative ophthalmology & visual science 1982;22:376-81.
[174] Rada JA, Cornuet PK, Hassell JR. Regulation of corneal collagen fibrillogenesis in vitro by corneal proteoglycan (lumican and decorin) core proteins. Experimental eye research 1993;56:635-48.
[175] Hicks CR, Crawford GJ, Lou X, Tan DT, Snibson GR, Sutton G, et al. Corneal replacement using a synthetic hydrogel cornea, AlphaCor: device, preliminary outcomes and complications. Eye (London, England) 2003;17:385-92.
[176] Germain L, Carrier P, Auger FA, Salesse C, Guérin SL. Can we produce a human corneal equivalent by tissue engineering? Progress in Retinal and Eye Research 2000;19:497-527.
[177] Bleckmann H, Holak S. Preliminary results after implantation of four AlphaCor artificial corneas. Graefe's archive for clinical and experimental ophthalmology = Albrecht von Graefes Archiv für klinische und experimentelle Ophthalmologie 2006;244:502-6.
[178] Chow CC, Kulkarni AD, Albert DM, Darlington JK, Hardten DR. Clinicopathologic correlation of explanted AlphaCor artificial cornea after exposure of implant. Cornea 2007;26:1004-7.
[179] Lemp MA. Cornea and Sclera. Archives of Ophthalmology 1976;94:473-90.
[180] Goodman WM, SundarRaj N, Garone M, Arffa RC, Thoft RA. Unique parameters in the healing of linear partial thickness penetrating corneal incisions in rabbit: immunohistochemical evaluation. Current eye research 1989;8:305-16.
[181] Gasset AR, Dohlman CH. The Tensile Strength of Corneal Wounds. Archives of Ophthalmology 1968;79:595-602.
[182] Liu W, Merrett K, Griffith M, Fagerholm P, Dravida S, Heyne B, et al. Recombinant human collagen for tissue engineered corneal substitutes. Biomaterials 2008;29:1147-58.
[183] Orwin EJ, Hubel A. In Vitro Culture Characteristics of Corneal Epithelial, Endothelial, and Keratocyte Cells in a Native Collagen Matrix. 2004.
[184] Alaminos M, Del Carmen Sánchez-Quevedo M, Muñoz-Avila JI, Serrano D, Medialdea S, Carreras I, et al. Construction of a complete rabbit cornea substitute using a fibrin-agarose scaffold. Investigative ophthalmology & visual science 2006;47:3311-7.

[185] Hashimoto Y, Funamoto S, Sasaki S, Honda T, Hattori S, Nam K, et al. Preparation and characterization of decellularized cornea using high-hydrostatic pressurization for corneal tissue engineering. Biomaterials 2010;31:3941-8.
[186] Carlsson DJ, Li F, Shimmura S, Griffith M. Bioengineered corneas: how close are we? Current opinion in ophthalmology 2003;14:192-7.
[187] Toksöz S, Guler MO. Self-assembled peptidic nanostructures. Nano Today 2009;4:458-69.
[188] Shah RN, Shah NA, Del Rosario Lim MM, Hsieh C, Nuber G, Stupp SI. Supramolecular design of self-assembling nanofibers for cartilage regeneration. Proceedings of the National Academy of Sciences of the United States of America 2010;107:3293-8.
[189] Mata A, Geng Y, Henrikson KJ, Aparicio C, Stock SR, Satcher RL, et al. Bone regeneration mediated by biomimetic mineralization of a nanofiber matrix. Biomaterials 2010;31:6004-12.
[190] Silva GA, Czeisler C, Niece KL, Beniash E, Harrington DA, Kessler JA, et al. Selective differentiation of neural progenitor cells by high-epitope density nanofibers. Science 2004;303:1352-5.
[191] Chow LW, Bitton R, Webber MJ, Carvajal D, Shull KR, Sharma AK, et al. A bioactive self-assembled membrane to promote angiogenesis. Biomaterials 2011;32:1574-82.
[192] Boateng SY, Lateef SS, Mosley W, Hartman TJ, Hanley L, Russell B. RGD and YIGSR synthetic peptides facilitate cellular adhesion identical to that of laminin and fibronectin but alter the physiology of neonatal cardiac myocytes. American journal of physiology Cell physiology 2005;288:C30-8.
[193] Fittkau MH, Zilla P, Bezuidenhout D, Lutolf MP, Human P, Hubbell JA, et al. The selective modulation of endothelial cell mobility on RGD peptide containing surfaces by YIGSR peptides. Biomaterials 2005;26:167-74.
[194] Massia SP, Rao SS, Hubbell JA. Covalently immobilized laminin peptide Tyr-Ile-Gly-Ser-Arg (YIGSR) supports cell spreading and co-localization of the 67-kilodalton laminin receptor with α-actinin and vinculin. Journal of Biological Chemistry 1993;268:8053-9.
[195] Saiki I, Murata J, Iida J, Sakurai T, Nishi N, Matsuno K, et al. Antimetastatic effects of synthetic polypeptides containing repeated structures of the cell adhesive Arg-Gly-Asp (RGD) and Tyr-Ile-Gly-Ser-Arg (YIGSR) sequences. British Journal of Cancer 1989;60:722-8.
[196] Walker JR, Roth JR, Altman E. An in vivo study of novel bioactive peptides that inhibit the growth of Escherichia coli. The journal of peptide research : official journal of the American Peptide Society 2001;58:380-8.
[197] Marletta G, Ciapetti G, Satriano C, Pagani S, Baldini N. The effect of irradiation modification and RGD sequence adsorption on the response of human osteoblasts to polycaprolactone. Biomaterials 2005;26:4793-804.
[198] Klenkler B, Sheardown H. Growth factors in the anterior segment: role in tissue maintenance, wound healing and ocular pathology. Experimental eye research 2004;79:677-88.
[199] Jester JV, Huang J, Fisher S, Spiekerman J, Chang JH, Wright WE, et al. Myofibroblast Differentiation of Normal Human Keratocytes and hTERT, Extended-Life Human Corneal Fibroblasts. Investigative Opthalmology & Visual Science 2003;44:1850-.
[200] Conrad AH, Zhang Y, Tasheva ES, Conrad GW. Proteomic analysis of potential keratan sulfate, chondroitin sulfate A, and hyaluronic acid molecular interactions. Investigative ophthalmology & visual science 2010;51:4500-15.
[201] Morgan AW, Roskov KE, Lin-Gibson S, Kaplan DL, Becker ML, Simon CG. Characterization and optimization of RGD-containing silk blends to support osteoblastic differentiation. Biomaterials 2008;29:2556-63.

[202] Etheredge L, Kane BP, Hassell JR. The effect of growth factor signaling on keratocytes in vitro and its relationship to the phases of stromal wound repair. Investigative ophthalmology & visual science 2009;50:3128-36.
[203] Reinstein DZ, Archer TJ, Gobbe M, Silverman RH, Coleman DJ. Stromal thickness in the normal cornea: three-dimensional display with artemis very high-frequency digital ultrasound. Journal of refractive surgery (Thorofare, NJ : 1995) 2009;25:776-86.
[204] Ishizaki M, Zhu G, Haseba T, Shafer SS, Kao WWY. Expression of collagen I, smooth muscle α-actin, and vimentin during the healing of alkali-burned and lacerated corneas. Investigative Ophthalmology and Visual Science 1993;34:3320-8.
[205] Gaudreault M, Carrier P, Larouche K, Leclerc S, Giasson M, Germain L, et al. Influence of Sp1/Sp3 Expression on Corneal Epithelial Cells Proliferation and Differentiation Properties in Reconstructed Tissues. Investigative Opthalmology & Visual Science 2003;44:1447-.
[206] Guo X, Hutcheon AEK, Melotti SA, Zieske JD, Trinkaus-Randall V, Ruberti JW. Morphologic characterization of organized extracellular matrix deposition by ascorbic acid-stimulated human corneal fibroblasts. Investigative ophthalmology & visual science 2007;48:4050-60.
[207] Vrana NE, Builles N, Justin V, Bednarz J, Pellegrini G, Ferrari B, et al. Development of a reconstructed cornea from collagen-chondroitin sulfate foams and human cell cultures. Investigative ophthalmology & visual science 2008;49:5325-31.
[208] Borene ML, Barocas VH, Hubel A. Mechanical and cellular changes during compaction of a collagen-sponge-based corneal stromal equivalent. Annals of biomedical engineering 2004;32:274-83.
[209] Crabb RAB, Chau EP, Evans MC, Barocas VH, Hubel A. Biomechanical and microstructural characteristics of a collagen film-based corneal stroma equivalent. Tissue engineering 2006;12:1565-75.
[210] Merrett K, Fagerholm P, McLaughlin CR, Dravida S, Lagali N, Shinozaki N, et al. Tissue-engineered recombinant human collagen-based corneal substitutes for implantation: performance of type I versus type III collagen. Investigative ophthalmology & visual science 2008;49:3887-94.
[211] Fagerholm P, Lagali NS, Carlsson DJ, Merrett K, Griffith M. Corneal regeneration following implantation of a biomimetic tissue-engineered substitute. Clinical and translational science 2009;2:162-4.
[212] Uzunalli G, Tumtas Y, Delibasi T, Yasa O, Mercan S, Guler MO, et al. Improving pancreatic islet in vitro functionality and transplantation efficiency by using heparin mimetic peptide nanofiber gels. Acta biomaterialia 2015;22:8-18.
[213] Olefsky JM. Prospects for Research in Diabetes Mellitus. JAMA 2001;285:628-.
[214] Kizilel S, Garfinkel M, Opara E. The bioartificial pancreas: progress and challenges. Diabetes technology & therapeutics 2005;7:968-85.
[215] Barrett-Connor E, Khaw KT. Diabetes mellitus: An independent risk factor for stroke? American Journal of Epidemiology 1988;128:116-23.
[216] Bild DE, Selby JV, Sinnock P, Browner WS, Braveman P, Showstack JA. Lower-Extremity Amputation in People With Diabetes: Epidemiology and Prevention. Diabetes Care 1989;12:24-31.
[217] Geiss LS, Herman WH, Teutsch SM. Diabetes and renal mortality in the United States. American Journal of Public Health 1985;75:1325-6.
[218] Moss SE, Klein R, Klein BEK. The Incidence of Vision Loss in a Diabetic Population. Ophthalmology 1988;95:1340-8.
[219] Nathan DM. Long-term complications of diabetes mellitus. New England Journal of Medicine 1993.

[220] LaPorte RE, Tajima N, Akerblom HK, Berlin N, Brosseau J, Christy M, et al. Geographic Differences in the Risk of Insulin-dependent Diabetes Mellitus: The Importance of Registries. Diabetes Care 1985;8:101-7.
[221] Leslie RD. Predicting adult-onset autoimmune diabetes: clarity from complexity. Diabetes 2010;59:330-1.
[222] Mellitus D. Diagnosis and classification of diabetes mellitus. Diabetes Care 2005;28:S37.
[223] Bloomgarden ZT. Diabetes Complications. Diabetes Care 2004;27:1506-14.
[224] Narang AS, Mahato RI. Biological and biomaterial approaches for improved islet transplantation. Pharmacological reviews 2006;58:194-243.
[225] Robertson RP. Islet transplantation as a treatment for diabetes - a work in progress. The New England journal of medicine 2004;350:694-705.
[226] Ryan EA, Paty BW, Senior PA, Bigam D, Alfadhli E, Kneteman NM, et al. Five-year follow-up after clinical islet transplantation. Diabetes 2005;54:2060-9.
[227] Nanji SA, Shapiro AMJ. Advances in pancreatic islet transplantation in humans. Diabetes, obesity & metabolism 2006;8:15-25.
[228] Paraskevas S, Maysinger D, Wang R, Duguid TP, Rosenberg L. Cell loss in isolated human islets occurs by apoptosis. Pancreas 2000;20:270-6.
[229] Menger MD, Vajkoczy P, Beger C, Messmer K. Orientation of microvascular blood flow in pancreatic islet isografts. The Journal of clinical investigation 1994;93:2280-5.
[230] Beger C, Cirulli V, Vajkoczy P, Halban PA, Menger MD. Vascularization of purified pancreatic islet-like cell aggregates (pseudoislets) after syngeneic transplantation. Diabetes 1998;47:559-65.
[231] Furuya H, Kimura T, Murakami M, Katayama K, Hirose K, Yamaguchi A. Revascularization and Function of Pancreatic Islet Isografts in Diabetic Rats Following Transplantation. Cell Transplantation 2003;12:537-44.
[232] Merchant FA, Diller KR, Aggarwal SJ, Bovik AC. Angiogenesis in cultured and cryopreserved pancreatic islet grafts. Transplantation 1997;63:1652-60.
[233] Vajkoczy P, Menger MD, Simpson E, Messmer K. Angiogenesis and vascularization of murine pancreatic islet isografts. Transplantation 1995;60:123-7.
[234] Mattsson G. The Endothelial Cells in Islets of Langerhans. Upsala Journal of Medical Sciences 2009.
[235] Vasir B, Aiello LP, Yoon KH, Quickel RR, Bonner-Weir S, Weir GC. Hypoxia induces vascular endothelial growth factor gene and protein expression in cultured rat islet cells. Diabetes 1998;47:1894-903.
[236] Kemp CB, Knight MJ, Scharp DW, Lacy PE, Ballinger WF. Transplantation of Isolated Pancreatic Islets into the Portal Vein of Diabetic Rats. Nature 1973;244:447-.
[237] Carlsson PO, Palm F, Andersson A, Liss P. Markedly Decreased Oxygen Tension in Transplanted Rat Pancreatic Islets Irrespective of the Implantation Site. Diabetes 2001;50:489-95.
[238] Selawry HP, Whittington K. Extended Allograft Survival of Islets Grafted into Intra-abdominally Placed Testis. Diabetes 1984;33:405-6.
[239] Perez VL, Caicedo A, Berman DM, Arrieta E, Abdulreda MH, Rodriguez-Diaz R, et al. The anterior chamber of the eye as a clinical transplantation site for the treatment of diabetes: a study in a baboon model of diabetes. Diabetologia 2011;54:1121-6.
[240] Kriz J, Vilk G, Mazzuca DM, Toleikis PM, Foster PJ, White DJG. A novel technique for the transplantation of pancreatic islets within a vascularized device into the greater omentum to achieve insulin independence. American journal of surgery 2012;203:793-7.
[241] Asai S, Kamei Y, Torii S. One-stage reconstruction of infected cranial defects using a titanium mesh plate enclosed in an omental flap. Annals of plastic surgery 2004;52:144-7.

[242] Vineberg AM. Revascularization of the entire heart by internal mammary artery implantation, epicardiectomy and free omental graft. Canadian Medical Association journal 1966;94:378-85.
[243] De La Torre JC, Goldsmith HS. Coerulospinal fiber regeneration in transected feline spinal cord. Brain Research Bulletin 1994;35:413-7.
[244] Merani S, Toso C, Emamaullee J, Shapiro AMJ. Optimal implantation site for pancreatic islet transplantation. The British journal of surgery 2008;95:1449-61.
[245] Thomas F, Wu J, Contreras JL, Smyth C, Bilbao G, He J, et al. A tripartite anoikis-like mechanism causes early isolated islet apoptosis. Surgery 2001;130:333-8.
[246] Beattie GM, Montgomery AMP, Lopez AD, Hao E, Perez B, Just ML, et al. A Novel Approach to Increase Human Islet Cell Mass While Preserving -Cell Function. Diabetes 2002;51:3435-9.
[247] Lucas-Clerc C, Massart C, Campion JP, Launois B, Nicol M. Long-term culture of human pancreatic islets in an extracellular matrix: morphological and metabolic effects. Molecular and Cellular Endocrinology 1993;94:9-20.
[248] Wang R. Maintenance of beta-cell function and survival following islet isolation requires re-establishment of the islet-matrix relationship. Journal of Endocrinology 1999;163:181-90.
[249] Jiang H, Guler MO, Stupp SI. The internal structure of self-assembled peptide amphiphiles nanofibers. Soft Matter 2007;3:454-.
[250] Stendahl JC, Rao MS, Guler MO, Stupp SI. Intermolecular Forces in the Self-Assembly of Peptide Amphiphile Nanofibers. Advanced Functional Materials 2006;16:499-508.
[251] Murphy MB, Blashki D, Buchanan RM, Fan D, De Rosa E, Shah RN, et al. Multi-composite bioactive osteogenic sponges featuring mesenchymal stem cells, platelet-rich plasma, nanoporous silicon enclosures, and Peptide amphiphiles for rapid bone regeneration. Journal of functional biomaterials 2011;2:39-66.
[252] Cui H, Webber MJ, Stupp SI. Self-assembly of peptide amphiphiles: from molecules to nanostructures to biomaterials. Biopolymers 2010;94:1-18.
[253] Mammadov R, Mammadov B, Toksoz S, Aydin B, Yagci R, Tekinay AB, et al. Heparin mimetic peptide nanofibers promote angiogenesis. Biomacromolecules 2011;12:3508-19.
[254] Gul ASD, Fadillioglu E, Karabulut I, Yesilyurt A, Delibasi T. The effects of oral carvacrol treatment against H2O2 induced injury on isolated pancreas islet cells of rats. Islets 2013.
[255] Mammadov R, Mammadov B, Guler MO, Tekinay AB. Growth factor binding on heparin mimetic peptide nanofibers. Biomacromolecules 2012;13:3311-9.
[256] Zheng X, Baker H, Hancock WS, Fawaz F, McCaman M, Pungor E. Proteomic analysis for the assessment of different lots of fetal bovine serum as a raw material for cell culture. Part IV. Application of proteomics to the manufacture of biological drugs. Biotechnology progress 2006;22:1294-300.
[257] Ayala JE, Samuel VT, Morton GJ, Obici S, Croniger CM, Shulman GI, et al. Standard operating procedures for describing and performing metabolic tests of glucose homeostasis in mice. Disease models & mechanisms 2010;3:525-34.
[258] Daoud J, Petropavlovskaia M, Rosenberg L, Tabrizian M. The effect of extracellular matrix components on the preservation of human islet function in vitro. Biomaterials 2010;31:1676-82.
[259] Greenfield NJ, Fasman GD. Computed circular dichroism spectra for the evaluation of protein conformation. Biochemistry 1969;8:4108-16.
[260] Stendahl JC, Kaufman DB, Stupp SI. Extracellular Matrix in Pancreatic Islets: Relevance to Scaffold Design and Transplantation. Cell Transplantation 2009;18:1-12.
[261] Ilieva A. Pancreatic islet cell survival following islet isolation: the role of cellular interactions in the pancreas. Journal of Endocrinology 1999;161:357-64.

[262] Gelain F, Bottai D, Vescovi A, Zhang S. Designer self-assembling peptide nanofiber scaffolds for adult mouse neural stem cell 3-dimensional cultures. PloS one 2006;1:e119-e.
[263] Knepper PA, Mayanil CS, Goossens W, McLone DG, Hayes E. The presence of transcription factors in fetal bovine sera. In Vitro Cellular & Developmental Biology - Animal 1998;34:170-3.
[264] Bennet W, Sundberg B, Lundgren T, Tibell A, Groth CG, Richards A, et al. Damage to porcine islets of Langerhans after exposure to human blood in vitro, or after intraportal transplantation to cynomologus monkeys: protective effects of sCR1 and heparin. Transplantation 2000;69:711-9.
[265] Shah S, Lowery E, Braun RK, Martin A, Huang N, Medina M, et al. Cellular basis of tissue regeneration by omentum. PloS one 2012;7:e38368-e.
[266] Lang R, Rutschman RL, Greaves DR, Murray PJ. Autocrine Deactivation of Macrophages in Transgenic Mice Constitutively Overexpressing IL-10 Under Control of the Human CD68 Promoter. The Journal of Immunology 2002;168:3402-11.
[267] Meiron M, Zohar Y, Anunu R, Wildbaum G, Karin N. CXCL12 (SDF-1) suppresses ongoing experimental autoimmune encephalomyelitis by selecting antigen-specific regulatory T cells. Journal of Experimental Medicine 2008;205:2643-55.
[268] Yano T, Liu Z, Donovan J, Thomas MK, Habener JF. Stromal cell derived factor-1 (SDF-1)/CXCL12 attenuates diabetes in mice and promotes pancreatic beta-cell survival by activation of the prosurvival kinase Akt. Diabetes 2007;56:2946-57.
[269] Singer AJ, Clark RA. Cutaneous wound healing. The New England journal of medicine 1999;341:738-46.
[270] Gurtner GC, Werner S, Barrandon Y, Longaker MT. Wound repair and regeneration. Nature 2008;453:314-21.
[271] Diegelmann RF, Evans MC. Wound healing: an overview of acute, fibrotic and delayed healing. Frontiers in bioscience : a journal and virtual library 2004;9:283-9.
[272] Bayat A, McGrouther DA, Ferguson MWJ. Skin scarring. BMJ (Clinical research ed) 2003;326:88-92.
[273] Deppermann C, Cherpokova D, Nurden P, Schulz J-N, Thielmann I, Kraft P, et al. Gray platelet syndrome and defective thrombo-inflammation in Nbeal2-deficient mice. The Journal of clinical investigation 2013;123:3331-42.
[274] Clark RA. Fibrin and wound healing. Annals of the New York Academy of Sciences 2001;936:355-67.
[275] Martin P. Wound Healing--Aiming for Perfect Skin Regeneration. Science 1997;276:75-81.
[276] Gillitzer R, Goebeler M. Chemokines in cutaneous wound healing. Journal of leukocyte biology 2001;69:513-21.
[277] Lazarus GS, Cooper DM, Knighton DR, Margolis DJ, Pecoraro RE, Rodeheaver G, et al. Definitions and guidelines for assessment of wounds and evaluation of healing. Archives of dermatology 1994;130:489-93.
[278] Miller M-C, Nanchahal J. Advances in the modulation of cutaneous wound healing and scarring. BioDrugs : clinical immunotherapeutics, biopharmaceuticals and gene therapy 2005;19:363-81.
[279] Lovvorn HN, Cheung DT, Nimni ME, Perelman N, Estes JM, Adzick NS. Relative distribution and crosslinking of collagen distinguish fetal from adult sheep wound repair. Journal of pediatric surgery 1999;34:218-23.
[280] Adolphe C, Wainwright B. Pathways to improving skin regeneration. Expert reviews in molecular medicine 2005;7:1-14.
[281] Madri Ja SSRAM. Angiogenesis. New York: Plenum Press; 1996. p. 355-71.

[282] Kimura H, Esumi H. Reciprocal regulation between nitric oxide and vascular endothelial growth factor in angiogenesis. Acta biochimica Polonica 2003;50:49-59.
[283] Brooks PC, Strömblad S, Sanders LC, von Schalscha TL, Aimes RT, Stetler-Stevenson WG, et al. Localization of matrix metalloproteinase MMP-2 to the surface of invasive cells by interaction with integrin alpha v beta 3. Cell 1996;85:683-93.
[284] Fairbrother WJ, Champe MA, Christinger HW, Keyt BA, Starovasnik MA. Solution structure of the heparin-binding domain of vascular endothelial growth factor. Structure 1998;6:637-48.
[285] Koolwijk P, van Erck MG, de Vree WJ, Vermeer MA, Weich HA, Hanemaaijer R, et al. Cooperative effect of TNFalpha, bFGF, and VEGF on the formation of tubular structures of human microvascular endothelial cells in a fibrin matrix. Role of urokinase activity. The Journal of cell biology 1996;132:1177-88.
[286] Pellegrini L. Role of heparan sulfate in fibroblast growth factor signalling: a structural view. Current opinion in structural biology 2001;11:629-34.
[287] Hoeben A, Landuyt B, Highley MS, Wildiers H, Van Oosterom AT, De Bruijn EA. Vascular endothelial growth factor and angiogenesis. Pharmacological reviews 2004;56:549-80.
[288] Zhou Z, Wang J, Cao R, Morita H, Soininen R, Chan KM, et al. Impaired angiogenesis, delayed wound healing and retarded tumor growth in perlecan heparan sulfate-deficient mice. Cancer research 2004;64:4699-702.
[289] Rajangam K, Behanna HA, Hui MJ, Han X, Hulvat JF, Lomasney JW, et al. Heparin binding nanostructures to promote growth of blood vessels. Nano letters 2006;6:2086-90.
[290] Shroff K, Rexeisen EL, Arunagirinathan MA, Kokkoli E. Fibronectin-mimetic peptide-amphiphile nanofiber gels support increased cell adhesion and promote ECM production. Soft Matter 2010;6:5064-.
[291] Metcalfe AD, Ferguson MWJ. Tissue engineering of replacement skin: the crossroads of biomaterials, wound healing, embryonic development, stem cells and regeneration. Journal of the Royal Society, Interface / the Royal Society 2007;4:413-37.
[292] Ghosh K, Ren X-D, Shu XZ, Prestwich GD, Clark RAF. Fibronectin functional domains coupled to hyaluronan stimulate adult human dermal fibroblast responses critical for wound healing. Tissue engineering 2006;12:601-13.
[293] Helary C, Bataille I, Abed A, Illoul C, Anglo A, Louedec L, et al. Concentrated collagen hydrogels as dermal substitutes. Biomaterials 2010;31:481-90.
[294] Zhong S, Teo WE, Zhu X, Beuerman R, Ramakrishna S, Yung LYL. Formation of collagen-glycosaminoglycan blended nanofibrous scaffolds and their biological properties. Biomacromolecules;6:2998-3004.
[295] Paramonov SE, Jun H-W, Hartgerink JD. Self-assembly of peptide-amphiphile nanofibers: the roles of hydrogen bonding and amphiphilic packing. Journal of the American Chemical Society 2006;128:7291-8.
[296] Smith CK, Withka JM, Regan L. A Thermodynamic Scale for the .beta.-Sheet Forming Tendencies of the Amino Acids. Biochemistry 1994;33:5510-7.
[297] Kweon D-K, Song S-B, Park Y-Y. Preparation of water-soluble chitosan/heparin complex and its application as wound healing accelerator. Biomaterials 2003;24:1595-601.
[298] Ito M, Yang Z, Andl T, Cui C, Kim N, Millar SE, et al. Wnt-dependent de novo hair follicle regeneration in adult mouse skin after wounding. Nature 2007;447:316-20.
[299] Mannor GE, Phelps RG, Friedman AH, Meltzer M. Eyelid healing after carbon dioxide laser skin resurfacing: histological analysis. Archives of ophthalmology (Chicago, Ill : 1960) 1999;117:913-6.
[300] Metcalfe AD, Ferguson MW. Tissue engineering of replacement skin: the crossroads of biomaterials, wound healing, embryonic development, stem cells and regeneration. J R Soc Interface 2007;4:413-37.

[301] Spyrou GE, Naylor IL. The effect of basic fibroblast growth factor on scarring. British journal of plastic surgery 2002;55:275-82.
[302] Galiano RD, Tepper OM, Pelo CR, Bhatt KA, Callaghan M, Bastidas N, et al. Topical vascular endothelial growth factor accelerates diabetic wound healing through increased angiogenesis and by mobilizing and recruiting bone marrow-derived cells. The American journal of pathology 2004;164:1935-47.
[303] Conway K, Price P, Harding KG, Jiang WG. The molecular and clinical impact of hepatocyte growth factor, its receptor, activators, and inhibitors in wound healing. Wound repair and regeneration : official publication of the Wound Healing Society [and] the European Tissue Repair Society;14:2-10.
[304] Islam MS, Zhou H. Isolation and characterization of putative epidermal stem cells derived from Cashmere goat fetus. European journal of dermatology : EJD;17:302-8.
[305] Matsumoto K, Nakamura T. Hepatocyte growth factor (HGF) as a tissue organizer for organogenesis and regeneration. Biochemical and biophysical research communications 1997;239:639-44.
[306] Nakanishi K, Uenoyama M, Tomita N, Morishita R, Kaneda Y, Ogihara T, et al. Gene transfer of human hepatocyte growth factor into rat skin wounds mediated by liposomes coated with the sendai virus (hemagglutinating virus of Japan). The American journal of pathology 2002;161:1761-72.

APPENDIX

Table of copyright permission of references that are used in the thesis.

Referance Number	Supplier	License Number
[9]	Nature Publishing Group	3767330324251
[10]	Nature Publishing Group	3767330508929
[57]	Nature Publishing Group	3767330227027
[162]	Royal Society of Chemistry	376789474458
[163]	Elsevier	3742020498985
[212]	Elsevier	3742020676334